CLIMATE AND HEALTH: EXTREME EVENTS, FOOD SYSTEMS, AND NUTRITION

by Aishwarya Venkat, MS

A dissertation submitted to Tufts University Friedman School of Nutrition Science and Policy in conformity with the requirements for the degree of Doctor of Philosophy in the Agriculture, Food, and Environment Program

Defense date: April 24, 2024

Thesis Chair:

Elena N. Naumova, PhD

Professor, Friedman School of Nutrition Science and Policy, Tufts University

Committee Members:

William A. Masters, PhD

Professor, Friedman School of Nutrition Science and Policy, Tufts University

Erin Coughlan de Perez, PhD

Associate Professor, Friedman School of Nutrition Science and Policy, Tufts University

Contents

Table of Figures

Table of Tables

Acknowledgements

I convey my deepest gratitude to my family, friends, mentors, teachers, and colleagues for their enduring support and patience throughout this journey. My family has always reminded me that my work should stand in service of the marginalized and this has informed my academic journey in profound ways. I also thank my partner for supporting my work and helping me envision and work towards the material realities of an equitable and just global food system. I thank my committee, Dr. Elena Naumova, Dr. Will Masters, and Dr. Erin Coughlan de Perez for their mentorship and guidance over the years on many disparate topics. I have worked with Dr. Naumova for almost a decade now and I am eternally obliged to work with a force for interdisciplinary collaboration and creativity. I am also grateful to the Tufts Initiative for the Forecasting and Modeling of Infectious Diseases and the Food Prices for Nutrition research groups for the rich collaboration and methodological developments at the heart of this dissertation. Finally, I extend heartfelt thanks to my colleagues at the Feinstein International Center (Dr. Anastasia Marshak, Dr. Helen Young, Dr. Paul Howe, and Dr. Dan Maxwell) and the Tufts Data Lab (Carolyn Talmadge and Kyle Monahan) for lending their technical expertise, ground-truthing model results against field experience, and helping me understand the limits of my analysis.

This dissertation was written within and around the cities of Boston, Massachusetts and Redmond, Washington. My community on the east coast is built, physically and collectively, on the traditional and ancestral land of the Massachusett, including the Mashpee and Aquinnah, Wampanoag, Nipmuc, and Massachusett tribes. On the west coast, my community is built on the ancestral lands of the Coast Salish people, including the Duwamish, Puyallup, Suquamish, Tulalip and Muckleshoot nations. In addition to physically inhabiting these lands, my discipline and the climate movement is enabled by the active stewardship and leadership of Indigenous communities around the world who have inhabited their homelands since time immemorial. I

honor and pay my respects to these people and lands, and I will stand in solidarity and action with you as our environment transforms.

I would also like to acknowledge that my socioeconomic and academic privileges allow me to be insulated from the worst impacts of climate change. I recognize that this dissertation comprises only secondary data analysis and does not include the direct voices and opinions of those on the frontlines of climate catastrophe. I understand that in many ways my identity reinforces the hegemony of privileged individuals in the climate sector, and I acknowledge that despite writing this dissertation I know little about the lived experiences of climate-vulnerable people. I will work to ensure that the conclusions presented in this dissertation are never incorrectly generalized or used in lieu of direct engagement with communities about their experiences with climate change. As someone who continues to benefit from the high environmental footprints of the global north, I also accept my responsibility to minimize my environmental footprint and contribute to climate adaptation and mitigation efforts in my communities.

This research is supported by various sources. Preliminary research on famine forecasting and extreme events was supported in part by the Office of the Director of National Intelligence (ODNI), Intelligence Advanced Research Projects Activity (IARPA), via 2017-17072100002. Chapter 3 was partly supported by the Food Prices for Nutrition project at Tufts University (INV-016158) funded by the Bill & Melinda Gates Foundation and the UK FCDO. Chapters 3 and 4 were developed under consultancy contracts with the World Bank and The Micronutrient Forum. The views and conclusions contained herein are those of the authors and should not be interpreted as necessarily representing the official policies, either expressed or implied, of any of the funders.

Abstract

Anthropogenic climate change has increased the frequency and severity of extreme weather, affecting approximately 3.6 billion people worldwide. In the food system, extreme weather directly and indirectly affects food production, consumption, livelihoods, and human health. Remote sensing data allows us to harmonize measurement to define and study extremes at high spatiotemporal resolution. This thesis explores extreme weather phenomena and their impacts on three dimensions of the global food system: retail food prices, acute malnutrition, and famine early warning systems. We utilize novel global datasets to investigate the magnitude of each outcome's response to a suite of extreme weather events including heatwaves, coldwaves, floods, droughts, and storms.

Aim 1 investigates how food prices respond to extreme weather using a database of over 2 million retail price observations in 78 countries during 2000 – 2022 extracted from three early warning systems. Each price was matched to food composition tables as well as market-specific contemporaneous and prior extreme weather occurrence to test if extreme weather is associated with overall higher prices for perishable foods. We discover heterogenous impacts across food groups and urban/rural markets, highlighting dynamic supply constriction and demand reduction in response to extreme weather. On average, storms are associated with 7% higher prices of Fruits and Vegetables, whereas droughts are associated with 5% higher prices of Breads and Cereals in both urban and rural markets. These results underscore the importance of monitoring retail prices of a diverse range of foods to inform climate adaptation and support healthy diets.

Aim 2 investigates seasonal wasting and extreme weather impacts among children under age five. We spatiotemporally align survey boundaries from three global cross-sectional survey databases to extract over 2.5 million anthropometry observations in 39 African countries during

2000 – 2022. Each observation was matched to Koppen climate classes, dominant precipitation type, and extreme weather occurrence during and preceding the survey month. Using multiple harmonic regression, we demonstrate that wasting is highly seasonal and geographically diverse. We further calculate peak timing and wasting prevalence estimates at high spatial and temporal resolution, and identify limited associations between extreme weather and wasting. These findings can inform climate-sensitive interventions and nutrition surveillance efforts to reduce seasonal wasting.

Aim 3 studies extreme weather's influence on famine early warning using a compilation of current and predicted acute food insecurity phase classifications from three databases of food insecurity analyses. We first develop a probabilistic approach to quantify the likelihood of predicting and observing particular phase transitions. We then test whether the conditional probabilities of predicting and observing particular transitions are significantly different in the presence of concurrent and preceding extreme weather. We find mixed results with preliminary evidence that months with severe floods are associated with marginally higher likelihood of underprediction. This probabilistic framework and extreme weather-specific findings can be utilized to iteratively improve the accuracy of food insecurity prediction in the context of a volatile climate.

Introduction

Anthropogenic climate change has resulted in higher temperatures across land, sea, and atmosphere, as well as increased frequency of weather extremes such as heatwaves, extreme precipitation, droughts, and tropical cyclones. These changes directly affect 3.3-3.6 billion people (IPCC, 2022). In the food system, these events are associated with reduced food production affecting both land-based and aquatic systems (Cottrell et al., 2019). Weather extremes such as floods and heatwaves are also associated with direct impacts on human health, particularly in the form of infectious diseases and respiratory illnesses. Among infants and children under age five, several etiological pathways link maternal and child exposure to extreme temperature or extreme precipitation with lower birthweights, growth faltering at critical ages, and lifelong consequences on morbidity, learning outcomes, and incomes. Exposure to extreme weather is thus an important determinant of food security and health.

However, research within food systems is biased. A recent scoping review found that 73% of studies on environmental shocks in the food system focused on production alone, and food consumption was included in only 15% of studies (K. F. Davis, Downs, & Gephart, 2021). This indicates that outsize research emphasis on food production occurs at the expense of other critical parts of the food chain such as storage, processing, retail, and consumption. Studying these facets of the food system can help illuminate weather-food linkages at policy-relevant spatial and temporal scales, and inform critical entry points for climate adaptation.
Conceptualization and measurement extreme weather is also highly heterogenous. One key challenge is that there are few standard measures of extreme weather phenomena, partly due to the diversity of vocabulary and indicators utilized across disciplines. One review found that in 10 years of academic literature on the topic of extreme events, majority of publications do not provide an explicit definition of the phenomenon under study (McPhillips et al., 2018). This ambiguity is further complicated by self-reported incidence of extreme weather, as well as

varied physical measures of different dimensions of extreme weather. These conceptualizations of extreme weather thus determine how the event is defined and how its impacts in the food system are measured. Comparability and generalizability of findings from studies using very different definitions of the underlying extreme is therefore limited.

This dissertation broadly explores extreme weather phenomena and their impacts on the food system. We first begin with an overview of how extreme weather is conceptualized, and conclude Chapter 1 by adopting the vocabulary of the risk framework and the spatial and temporal limits of an eventist approach in our definition of climate hazards. We then proceed to a review of climate hazards and their relationship to human health and nutrition in Chapter 2. This review focuses on nutrition outcomes and extreme weather. We find that regression approaches and deviation-based measures of continuous weather phenomena are most commonly utilized in this literature. Causal inference to establish a robust link between extreme weather and health outcomes is rare. The review further finds that less than 10% of reviewed publications provide at least three of five criteria to describe the climate hazard under study. The review allows us to acknowledge the complexity of existing approaches and limited causal inference feasible from secondary studies. Chapter 3 details common techniques and workflows utilized across chapters that are referenced in further chapters.

The rest of the dissertation chapters sequentially explore climate hazards in three different dimensions of food systems. Due to the diversity of topics covered, each chapter includes a smaller introduction of relevant literature. In Chapter 4 we turn to retail food prices extracted from three early warning system databases: the Global Information and Early Warning System (GIEWS) by the Food and Agriculture Organization (FAO) of the United Nations (UN); the Famine Early Warning System Network (FEWSNET) produced by USAID; and the Vulnerability Analysis and Mapping (VAM) system from the World Food Programme (WFP). In Chapter 5 we turn to human health outcomes, particularly undernutrition in the short term (wasting). We

explore these outcomes using three datasets: a compilation of Standardized Monitoring and Assessment of Relief and Transition (SMART) surveys; a database of USAID Demographic Health Surveys (DHS) matched to geospatial coordinates in the IFPRI Advancing Research on Nutrition and Agriculture (AReNA) GIS dataset; and a manually standardized compilation of 52 Multiple Indicator Cluster Surveys implemented by the United Nations International Children's Emergency Fund. These three datasets together provide 23 years of anthropometry data for a nuanced comparison of extreme weather effects on stunting and wasting. Finally, we turn to famine early warning systems in Chapter 6 for a systems-level perspective on acute food insecurity. Since there are no standard measures of system performance for famine early warning systems, Section 1 of Chapter 5 introduces a Markov probabilistic framework utilized to develop metrics such as transition probabilities, persistence, volatility, and crisis duration. Section 2 of Chapter 5 applies these metrics to measure the influence of extreme weather on phase classifications from three famine early warning systems: FEWSNET, the Integrated Phase Classification (IPC), and the Cadre Harmonisee (CH). We conclude with Chapter 7: Conclusions and Recommendations, which outlines key policy takeaways, limitations to the data and analysis, and future directions from each chapter.

Chapter 1: Origins of Extreme Weather

Physical Basis

Extreme events refer, with varying precision, to a spectrum of phenomena including disasters, catastrophes, emergencies, and crises. Such events are classified into families and main events as shown in Table 1 (IRDR, 2014).

Table 1 Peril Classification (adapted from IRDR 2014, Figure 2)

Family	Geophysical	Hydrological	Meteorological	Climatological	Biological
Main Event	Earthquake Mass movement Volcanic activity	Flood Landslide Wave action	Storm Extreme temperature Fog Tropical cyclone	Drought Wildfire Glacial lake outburst	Animal incident Disease Insect infestation

The geophysical family relates to disasters caused by deformations below the earth surface in the lithosphere. Ruptures or rock movements along geologic faults can release sufficient energy to generate shaking, vibrations, and surface shifts, altogether known as earthquakes. Tectonic earthquakes may radiate seismic waves from the epicenter to several thousand kilometers. Tectonic activity proximal to a volcano, or pressure changes due to movement of magma within a volcanic system, may also lead to volcanic-tectonic earthquakes. The primary impact of earthquakes on humans occurs through injuries and physical damage to infrastructure and utilities such as electricity grids and telephone networks. Earthquakes may also trigger secondary phenomena such as landslides, flash floods, and tsunamis (Hyndman & Hyndman, 2016; Keller & DeVecchio, 2016).

The water cycle can also lead to extreme volumes of water in a location which triggers hydrologic disasters. Floods are defined as “an overflow of water on normally dry land”, and occur mainly due to heavy rain in conjunction with other atmospheric phenomena. Fluvial or

river floods occur due to rising levels in water bodies, which may lead to breaching of water infrastructure such as dams and levees. Pluvial or flash/surface floods occur independent of water bodies. Coastal storms may also generate flooding as a result of high speed winds forcing high tidewaters onto land in the form of storm surges (Maidment, 1993). Offshore factors can lead to development of high-energy waves which can propagate inland during storms. Depending on topology, floods may also trigger landslides, or movement of rocks and earth downslope. The type of flood affects the length of the warning period to undertake protective activities. Fluvial and coastal floods are often slow to unfold and easily forecasted, and thus provide communities critical evacuation time before damage occurs. Flash floods are often more destructive and provide little preparation or evacuation time (Keller & DeVecchio, 2016).

Atmospheric heat from the sun in conjunction with the global water cycle drives global patterns of temperature and precipitation. The combination of these forces can generate fog, which is defined as a suspension of water droplets in the atmosphere near the earth surface. Instability in the atmosphere in the presence of high temperatures, moisture, and winds can also generate tropical cyclones. These phenomena usually originate around the equator from warm ocean waters, and are also known as hurricanes, storms, and typhoons. Wind damage and flooding from severe tropical cyclones can devastate coastal communities. Prolonged exposure to extreme temperatures such as heatwaves can also occur due to atmospheric forces trapping high pressure systems close to the earth surface. Human impacts from heatwaves include plant stress in agricultural systems, wildfires, strained electricity grids, and physiological exhaustion (Hyndman & Hyndman, 2016; Keller & DeVecchio, 2016).

Beyond short-term phenomena such as tropical cyclones, interactions between global temperature and water cycles also unfold over years and decades. For example, meteorological droughts occur due to consistently low seasonal precipitation as a result of altered weather patterns, land use, and/or ecosystems-level changes. These factors may also accelerate

seasonal phenomena such as wildfires and glacial melt, increasing the frequency and severity of resulting devastation. Long-term climate cycles also form the foundation of ecosystems including microbiota, flora, and fauna. Long-term disruptions to climate have downstream effects on ecosystems through altered pathogen, pest, and disease cycles, changing animal ranges, and increased rates of human/animal interactions (Hyndman & Hyndman, 2016; Keller & DeVecchio, 2016)

All aforementioned disasters have also been influenced by human activities. Climate change is “unequivocal and ongoing” (Ara Begum et al., 2022) and scientific consensus indicates that human influence has increased mean sea level and temperature extremes around the world (Eyring et al., 2021). These influences have led to an increased frequency and/or intensity of weather extremes in recent decades, including temperature and precipitation extremes, tropical cyclones, and worsening droughts (Seneviratne et al., 2021). As the climate continues to evolve in response to human forcings, improved characterization of disaster risk perception and decision-making is key for robust adaptation and mitigation responses.

Origins of Disaster Study

Although the physical basis of extreme events are mostly universal, the applied definitions of these phenomena vary greatly by discipline, subject, and spatial and temporal scale (Enrico Louis Quarantelli & Ronald W Perry, 2005). *Disaster* was the preferred terminology for an extreme event since the inception of the field of disaster research in the 1950s (K. J. Tierney, 2007). One early definition indicates that a disaster is “any event in a geophysical system displaying relatively high variance from the mean” (Alexander, 1993; White, 1974). This definition emphasizes that disasters are significant deviations from an established normal within the context of natural systems. Disasters were historically understood to originate as hazards in earth systems and subsequently affect human life through property damage or impeded lives and livelihoods (Perry, 2007; K. J. Tierney, 2007). This objective or ‘*eventist*’

framing renders the environmental system as independent from human influence or impact. The study of environmental occurrences has conventionally been the focus of physical sciences in earth sciences and engineering, whereas human-environment interactions were investigated in sociology, anthropology, and related fields (Alexander, 1993; Burton, Kates, & White, 1993; Perry, 2007).

Disasters may also be defined as dependent on their social impacts, particularly on human social structures (Gary A. Kreps, 1989). For example, a disaster can be “a naturally occurring or man-made geologic condition or phenomenon that presents a risk or is a potential danger to life or property” (American Geological Institute, 1984). It can also be defined as “an event, concentrated in time and space which threatens a society or a relatively self-sufficient subdivision of a society with major unwanted consequences as a result of the collapse of precautions which had hitherto been culturally accepted as adequate” (Turner, 1976). This intersection is reflected in the current global consensus definition of disasters in the United Nations International Strategy for Disaster Reduction (UNISDR):

> “a serious disruption of the functioning of a community or a society involving widespread human, material, or environmental losses and impacts which exceeds the ability of the affected community to cope using only its own resources” (UNISDR, 2009)

Disasters are thus events that overwhelm communities, and are inherently social phenomena (Dynes, 2005; Perry, 2007; K. J. Tierney, 2007). Vulnerability to disasters often parallels social vulnerabilities along gender, race, ethnicity, class, caste, and other dimensions (Cutter, 1996, 2003; Enrico L Quarantelli & Ronald W Perry, 2005; K. Tierney, 2014a). In addition to direct impacts, social stratification further affects perceptions of disasters, in turn affecting upstream conceptualization and measurement decisions (Burton et al., 1993; Cutter, 1996; Drabek, 1989; Hewitt, 1983). In the human experience of disasters, the event cannot be separated from the social contexts in which they occur (Hewitt, 1983). Thus, a social definition

of disaster may address these events broadly as “nonroutine social problems” (Drabek, 1989; Hewitt, 1983; Gary A Kreps, 1989). In a more continuous sense, disasters may be considered as common experiences reflective of social structures and vulnerabilities rather than purely environmental anomalies. This constructivist view of disasters sees them as “foreseeable manifestation[s] of the broader forces that shape societies” (K. J. Tierney, 2007). Our definitions and experience of disasters evolve in parallel with a dynamic society (Alexander, 2005; Gary A. Kreps, 1989).

Eventist and constructivist approaches also determine spatial and temporal extents of disaster study. Early eventist definitions in systems theory characterize disasters as short-term disruptions to a natural system (Alexander, 1993; Fritz, 1961; Turner, 1976). The duration of most disasters is at the scale of hours or days (Alexander, 1993) in eventist framings; however in social conceptions of time, the factors causing vulnerability during a disaster may unfold over a period of years or decades (Dynes, 2005; Perry, 2007; K. J. Tierney, 2007). The question of when a disaster ends may elicit different responses as well. A disaster was initially theorized as a disruption followed by an onset or emergency period, a first-stage adjustment period, and an eventual return to the established norm (Turner, 1976). The chosen system boundaries therefore determine the temporal extent of analysis. An eventist focus on the environmental agent indicates that the disaster period ends when the specific environmental system returns to an expected range. From a constructivist standpoint, human routines may remain affected for several months or years after a disaster, and exacerbated from compound vulnerabilities. In the spatial domain, eventists may limit their region of interest to the geographic boundaries of a disaster-affected area, whereas constructivists may extend these boundaries to include social spaces, e.g. kinship networks, ethnicity or clan groups, and institutional extents (Dynes, 2005; Perry, 2007). The spatial and temporal extent of disaster analysis is thus influenced by disciplinary approaches.

The remainder of this chapter will explore various disciplinary approaches to conceptualizing and measuring extreme events. This non-exhaustive tour will then extend to specific metrics used to operationalize extreme event measurements, with a specific focus on how the spatial and temporal domains are constructed for each. We will then end with some conclusions and applications relevant to food systems to introduce Chapter 2: Nutrition Impacts of Extreme Events.

Conceptualizations

Sociological Framings

The 'social productions of disaster' and vulnerabilities are of particular concern in disaster research (Cutter, 1996; Hewitt, 1983; Mileti, 1999). Thus, the sociological approach studies how disasters differentially impact various groups, and how individuals interact with disasters through perceptions, attitudes, and behaviors (Alexander, 1993; Paul, 2011). The latter attention on attitudes and beliefs constitutes the behavioral or human ecological lens towards disaster study (Cutter, 2003; Hewitt, 1983; Paul, 2011; Tobin & Montz, 1997a). A common definition of a disaster from the human ecological standpoint may be an occurrence that exhausts or overwhelms the adjustment options available to an individual or otherwise severely limits their choices. This approach is very effective at influencing hazards policy because it interrogates affected individuals about their understanding of disasters (Paul, 2011).

The structuralist or political ecological approach involves studying the underlying human circumstances which determine vulnerability to extreme events (Hewitt, 1983). Generally, disasters disproportionally impact the poorest and most marginalized individuals in a society (K. Tierney, 2014b). Therefore, potential determinants of vulnerability include individual, household, communal, regional, and often institutional, national, and international factors (Palm, 1990; Wisner, Blaikie, Cannon, & Davis, 2004). A shared definition of disaster from this lens may be

an event that disproportionately impacts the most marginalized social groups in a region. The political ecological approach conceptualizes social and institutional linkages at multiple spatial and social scales, leading to a holistic treatment of human-environment interactions (Cutter, 1996; Paul, 2011). More recently, geographers have integrated the physical and sociological aspects of disaster into a 'hazards in context' approach which incorporates these complex interactions into spatial models of vulnerability (Cutter et al., 2008; Palm, 1990).

Risks and Hazards

The field of disaster risk management utilizes a probabilistic approach to define risk and its constituent components. A plurality of definitions exist for the concept of risk, including the expected losses from a disaster, probability of an undesirable event or loss, and severity of consequences of an event (Aven, 2012; León, 2006; UNDRR, 2017; Wisner et al., 2004). Within risk management frameworks, risk is defined as a complex manifestation of the interactions between a potentially destructive system or event (hazard, *H*), and social vulnerabilities (*V*) which determine physical and social exposure to the hazard (*E*). Risk is thus often expressed mathematically as $R = H \times E \times V$ (Keller & DeVecchio, 2016; UN/ISDR, 2009; UNDRR, 2017; Wisner, Gaillard, & Kelman, 2012). Risk assesses the potential for negative consequences, and is therefore forward-looking, continuous, and dynamic (Keller & DeVecchio, 2016). Risk assessments aim to evaluate hazards and minimize the level of risk through adjustments (Alexander, 1993; Keller & DeVecchio, 2016).

Disaster risk is specifically defined as: "the likelihood of loss of life, injury or destruction and damage from a disaster in a given period of time" (UNDRR, 2017; UNISDR, 2009). Twigg (2001) links the structuralist framing to the risks framework by clarifying: "A disaster is the result of a hazard's impact on society" (Twigg, 2001). If a hazard occurs in the absence of exposure and therefore there is no vulnerability, then there is no risk. Expressions of risk may be

subjective (based on knowledge systems and uncertainty), and/or probabilistic (based on empirical frequencies of occurrence) (Aven, 2012; Wisner et al., 2012).

Hazards are a critical component of risk. A hazard is formally defined as “a dangerous phenomenon, substance, human activity or condition that may cause loss of life, injury or other health impacts, property damage, loss of livelihoods and services, social and economic disruption, or environmental damage” (UNDRR, 2017). Hazards have various characteristics that influence risk:

- ***Identity and Origin***: the nature of the hazard itself determines the mechanism of potential impact (Hewitt & Burton, 1973; Keller & DeVecchio, 2016; Tobin & Montz, 1997b). For example, floods are hydrological hazards, and knowledge about streamflow or floodplain dynamics can better inform risk management.
- ***Magnitude***: the magnitude of a hazard is determined by the strength of the underlying physical process. Calculations of magnitude allow for comparisons of different hazards and determine thresholds to define the events with greatest potential for damage. For example, the amount of energy released in an earthquake directly informs the magnitude of the earthquake on the Richter scale, and a threshold value of 6 is used to identify potentially damaging earthquakes (Alexander, 1993; Burton, Kates, & White, 1978; Tobin & Montz, 1997b).
- ***Intensity***: intensity refers to the localized impact of a hazard at a location and time. This response is usually measured as an index or scale, and includes a range of possible impacts on ecosystems, property, or human beings. For example, the intensity of an earthquake is measured using the Modified Mercalli Scale, which incorporates outcomes like falling objects, tree and building damage, and overturned furniture (Keller & DeVecchio, 2016; Tobin & Montz, 1997b).

- ***Spatial Properties***: the physical space affected by a hazard. The affected area is dependent on the origins, magnitude, and intensity of the hazard, as well as spatial factors including elevation, proximity to coastline, presence of forests or wetlands, etc. Several authors have theorized concentric regions of hazard impact (Alexander, 1993), which include:
    - ***Zone of total impact***: area which experiences the highest direct impact of a hazard
    - ***Zone of marginal impact***: surrounding area where hazard impact is significantly lower
    - ***Zone of filtration***: the closest 'safe ground' for victims from previous zones, and therefore hosts refugees and victims seeking shelter or aid
    - ***Zone of aid***: regions where supplies and aid is gathered to support individuals in all impacted zones
- ***Temporal Properties***
    - ***Duration***: the length of time taken for a disaster to unfold ranges from a few seconds (e.g. tornado) to several years (e.g. drought). This definition excludes human impacts, which may last for years or decades. Chronological time provides one dimension for comparison of different events, and is particularly important for risk management and planning (Alexander, 1993; Tobin & Montz, 1997b). In general, longer-duration events allow for greater opportunities for adjustment planning and implementation (Tobin & Montz, 1997b)
    - ***Frequency***: the expected occurrence of a disaster of a particular magnitude and duration based on the long-run average. There is a nonlinear and negative relationship between frequency and magnitude, such that high magnitude events have relatively low frequency and vice versa (Alexander, 1993; Maidment, 1993). Higher frequency events are also generally associated with greater risk perception

and understanding (Cutter et al., 2008). Frequency analysis forms the foundation of hazard estimation, prediction, and early warning systems.

- ***Rate of Onset***: The length of time between initial activity to peak hazardous state. The rate of onset determines immediate response times and the length of the warning period (Cutter et al., 2008)
- ***Return Period***: the time between occurrences of a disaster of a particular magnitude and duration. This statistic may also be defined as the probability of exceedance or the inverse of the average frequency of occurrence (Maidment, 1993). Rarer events often tend to be more destructive due to less time for forewarning and preventative action.
- ***Sequence***: successive hazards of same or different origins may also inflict compounded damage; e.g. an earthquake generating a tsunami leading to flooding (Cutter, 2018). These successive events may be cascading hazards if they are proximate in time, space, and origin. If the causes of a disaster are natural and anthropogenic, with multiple vulnerabilities and often conflict, then the disaster may evolve into a complex emergency requiring humanitarian response (Cutter, 2018).

Disturbances

In ecology, extreme events and hazards are framed as disturbances or perturbations which affect populations and ecosystems (Grimm, Pickett, Hale, & Cadenasso, 2017). Such perturbances share many characteristics of hazards such as intensity or magnitude, spatial extent, duration, and timing (Grimm et al., 2017; Peters et al., 2011). These features are often used to characterize disturbance regimes which in turn affect system structure and function (Dale, Lugo, MacMahon, & Pickett, 1998; Grimm et al., 2017).

Comprehensive understanding of the target ecological system is required to assess the impact of a disturbance. Generally, the equilibrium state of a system or population is first

defined, and its responses to short-term and long-term perturbations, known as pulses and presses respectively, are assessed (Ives & Carpenter, 2007; May, 1974). The impact of a pulse event can be assessed by a community's rate of return to its equilibrium state (May, 1974). Experience of stochastic pulses also generates community resilience, which is defined as the change in combined densities in response to repeated disturbances (Pimm, 1984). Higher resistance leads to rapid return rates and therefore less overall variability in the system (Ives & Carpenter, 2007; Pimm, 1984). Long-term perturbations or presses may lead to changes in community composition and/or dynamics, leading to newer equilibrium states or community identities (Grimm et al., 2017; Peters et al., 2011). Existing feedback loops within ecosystems may also be impacted during and due to pulse or press events (Grimm et al., 2017; Peters et al., 2011).

Although the disturbance framing has much in common with both risk and sociological definitions of disasters, there are some key differences. The spatial scale of ecological systems is highly variable, and includes orders of magnitude differences between communities (e.g. microbiota vs. cities). The temporal distinction between pulse and press events also depends greatly on the specified system boundaries (Collins et al., 2010; Pickett & Cadenasso, 2008; Pickett, Kolasa, Armesto, & Collins, 1989). Disturbance events are characterized by a sequence of onset, duration, and release but these events are highly variable in sequence and scale (Dale et al., 1998; Pickett et al., 1989). Ecological approaches further recognize the interconnectedness of complex systems through feedback loops and cascades, and emphasize that the system changes dynamically through its experience of disturbances (Donohue et al., 2016; Grimm et al., 2017; Peters et al., 2011). Despite these differences, the ecological lens has influenced development perspectives on resilience, e.g. through DFID's disaster resilience strategy (DFID, 2011).

Shocks and Stressors

All perspectives discussed above have significant influence on how disasters are conceptualized in development. Development aims to reduce vulnerability and rebuild in the aftermath of disaster. It also promotes stability and "the sense that people can control their own economic destiny" (Anderson, 1991). On the other hand, disasters "turn back the development clock" (Sanderson, 2000) and upend communities and livelihoods. The political economy approach (Hewitt, 1983; Wisner et al., 2004) is most closely aligned with developmental perspectives on vulnerability and resilience. Current frameworks emphasize the continuous nature of resilience as an intermediate outcome towards a long-term goal such as improved nutrition or escaping poverty (Béné, Frankenberger, & Nelson, 2015; Constas, Frankenberger, & Hoddinott, 2014).

More recent livelihoods frameworks emphasize the role of actions and activities at various scales as expressions of resilience (Chambers & Conway, 1991; Sanderson, 2000). Chambers and Conway (1991) define livelihoods as: "the capabilities, assets (both natural and social) and activities required for a means of living" (Chambers & Conway, 1991). Livelihoods occur primarily in the economic domain, and therefore concern factors related to production, consumption, trade, and income generating activities (Bujones, Jaskiewicz, Linakis, & McGirr, 2013). These activities further intersect with identities, capitals, and social structures to construct vulnerability to disasters (Wisner et al., 2004).

In this context, shocks are defined as "external short-term deviations from long-term trends [which] have substantial negative effects on people's current state of well-being, level of assets, livelihoods, or safety, or their ability to withstand future shocks" (Zseleczky & Yosef, 2014). Stresses are long-term factors that reduce stability and increase vulnerability (Bujones et al., 2013). Naturally occurring shocks such as floods and droughts can damage crops and livestock, destroy assets, and impede physical access to livelihoods (Béné, Frankenberger, et

al., 2015; Bujones et al., 2013). Such shocks also impact individual health through disease pathways, leading to lower productivity, increased expenditures on healthcare, and resulting vulnerability (Béné, Frankenberger, et al., 2015; Constas et al., 2014; Emmanuel Skoufias, 2003). Man-made shocks such as market, conflict, or technological shocks can also impede movement and livelihoods. Finally, economic shocks such as trade restrictions and financial crises can impact wages and prices, and affect labor demand, market function, and nutrition status at regional scales (Béné, Frankenberger, et al., 2015; Constas et al., 2014; Emmanuel Skoufias, 2003). The plurality of pathways from shocks to food system and nutrition impacts are detailed in Chapter 2.

Shocks and stressors rarely occur as isolated events and are often interrelated. For example, degraded natural resources may be both the cause or consequence of conflict, and lower labor opportunities in one location may lead to outmigration and population pressures elsewhere (R. Choularton, Frankenberger, Kurtz, & Nelson, 2015; Constas et al., 2015). Resilience to one shock therefore does not confer resilience to another shock or stressor (Constas et al., 2014). Multiple shocks and their interactions must be disaggregated and studied for a complete picture of resilience and responses (R. Choularton et al., 2015). Due to the intensive nature of many shocks, the unit of analysis for resilience studies extends beyond households to include communities, ecosystems, and institutions (Béné, Frankenberger, et al., 2015).

The operationalization of shocks in development theory and programming has yielded subjective and objective measures. Objective measures of shocks derive from global monitoring systems, early warning systems, and satellite-derived data (Béné, Frankenberger, et al., 2015; R. Choularton et al., 2015). These data sources often monitor changes in atmospheric phenomena to identify shifts in food production and livelihoods. Subjective measures of shock derive from household surveys which collect data on income, assets, and responses to shocks.

Although most surveys include questions about shock experience, there is a lack of standardization and uniformity on what shocks mean across surveys (Béné, Frankenberger, et al., 2015; Carletto, Banerjee, & Zezza, 2015). The self-reported nature of shocks in household surveys fails to separate impact from exposure, and does not provide information about the magnitude or duration of the shock itself (Carletto et al., 2015; Edwards, Gray, & Borja, 2021). Classification of shocks as covariate (affecting large areas or populations) or idiosyncratic (affecting a few households) further obscures event and impact. Most recently, community rating and mixed methods combine objective measures of shock magnitude and duration with subjective measures of shock perception to better capture complex interactions and trajectories of recovery (R. Choularton et al., 2015; Edwards et al., 2021; Dan Maxwell, Constas, Frankenberger, Klaus, & Mock, 2015).

Subjective and objective definitions of shocks may also differ in the temporal domain. The low frequency of survey administration limits available data on exposure to shocks and stressors (R. Choularton et al., 2015). Household surveys are often implemented once every few years, and may often collect information about shocks several years after the event (R. Choularton et al., 2015). As a result, resilience programs and household surveys are biased towards large-scale covariate shocks that affect communities. However, vulnerable households most commonly experience lower intensity, higher frequency shocks which result in greater share of economic losses (Béné, Frankenberger, et al., 2015; R. Choularton et al., 2015; Oxley, 2013; UNDRR, 2019). Objective measures of shock may also overlook regular or seasonal extensive shocks due to the search for significant deviations from long-term averages. High-frequency data on both shocks and stressors, and their varied impacts across multiple spatial scales and social structures, is very rarely collected (Béné, Frankenberger, et al., 2015).

Thresholds and Tipping Point

A tipping point is broadly defined as “a limit beyond which a system cannot return directly to its former state” or a point at which major changes occur in system dynamics (Donohue et al., 2016; Ives & Carpenter, 2007). This concept derives from ecology and systems theory with broad application to economics, resilience, and development. Tipping points have been applied to explain poverty traps and resilience (Barrett & Constas, 2014). In social settings, formal or informal threshold values can help decisionmaking for disaster management .

In the context of the macroclimate, tipping points are associated with self-perpetuating system dynamics which proceed uninhibited beyond a safe operating range (Seneviratne et al., 2021). Several tipping elements which can lead to catastrophic change in the global climate system have been identified (Ara Begum et al., 2022; Armstrong McKay et al., 2022; Lenton & Ciscar, 2012). The causes of tipping within ecosystems are highly variable, nonlinear, and are often linked to positive feedback loops (Ara Begum et al., 2022; Lenton & Ciscar, 2012). The application of tipping point theory to engineering and climate change adaptation is fairly new (Ahmed, Khan, Warner, Moors, & Terwisscha Van Scheltinga, 2018; Lenton & Ciscar, 2012). Adaptation tipping point approaches aim to model human responses to hazards and mitigation measures, but have only been used in small case studies of flood resilience in Bangladesh and the Netherlands (Ahmed et al., 2018). Applications of tipping point theory to food insecurity, droughts, heatwaves, and floods are also emergent (Ahmed et al., 2018; Krishnamurthy R, Fisher, Schimel, & Kareiva, 2020; Park, Seager, Rao, Convertino, & Linkov, 2013; van Herk, Schot, Gersonius, & Koukoui, 2015). Analytical methods are diverse at present but generally involve a constructed climate damage function with varied functional forms (Lenton & Ciscar, 2012).

Impact-Based Measures

Various other definitions of disasters exist across disciplines. The total losses sustained during an event has been used as one definition of disaster from an economic standpoint. The original threshold of $1 million has since been updated to an increasingly common occurrence of “billion dollar disasters” (Burton et al., 1978; Cutter, 2018). Event-specific morbidity or mortality has also been used as a threshold for disaster. Such a threshold is utilized in the Centre for Research on the Epidemiology of Disasters (CRED) Emergency Events Database (EM-DAT), the most detailed compilation of disasters utilized by humanitarians. EM-DAT requires at least one of the following criteria to be met for inclusion in the database: 10 or more people killed, 100 or more people affected, declaration of a state of emergency, or call for international assistance (Guha-Sapir & Below, 2022). The EM-DAT database forms the basis of large system-wide analyses such as the Global Assessment of Risk which are used to target progress towards global agendas of disaster risk reduction. However, the impact-based definition of disaster in EM-DAT means that small- and medium-scale, localized, and frequent disasters which cause 68% of economic losses (UNDRR, 2019) may go unrecorded. In the humanitarian domain, an Integrated Phase Classification assessment of Phase 3 is used as a critical threshold for potential severe food insecurity (IPC Global Partners, 2019). More recent approaches to measuring disaster impacts include Disability-Adjusted Life Years (Noy, 2016) and ‘social barometers’ of disaster exposure from community ratings and social media (Edwards et al., 2021; Niles, Emery, Reagan, Dodds, & Danforth, 2019).

Conclusions

There exists a plurality of conceptualizations and operational definitions of hydrological, meteorological, climatological, and biological hazards across disciplines. At the individual and communal scales, risk exposure and perceptions and quantified through interview methods which aim to capture varied beliefs and opinions around vulnerability, risk, and resilience. In the

engineering and hydrological sciences, hazards are often calculated at the watershed scale as the outcome of modeling exercises which utilize inputs of historical meteorological records, morphological features, and land use. At the global scale, atmospheric scientists utilize evolving data on the natural system to generate climate projections which further inform scenario generation and analysis across disciplines.

This dissertation adopts the risk framework approach to utilizes the term “hazard” instead of the varied terminology of extreme event, shock, disturbance, or risk. This definition is consistent with the UNDRR definition of hazard as a “potentially destructive system or event”. Further, the use of hazard terminology is critical in our secondary analyses of outcomes in the food system as we cannot and do not study any measures of exposure or vulnerability across populations. In contrast to the economic framing of shocks which often relies on self-reported experience of natural hazards, we utilize gridded data derived from remote sensing to calculate the magnitude of hazard across study regions. This measurement of hazards based only on environmental variables is an eventist framing as it treats the environmental as independent of human influence or impact despite extensive evidence to the contrary. Among identified extremes, this dissertation also endeavors to study the relationship between different hazard magnitudes and responses observed in the food system.

Chapter 2: Measures of Climate Hazards and Human Health

Introduction

Weather shocks impact human health through increased risk of mortality and morbidity via multiple pathways. Among adults, extreme heat is associated with exhaustion, dehydration, lower labor productivity, and lower wages (Kjellstrom & Crowe, 2011; Zhao, Lee, Kjellstrom, & Cai, 2021). Long-term shocks such as seasonal droughts may cause households to utilize coping strategies such as reduced consumption and asset sales (Belesova, Agabiirwe, Zou, Phalkey, & Wilkinson, 2019; Dimitrova, 2021). On the other hand, short-term shocks such as floods and storms may cause physical injury from debris or drowning due to fast-moving floodwaters (K. Alderman, Turner, & Tong, 2012). Floods and storms may also increase likelihood of fecal-oral transmission and risk of vector-borne illnesses such as malaria and dengue, leading to illness, lower diet diversity, lower food consumption, and/or nutrient malabsorption (Ahern, Kovats, Wilkinson, Few, & Matthies, 2005; K. Alderman et al., 2012; Sajid & Bevis, 2021; Stanke, Kerac, Prudhomme, Medlock, & Murray, 2013).

The effects of extreme weather during infancy and early life is of particular interest due to the importance of this time period for child growth and development. Shocks and stressors during critical growth periods can have lifelong impacts (Barker, 1994). Growth faltering early in life can lead to lower human capital development (Abiona, 2017; Rosales-Rueda, 2018), cognitive development (Aguilar & Vicarelli, 2022; Ampaabeng & Tan, 2013; Dewey & Begum, 2011; Rosales-Rueda, 2018), educational attainment (Aizer, Stroud, & Buka, 2016; H. Alderman, 2006; Almond & Currie, 2011), reduced income and wealth (Maccini & Yang, 2009; Shah & Steinberg, 2017), and worse health in adulthood (Black et al., 2013; Isen, Rossin-Slater, & Walker, 2017). The first thousand days thus remains a critical window for anthropometric

attainment (Black et al., 2013), and growth faltering during this period can affect life outcomes (H. Alderman & Headey, 2018; Roth et al., 2017; Tusting et al., 2020).

The relationship between precipitation shocks and child health is well-studied. In tropical regions, rainfall quantity and variability is consistently found to be a critical factor in child growth (Cornwell & Inder, 2015; Maccini & Yang, 2009; Omiat & Shively, 2020; G. E. Shively, 2017). Positive rainfall shocks, or floods, have mixed effects on household incomes and nutrition. Seasonal flooding can improve yields and incomes for agricultural households; however, extreme flooding can inundate fields and upend infrastructure, leading to reduced yields from spoilage and impaired access. During such extremes, agricultural households may experience reduced incomes, increased food prices, and thus constrained consumption and diet diversity (Brown & Kshirsagar, 2015; Sajid & Bevis, 2021). Empirical studies link floods to worse nutrition (Cooper, Brown, Azzarri, & Meinzen-Dick, 2019; Cornwell & Inder, 2015; Le & Nguyen, 2021; Rosales-Rueda, 2018), worse health (Aguilar & Vicarelli, 2022; E. Skoufias & Vinha, 2012), lower birth weight (Chacón-Montalván et al., 2021; Grace, Davenport, Hanson, Funk, & Shukla, 2015), and cognitive impacts (Aguilar & Vicarelli, 2022; Maccini & Yang, 2009; Rosales-Rueda, 2018). Negative rainfall shocks and droughts, particularly in rainfed cereal-producing regions, are also associated with temperature- and water-stressed plants and thus reduced yields. Similar health outcomes of limited consumption and reduced diet diversity follow for agricultural households (Brown & Kshirsagar, 2015; Dillon, McGee, & Oseni, 2015; Yamano, Alderman, & Christiaensen, 2005). Drought-related conflict has also been associated with increased child stunting (Delbiso, Rodriguez-Llanes, Donneau, Speybroeck, & Guha-Sapir, 2017; Kinyoki et al., 2017). Beyond individual outcomes, Phalkey et al (2015) conclude that there is “limited comprehensive empirical evidence at the household level” for a relationship between precipitation deviation and child undernutrition (Phalkey, Aranda-Jan, Marx, Hofle, & Sauerborn, 2015).

Emergent literature on temperature shocks and child development are inconclusive. Reduced food production and lower incomes from heat-stressed crops provides an important pathway to undernutrition (Dillon et al., 2015). Etiological pathways between extreme temperatures and fetal growth include fetal oxidative stress, less effective thermoregulation and increased water demands during pregnancy (Bakhtsiyarava et al., 2022; Rocha & Soares, 2015), and maternal malnutrition and respiratory illnesses during temperature extremes (Molina & Saldarriaga, 2017). Both hot and cold extremes have been associated with lower birthweight with overall inconclusive results (Andalón, Azevedo, Rodríguez-Castelán, Sanfelice, & Valderrama-González, 2016; Baker & Anttila-Hughes, 2020; Bakhtsiyarava et al., 2022; Chersich et al., 2020; Deschenes, Greenstone, & Guryan, 2009). Evidence from cross-sectional studies indicate worse health outcomes in the short-term following extreme temperature incidence (Davenport, Dorélien, & Grace, 2020; Grace et al., 2015; Randell & Gray, 2016; E. Skoufias & Vinha, 2012; Thiede & Strube, 2020).

Thus, the growing literature on climate change and climate shocks' effects on nutrition is exceedingly diverse. Studies at this intersection derive from several disciplines including engineering, climate science, nutrition, economics, medicine, and public health. The variables used to define climate and weather extremes are equally diverse, as are the nutrition indicators and analytical methodologies to examine this relationship. Existing reviews indicate several gaps in the literature, including limited causal inference from secondary data, absent accounting of adaptation measures, and confounding across studied environmental variables (e.g. air pollution and temperature, temperature and precipitation) (Chersich et al., 2020). Analytical gaps include robust methodologies to disentangle the role of the continuous environment from shocks or deviations from historic averages, identification of appropriate timescales for measurement of precipitation shocks (Cooper et al., 2019), measurement of acute weather shocks, investigation of micronutrient deficiency outcomes, and measurement of urban and rural

food security alongside anthropometric indicators (Phalkey et al., 2015). The first step to addressing these gaps is taking stock of the plurality of environmental and nutrition indicators utilized in this burgeoning field, and documenting the specific shocks and analytical methodologies utilized in existing studies. At present there are no best practices for reconciling various spatial and temporal scales for developing tailored climate indicators for particular nutrition outcomes.

This review aims to identify common themes in how extreme weather is specifically treated in the literature on human health and nutrition. Rather than focusing on the magnitude of observed effects, which are known to be difficult to compare, we focus on described characteristics of climate hazards, the operational definition of hazards, types of data utilized to measure these hazards, and methodological approaches and their limitations. We further identify key assumptions about climate hazards made in nutrition studies, and

Targeted Literature Review

Scope of Review

A broad literature search was conducted for peer-reviewed articles using Web of Science, PubMed, Scopus, and EconLit databases. Each extreme event and its synonyms were used to develop event keywords as shown in Table 2. A query consisted of each event keyword in the title of the publication AND any of the following nutrition-related keywords in the article abstract: stunt*, wast*, weight, vitamin*, deficien*, diet*, food security, or food consumption. Further keywords were added to the title and abstract fields to limit the scope of the study to those conducted at the child or household level (AND [child* OR household*]), and those that specifically addressed nutrition or health outcomes (AND nutrition OR health).

Table 2 Event Keywords

Flood	***Landslide***	***Storm***	***Temperature***	***Drought/Fire***	***Other Hazards***

Flood*	Landslide*	Storm*	Temperature*	Drought*	Shock*
Inundate*	Mudslide*	Typhoon*	Heat*	Fire*	Disaster*
Rainfall	Rockslide*	Hurricane*	Cold*	Wildfire*	Catastroph*
Precipitation	Rockfall	Cyclone*	Frost*	Forest Fire	
			Freez*		

This approach has several distinctions compared to existing reviews on the subject of climate and undernutrition. Compared to Brown et al 2020 and Belesova et al 2019, we employ narrower search queries on a range of specific environmental extremes and hazards rather than continuous environmental factors. Although papers on the continuous environment are included in this analysis, the underlying search query is different. We further focus on studies at the child- and household-level rather than country- and regional studies. This criteria effectively excludes several simulation studies on crop yield and downstream food security outcomes due to differences in model assumptions and lack of comparability. In contrast to Brown et al 2020 and Phalkey et al 2015, we include nutrition outcomes related to physiological malnutrition including vitamin and mineral deficiencies per Belesova et al 2019, as well as diet diversity, food security, and food consumption. Finally, in a critical augmentation to all existing reviews, we characterize the spatial and temporal extent and resolution of each study to enable future comparisons on similar topics.

Screening Process

The initial search yielded a total of 992 unique entrie. Of these, 990 (99% of original) English language publications were retained. Subsequently we excluded surveys, interviews, editorials, guidelines, protocols, editorials (including letters, notes, and comments), event-specific outputs (documents from congresses, conferences, or proceedings), and any retracted publications or errata. This criteria yielded 788 original publications (79% of original).

At first stage, title and abstracts of all 788 publications were screened to identify whether each study addressed climate-impacted nutrition outcomes in humans. 361 studies (46%) were

excluded for relevance. Next, articles on related topics which do not directly address nutrition or food consumption, e.g. income and yield impacts, were excluded (n=26) Additionally, investigations around knowledge, attitudes, and practices around diets and nutrition were excluded unless quantitative measures of nutrition were also investigated (n=73). Publications on non-environmental hazards, e.g. Covid-19, catastrophic health expenditures, and earthquakes, were also excluded (n=70). Finally, studies utilizing only primary data, such as self-reported shocks, were excluded due to limited comparability across regions (n = 20). At the end of first stage, 530 publications (53%) were classified for exclusion. Excluded publications generally belonged to food technology, hydrology, energy, medicine, and agricultural economics disciplines. Included publications (n = 238, 30%) generally consisted of articles in nutrition, economics, and public health disciplines. Of these, 10 were reviews which were excluded from the main analysis but retained as supporting studies for cross-referencing of included publications. 6 publications could not be reviewed due to missing abstracts or insufficient evidence for an inclusion decision.

Several characteristics were gathered from each included study to inform this review. A complete list of identified characteristics is presented in Table 3.

Table 3 Data Extraction Sheet Fields

Category	***Field Name***	***Operational Definition***	***Options (if any)***
Spatial Extent	Country of study	Country or countries where study was conducted	Any
	Location of study	Names of study sites or geographic regions included in study	Any
	Spatial Resolution	Administrative level classification of study unit according to Geonames	ADM1 – ADM5
Temporal Extent	Study Period	Study period as defined by authors	
	Time of Data Collection	Time when survey was administered	Month, Year
	Recall Period of Survey	Recall period of survey if applicable	*n* days, *n* weeks, *n* months, long-term
Study Summary	Outcome Category	Type of undernutrition addressed in study (Belesova et al., 2019)	Acute, Chronic, Mixed, Micronutrient Deficiency

	Outcome Measure(s)		WHZ, MUAC, GAM, HAZ, WAZ, Blood measure, Diet Score
	Independent Variables	Categories of independent variables addressed (Phalkey et al., 2015)	Environment, Agriculture, Crop, Livelihoods, Socioeconomics, Demography, Diet, Morbidity
	Methodology	Categories of how the relationship between variables is assessed	Group comparisons, Association, Advanced Association, Causal (Observational), Causal (Experimental), Prediction
Hazard Characteristics	Hazard	Specific hazard or shock studied	Flood, Landslide, Drought, Temperature Extremes, Storm
	Hazard Measure	Measure used to characterize hazard/shock	Any

Findings

Summary of Studies

Descriptive statistics from the 238 publications included in this review are presented in the sections below. As seen in Figure 1, the number of relevant publications has notably increased since 2014, with a parallel increase in the types of weather phenomena being studied. Floods (79 studies, 33%) and droughts (62 studies, 26%) are the most frequent extreme events studied. Continuous measures of temperature, including hot and cold extremes comprise 44 studies or 18% of the sample. 16 studies (7%) were found involving storms or tropical cyclones, and only four studies were found addressing landslides and their impacts on nutrition.

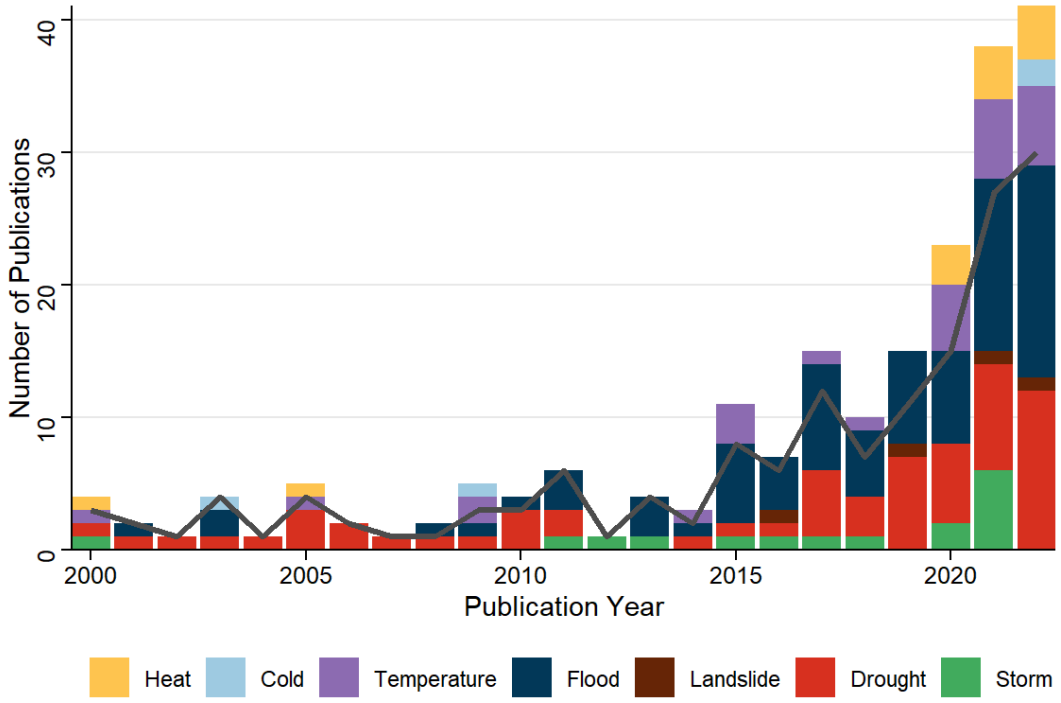

Figure 1 Counts of reviewed publications by year and weather phenomena studied. Grey line indicates total number of publications. Studies investigating multiple phenomena (e.g. heat and cold) are included multiple times in underlying bar graph.

Nutrition Outcomes

Figure 2 presents the variety of nutrition indicators studied across reviewed articles. Anthropometric indicators are most frequent outcome measure, utilized in 42% of reviewed publications. Among these indicators, a small difference is observed between frequency of Height-for-Age Z score (HAZ) and Weight-for-Height Z Score (WHZ), indicating comparable research interest in both chronic undernutrition (stunting) and acute undernutrition (wasting). Consumption-based indicators and birth outcomes are the next most frequent indicator category, appearing in 10% and 4% of studies respectively. Indexed and self-reported measures of diet diversity and food security are the rarest in our analysis, comprising less than 6% of reviewed publications.

As in Figure 1, floods and droughts are the most well-studied extreme weather phenomena and comprise the greatest diversity (over 18) of associated nutrition indicators. Majority of these

studies utilized anthropometric indices or binary assessments of stunted or wasted status (n=25). Studies of temperature impacts on nutrition utilized 11 unique nutrition indicators, with four studies investigating birth outcomes. A particular research focus on temperature influences on birth outcomes is therefore observed in the literature. Studies of storm impacts on nutrition utilized 7 unique nutrition indicators mostly related to anthropometry.

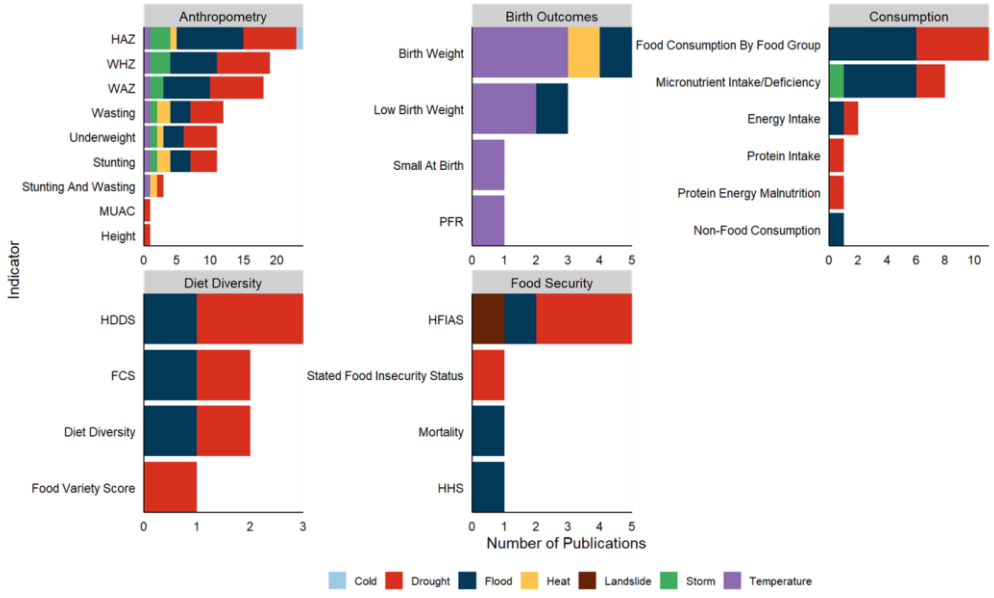

Figure 2 Counts of publications by nutrition indicator and extreme weather phenomenon studied

Climate Indicators

Figure 3 presents the variety of environmental measures utilized in reviewed publications. Deviation or anomaly measures, e.g. standard deviation from historic average precipitation, is the most frequently used climate indicator. Positive and negative rainfall anomalies from varied reference periods are often used to study household impacts of floods and droughts. Recent multi-county studies (n = 25) favor precipitation indices such as the Standardized Precipitation Index (SPI) and the Standardized Precipitation and Evapotranspiration Index (SPEI) as a more reliable measure of flood and drought across geographies. Three studies were found to utilize both continuous SPEI and thresholded SPEI values to create different categories of severity (Dimitrova, 2021; Freudenreich, Aladysheva, & Brück, 2022; Rustad, Rosvold, & Buhaug,

2019). Threshold-based indicators are also frequently utilized in temperature studies to operationalize increasing severity of heat stress (Isen et al., 2017; Tusting et al., 2020). Averages and Z-scores are similarly common; however, few studies utilize percentile-based climate indicators, perhaps due to the higher data demands of this measure (Block, Haile, You, & Headey, 2021). Finally, there is a large degree of overlap between Self-Report and Known Event measures, as the surveys that seek to identify whether households experienced a shock or not are targeted to particular regions and time frames.

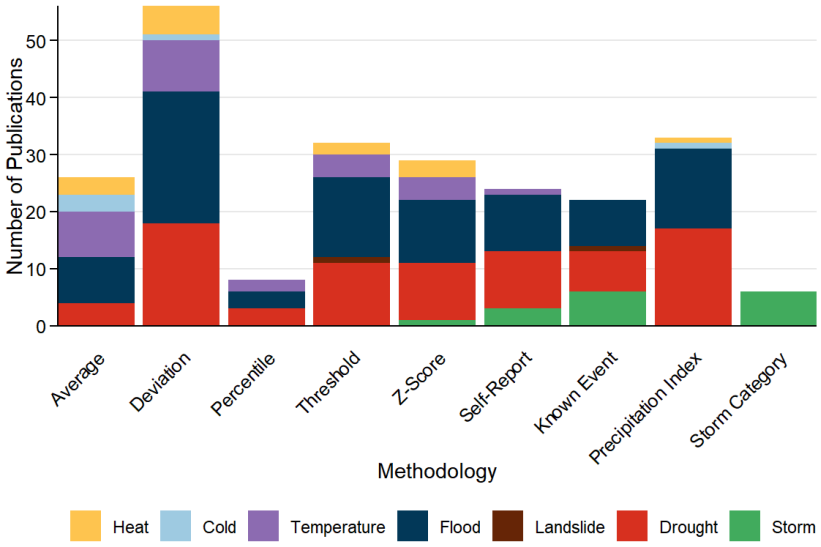

Figure 3 Counts of publications by type of climate indicator utilized and extreme weather phenomenon studied. Note: studies utilizing multiple indicators for one or more variables are included as multiple entries

Analytical Methods

Figure 4 presents the reviewed publications by the analytical methodologies utilized. Advanced association in the form of OLS or linear regression is the most frequently observed analytical methodology in this review. Advanced econometric techniques to establish causality are less frequently observed, but often utilized for investigations of welfare schemes and market interventions through cohort studies or randomized controlled trials. Compared to other methods, causal investigations using observational data are often used to study responses to floods and droughts. Predictive studies are least frequent in this review, with a total of five

studies attempting to predict consumption responses to simulated temperature and drought conditions from future climate scenarios. Simpler methods such as comparisons and correlations of outcomes between communities that were exposed and not exposed to the same extreme weather event, are much more commonly observed. These techniques were most frequently used in small-scale studies investigating localized impacts.

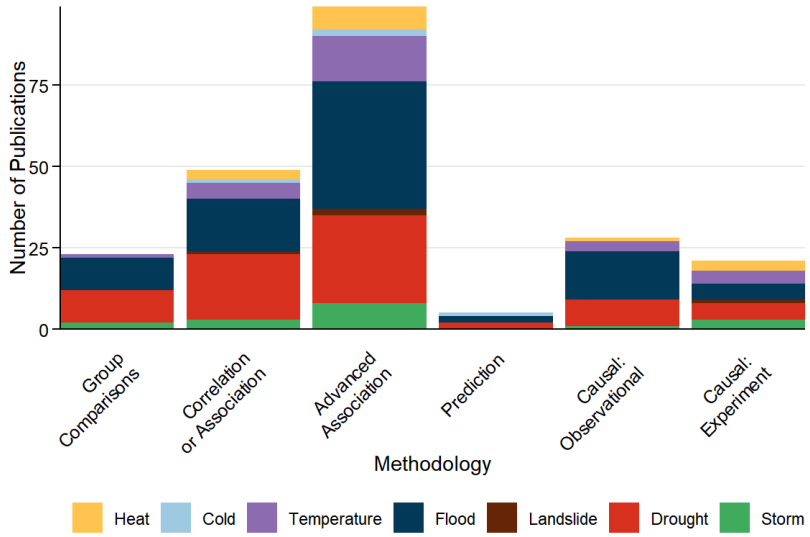

Figure 4 Counts of publications by type of methodology utilized and extreme weather phenomenon studied

Geographical Distribution of Studies

This review includes studies conducted in 51 countries, most of them in the global south. India (n=19), Bangladesh (n=14), and Ethiopia (n=14) are the most well-represented countries in this review. Among these countries, droughts (25 studies) and floods (20 studies) are the most frequently studied extreme weather events, and anthropometric outcomes are the best studied (n=35).

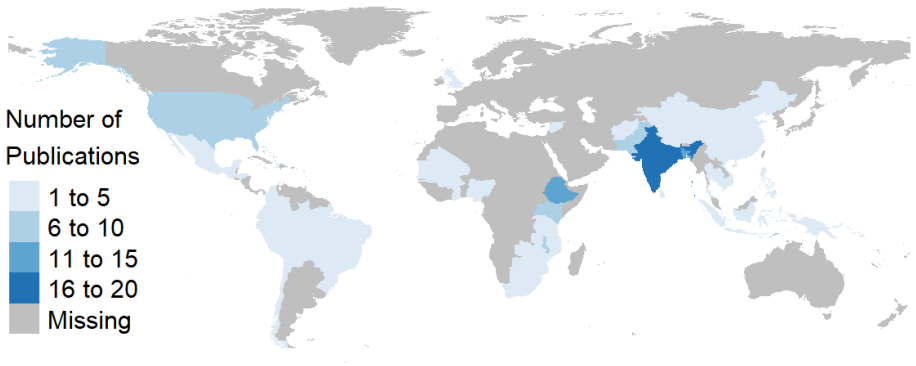

Figure 5 Counts of publications by study location. Note: Multi-country studies are not included in this map.

Main Assumptions

Reviewed studies set forth several methodological assumptions as the basis of their estimation strategies. Most studies of secondary data assume that weather shocks are exogenous to nutrition or health outcomes. This assumption directly affects the production, consumption, and infectious disease pathways to malnutrition discussed above. Several studies rely on this exogeneity assumption to derive individual climatological histories to match maternal and child anthropometries, birthweight, and mortality outcomes. When the exogenous variation in weather is used as an instrument, it is often tested through comparisons across exposed/unexposed subgroups (Aguilar & Vicarelli, 2022; Dillon et al., 2015) and birth clustering (Isen et al., 2017).

Most studies also assume limited exposure misclassification, or that respondents' location and survey timing can accurately represent individual exposure to a range of climate variables. This assumption is important as individual measures of climate adaptation strategies and mobility are often absent in multi-country, cross-sectional studies. USAID Demographic and Health Surveys, for example, ask respondents about the administrative region of prior residence if applicable. In the absence of this information, researchers must assume that individuals have limited movement ranges from survey locations. In the absence of detailed individual information about adaptation strategies to weather extremes, researchers frequently use household characteristics (roof material, floor material, access to piped water, access to electricity) and

wealth indices to proxy for how effectively households may be able to physically and physiologically protect themselves from weather extremes.

Several population-level assumptions are identified. For secondary studies studying in-utero outcomes, all pregnancies are assumed to last nine months due to missing data on actual pregnancy duration. Area-specific trends such as localized disease outbreaks or incidence of violence are also often not observed and these factors may affect observed effect sizes beyond month- and region-level fixed effects.

Conclusions

The targeted review provides a summary of the variety of indicators commonly used for both independent and dependent variables in comparable nutrition analyses. Anthropometry and standard deviations of environmental variables are most common in the literature. As noted in several reviews, temperature extremes, floods, and droughts are best represented across studies. Regression methods are often utilized to establish association between environment and health outcomes; however, specifications aimed at disentangling causality are rare, particularly across multi-country studies.

Chapter 3: Techniques and Workflows for Spatial and Temporal Alignment

Introduction

This dissertation develops and applies several methodologies across the remaining chapters, specifically multiple harmonic regression, fuzzy matching of survey administrative regions to spatial boundaries, and extraction of weather extremes. An overview of these techniques is provided here for brevity and referenced throughout the remainder of the document. Firstly, we investigate multiple harmonic regression, which extends established delta methods from single-peak harmonic regressions to a more flexible approach which accounts for multiple peaks. We then present fuzzy string matching, which allows us to match spatial boundaries to survey regions retroactively based on similarities in fields describing the spatial extent of survey. This technique allows us to investigate seasonal wasting from the SMART and MICS datasets in Chapter 5: Acute Malnutrition Seasonality in Cross-Sectional Data, and include valuable famine early warning data from the Cadre Harmonisee system in Chapter 6: Probabilistic Applications for Famine Early Warning Systems. Finally, the choice of datasets and metrics utilized to study extreme weather is discussed in Technique 3: Extraction of Weather Extremes from Gridded Data. We investigate three cities with very different climatologies: Dhaka, Bangladesh; Mexico City, Mexico; and N'Djamena, Chad. This investigation allows us to uncover critical differences across metrics, and motivates the choice of extreme weather indicators utilized in the remainder of this dissertation.

Technique 1: Multiple Harmonic Regression

Harmonic regression is a methodology for analysis of seasonal patterns that utilizes continuous temporal variables to build a seasonal curve. This approach is particularly useful for modeling cyclical processes such as precipitation or disease without discretizing or aggregating temporal

variables (Lofgren, Fefferman, Doshi, & Naumova, 2007; Elena N. Naumova & MacNeill, 2007a; Ramanathan et al., 2020). Simple sine and cosine functions are utilized to decompose the temporal variable into continuous time at reasonable frequencies of days, months, or years. One key advantage of harmonic regression is the ability to extract features of the seasonal curve, such as peak timing and maximum expected value, as well as confidence intervals around each estimate. These metrics are particularly valuable in epidemiology for the estimation of seasonal disease burdens of infectious diseases (Bhaskaran, Gasparrini, Hajat, Smeeth, & Armstrong, 2013; Cameron & Trivedi, 2013; Lofgren et al., 2007) and foodborne illnesses (Simpson, Zhou, & Naumova, 2020). Harmonic regression has also been used to study seasonality in retail food prices (Yan Bai, Naumova, & Masters, 2020).

Canonical harmonic regression utilizes one pair of sine and cosine terms to describe cyclical time. This formulation is the basis of the δ-method used to extract seasonal characteristics including peak timing and maximum expected values. (T. M. Alarcon Falconi, Cruz, & Naumova, 2018; E. N. Naumova et al., 2007; Elena N. Naumova & MacNeill, 2007b; Ramanathan et al., 2020; Simpson et al., 2020). One sine and one cosine term in the harmonic regression are sufficient to calculate seasonal characteristics in cases where there is one and only one peak during the cycle, as shown in Panel A in Figure 6. However, in cases where multiple peaks may be possible, such as Panels B and C in Figure 6, the canonical formula is no longer sufficient to fully describe the seasonal curve. Inclusion of a second pair of sine and cosine terms at double the cycle frequency is required to allow for the possibility of a second peak in the cycle (Tania M. Alarcon Falconi, Estrella, Sempértegui, & Naumova, 2020; Elena N. Naumova & MacNeill, 2007a; Ramanathan et al., 2020). The first harmonic pair thus includes only 2π terms, and the second harmonic pair includes 4π terms. This complete formulation of multiple harmonic regression is shown in Equation 1, where outcome *O* is observed at continuous time *t,* recorded as a continuous sequence of days or months in the study period. Assuming an annual cycle, ω

refers to a constant cycle duration of 12 months or 365.25 days which constitutes the calendar year. *T(t)* is a cubic polynomial of to accommodate nonlinear fluctuations and long-term trends.

$$0 = \beta_0 + \beta_1 \sin(2\pi\omega t) + \beta_2 \cos(2\pi\omega t) + \beta_3 \sin(4\pi\omega t) + \beta_4 \sin(4\pi\omega t) + \beta_5 T(t) \quad 1$$

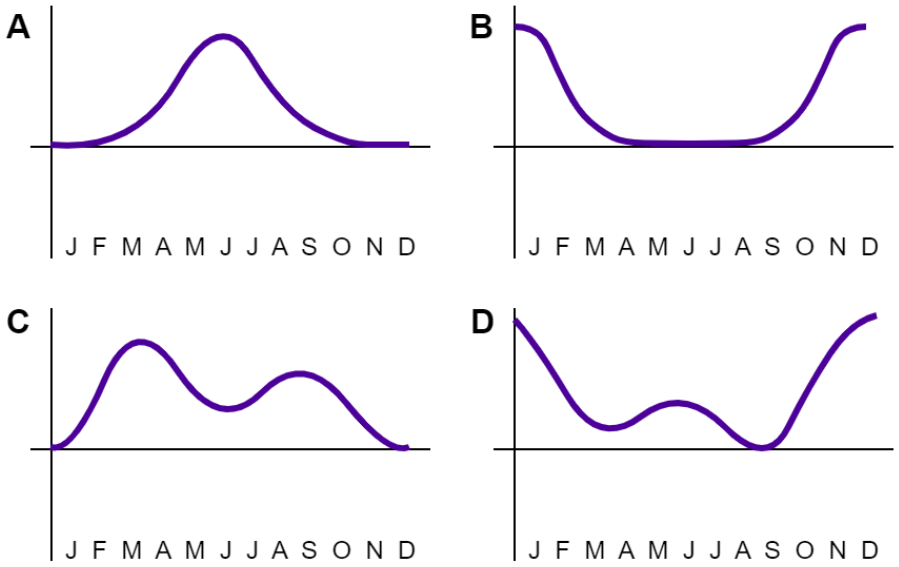

Figure 6 Example seasonal curves during a calendar year. Panel A describes a canonical (unimodal) formulation with one clear peak during the middle of the calendar year; Panel B describes a similar unimodal curve with a peak towards the end of the calendar year. Panel C presents a seasonal curve with two distinct peaks during the calendar year, and Panel D presents a seasonal curve where the main peak is towards the end of the calendar year and the smaller peak (shoulder) is in the middle of the calendar year.

Compared to canonical harmonic regression, multiple harmonic regression includes a few modifications to extract comparable measures of peak timing, peak values, amplitudes, and confidence intervals of each measure. The mathematical and vernacular definitions of each feature in both the single harmonic (unimodal) and the multiple harmonic (bimodal) formulation is presented in Table 4.

The main difference between traditional and multiple harmonic methods is that features of the multiple harmonic curve are calculated arithmetically using the second and third derivatives of the predicted harmonic curve to empirically identify global and local maxima (peaks) and minima (nadirs). Confidence intervals for each measure are derived from 999 simulations from two possible scenarios:

i. if more than 300 data points are available, each simulation randomly drops up to 50% of the dataset to calculate seasonal characteristics

ii. if fewer than 300 data points are available, an ARIMA model is fitted to the original time series and simulated using fitted features. If the cross-correlation function between the simulated time series and the original time series at Lag 0 is statistically significant at the 95% level, then seasonal characteristics are calculated from the simulated time series. Seasonal characteristics are derived by averaging measures from the 999 simulated time series.

To accommodate the possibility that either the unimodal, bimodal, or neither formulation best fits the dataset in question, a logical sequence is utilized. Both unimodal and bimodal regressions are first calculated and coefficient estimates and standard errors are extracted. If either of the second harmonic terms (β_3 and β_4) are statistically significant at the 95% level, the bimodal formulation is used to calculate seasonal features. If neither of the second harmonic terms is significant, the first harmonic terms from the unimodal formulation are examined for statistical significance (β_1 and β_2). If either of these terms are found to be statistically significant, the unimodal formulation is used to calculate seasonal features. If none of the harmonic terms are found to be statistically significant at the 95% level in either regression, then we assume that no statistically significant seasonal pattern can be deduced from the data and do not proceed further.

Several sensitivity analyses can be performed to validate the seasonal features. One extension can be a comparison of different seasonal frequencies (e.g. months vs. days) if these data are available. The effect of temporal aggregation has been explored before, and concurrent results from data with low and high temporal resolution can help confirm observed characteristics (Tania M. Alarcon Falconi et al., 2020). For highly seasonal outcomes with environmental linkages, e.g. waterborne disease incidence and precipitation, comparing seasonal curves of

related phenomena can further elucidate leading or lagging effects and potential differences in amplitudes during key periods such as monsoons.

Table 4 Estimation of Seasonal Characteristics from Harmonic Regression

Characteristic	**Unimodal (2π)**		**Bimodal (4π)**
	Gaussian Linear Model	*Log-Linear Model*	*Gaussian Linear or Log-Linear*
Regression Model	$Y_t = \beta_0 + \beta_1 \sin(2\pi\omega t) + \beta_2 \cos(2\pi\omega t) + \beta_3 T(t)$	$\ln(E[Y_t]) = \beta_0 + \beta_1 \sin(2\pi\omega t) + \beta_2 \cos(2\pi\omega t) + \beta_3 T(t)$	$Y_t \text{ or } \ln(E[Y_t]) = \beta_0 + \beta_1 \sin(2\pi\omega t) + \beta_2 \cos(2\pi\omega t) + \beta_3 \sin(2\pi\omega t) + \beta_4 \cos(2\pi\omega t) + \beta_5 T(t)$
Amplitude (γ)	$\gamma = \sqrt{{\beta_1}^2 + {\beta_2}^2}$	$\gamma = e^{\sqrt{{\beta_1}^2 + {\beta_2}^2}}$	$A = P_G - N_G$
95% Confidence Interval of Amplitude $(CI(\gamma))$	$Var(\gamma) = \frac{{\beta_1}^2{\sigma_1}^2 + {\beta_2}^2{\sigma_2}^2 + 2\sigma_{\beta_1\beta_2}\beta_1\beta_2}{{\beta_1}^2 + {\beta_2}^2}$ $CI(\gamma) = \gamma \pm 1.96\sqrt{Var(\gamma)}$	$Var(\gamma) = \gamma^2\left(\frac{{\beta_1}^2{\sigma_1}^2 + {\beta_2}^2{\sigma_2}^2 + 2\sigma_{\beta_1\beta_2}\beta_1\beta_2}{{\beta_1}^2 + {\beta_2}^2}\right)$ $CI(\gamma) = \gamma \pm 1.96\sqrt{Var(\gamma)}$	Estimated arithmetically from 999 simulations which randomly drop up to 50% of dataset $CI(\hat{\gamma}) = \sum_{n=1}^{n=999} P_G - N_G$
Peak (P)	$P = \beta_0 + \gamma$	$P = e^{\beta_0} + \gamma$	Estimated arithmetically from first, second, and third differences of the predicted seasonal curve. P_L = local maximum where C' = 0 and C'' < 0 P_G = global maximum, largest value of all P_Ls
Nadir (P)	$N = \beta_0 - \gamma$	$N = e^{\beta_0} - \gamma$	Estimated arithmetically from first, second, and third differences of the predicted seasonal curve. N_L = local minimum where C' = 0 and C'' > 0 N_G = global minimum, smallest value of all N_Ls
Peak Timing (P_T)	Phase shift $\Theta = \arctan\left(\frac{\beta_1}{\beta_2}\right)$ If $\beta_1 > 0$ and $\beta_2 > 0$, $P_T = (\Theta)\frac{M}{2\pi}$ If $\beta_2 < 0$, $P_T = (\Theta + \pi)\frac{M}{2\pi}$ If $\beta_1 < 0$ and $\beta_2 > 0$, $P_T = (\Theta + 2\pi)\frac{M}{2\pi}$		Estimated arithmetically from first, second, and third differences of the predicted seasonal curve. $P_{T,L}$ = Timing of P_L, $P_{T,G}$ = Timing of P_G

95% Confidence Interval of Peak Timing ($CI(\Theta)$)	$Var(\Theta) = \frac{{\beta_1}^2{\sigma_2}^2 + {\beta_2}^2{\sigma_1}^2 - 2\sigma_{\beta_1\beta_2}\beta_1\beta_2}{({\beta_1}^2 + {\beta_2}^2)^2}$ $CI(\Theta) = \Theta \pm 1.96\sqrt{Var(\Theta)}$		Estimated arithmetically from 999 simulations which randomly drop up to 50% of dataset $CI(\widehat{P_T}) = \sum_{n=1}^{n=999} P_{T,G}$
Characteristic	**Unimodal (2π)**		**Bimodal (4π)**
	Gaussian Linear Model	*Log-Linear Model*	*Gaussian Linear or Log-Linear*
Absolute Intensity (I_A)	$I_A = (\beta_0 + \gamma) - (\beta_0 - \gamma)$	$I_A = (e^{\beta_0} + \gamma) - (e^{\beta_0} - \gamma)$	Estimated arithmetically from first, second, and third differences of the predicted seasonal curve. $N_{T,L}$ = Timing of N_L, $N_{T,G}$ = Timing of N_G
Confidence Interval of Absolute Intensity ($CI(I_A)$)	$Var(I_A) = 4\,Var(\gamma)$ $CI(I_A) = I_A \pm 1.96\sqrt{Var(I_A)}$		Estimated arithmetically from 999 simulations which randomly drop up to 50% of dataset
Relative Intensity (I_R)	$I_R = \frac{\mathrm{P}}{N}$		$I_R = \frac{P_G}{N_G} + \frac{P_L}{N_L}$
Confidence Interval of Relative Intensity ($CI(I_R)$)	$Var(I_R) = \frac{{\beta_0}^2}{(\beta_0 - \gamma)^4}\,Var(I_A)$ $CI(I_R) = I_R \pm 1.96\sqrt{Var(I_R)}$	$Var(I_R) = \frac{e^{2\beta_0}}{(e^{\beta_0} - \gamma)^4}\,Var(I_A)$ $CI(I_R) = I_R \pm 1.96\sqrt{Var(I_R)}$	
Seasonal Intensity (I_S)	$I_S = e^{2A-1}$		$I_S = e^{2A-1}$

Technique 2: Matching Surveys to Spatial Boundaries with Fuzzy Matching

Most large surveys collect information describing the spatial location of the surveyed population. The collected location fields may have variable spatial resolution, but generally classify the surveyed region into increasingly smaller administrative units or geographic boundaries (e.g. country, region, state, county, etc.). If the survey extent covers a large area and includes variable population densities, the survey may also include information about whether the surveyed area was urban, sub-urban, or rural. Once standardized, these fields can be utilized to match the survey location to a representative digital spatial feature. This feature can facilitate further spatial analysis by allowing for matching survey outcomes to other environmental, demographic, or socioeconomic characteristics. The preliminary task of matching a survey location to a spatial feature is easily accomplished when the spatial extent of the survey is limited to the country (first-order administrative level) or subnational (second-order administrative level) scale. However, for large cross-sectional surveys spanning multiple countries with different spatial data collected in each survey, we outline a workflow to facilitate this matching.

We first begin by collecting and standardizing fields containing location information. If surveys are implemented in multiple languages, this requires combing through survey metadata and codebooks to compile a glossary of all relevant place-names, administrative level names, and urbanicity fields. Words with special characters and accents may also require cleaning and/or duplication to ensure that words can be matched across different encodings. The result of this step is a large vector of location words that can be compared against survey codebooks to extract survey fields containing location information.

Once location fields are identified, they can be extracted from the survey and concatenated together to create one string that describes each unique survey location. This step may require removing duplicated location fields, removal of descriptive words (e.g. district, division, province,

etc.) from place-names, and validation to ensure that all relevant fields are included in the final string.

Text matching requires a spatial reference, or a database to compare the survey location against to extract a likely match. To create this reference database, we create a list of place names compiled from the FAO Global Administrative Unit Layers (GAUL) dataset (FAO, 2015), Global Administrative Boundary Database (GADM) (Global Administrative Areas (GADM), 2012), and the United States Agency for International Development (USAID) Demographic and Health Survey (DHS) Spatial Data Repository (ICF, 2019). These three datasets combined include the majority of enumerated subnational administrative boundaries around the world. Combining these databases ensures that countries which may not be represented in one dataset are included in another (e.g. China's administrative boundaries is missing in DHS, but is available in GADM). Redundancies across datasets also allow for matching varied spellings. The inclusion of DHS shapefiles further allow for common geographic aggregations (e.g. North, East) used for survey purposes in many countries which might be absent in official subnational listings of the GAUL and GADM datasets. Location information at each administrative level is subsequently concatenated such that administrative levels with increasingly higher resolution can potentially be matched. An example of this process is shown in Figure 7. The feature ID from the original shapefile is also retained so that the source feature can be identified after matching.

With the target and reference strings compiled, fuzzy string matching can be implemented to compare strings. The goal of this process is to identify the most plausible reference string that matches the level of detail provided in the target string of concatenated location names. String similarity is assessed using a variety of metrics as follows:

- *The Levenshtein distance*: computes the number of character changes required to make the target string similar to each possible reference string;

- A series of ratios calculate the similarity between each pair of target and reference strings, scaled to a range of [0, 100]:
    - *Partial Ratio Score*: calculates similarity (i.e. number of common characters) between the target string and each word in each reference string, returning the maximum;
    - *Partial Token Sort Ratio*: calculates similarity by first splitting strings into tokens and sorting them, and then calculating the partial ratio score;
    - *Partial Token Set Ratio*: same as the Partial Token Sort Ratio after removing duplicate words;
    - *Overlap coefficient or Jaccard measure*: calculated as the number of overlapping characters between the target and reference strings divided by the smaller of the sets

The above measures are calculated for each word comprising the target string. In other words, following the example illustrated in Figure 7, string match metrics are calculated five times: first individually for “Pakistan”, “Dera Ghazi Khan”, and “Muzaffargarh”; and then for their sequential combinations: “Pakistan – Dera Ghazi Khan” and “Pakistan – Dera Ghazi Khan – Muzaffargarh”. This ensures that all possible matches from reference strings are considered, especially when a particular administrative level or location word is missing from the target string. In this example, the state-level descriptor of Punjab is missing from the target string; however, because fuzzy string matching is implemented on multiple levels, we can be confident that reference strings including this information will not be penalized for this exclusion. Calculated scores for each reference string is then averaged, and the string matched to the highest score is retained. If multiple matches are found, the longest reference string providing the most detailed administrative boundary is retained. If multiple matches are found using this criteria, the following logic is used to prioritize datasets: GADM > DHS > GAUL.

The result of fuzzy string matching is that the target string is matched to the best available reference string. After this step, the ID of the spatial feature corresponding to the matched reference string is referenced. This final step matches the target string with its corresponding spatial feature.

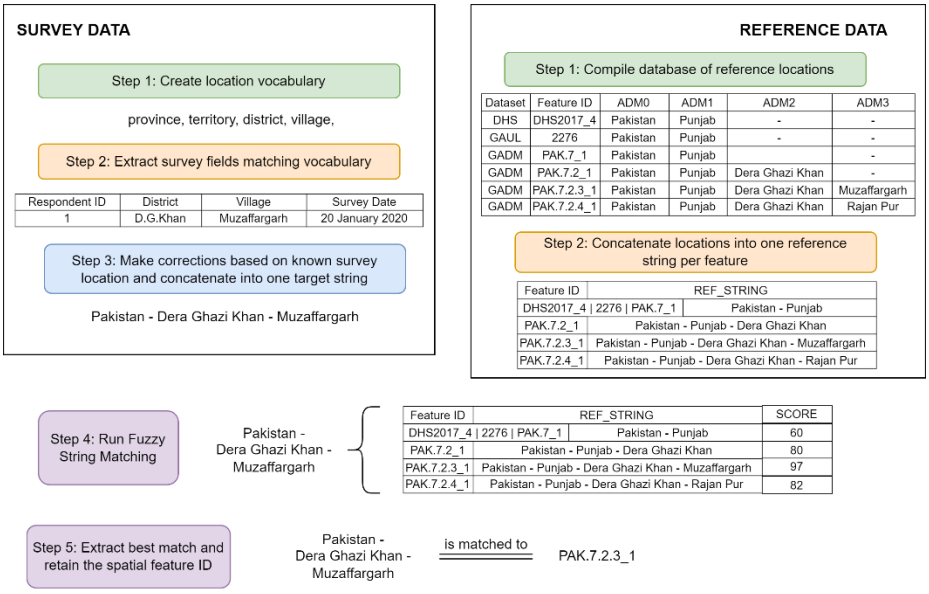

Figure 7 Example process of fuzzy string matching

Technique 3: Extraction of Weather Extremes from Gridded Data

Storms

Data on tropical cyclones and storms were extracted from the International Best Track Archive for Climate Stewardship (IBTrACS) storm track database (Knapp, Kruk, Levinson, Diamond, & Neumann, 2010). This dataset provides the storm path, or track, as vector information compiled from GPS point locations of the center of the tropical cyclone. Point locations are most often collected at 6-hour intervals.

Defining a radius for each storm is the most relevant challenge for this analysis. The chosen radius will serve as our measure of storm-impacted area and thus influence downstream results. Multiple definitions of this radius are provided in the IBTrACS dataset as described in Table 5. These fields record information from several international agencies and serve as a compilation

of various datasets tracking storm characteristics. While exploring the IBTrACS dataset, it was noted that the radius of maximum mean winds (RMW) field from US reporting agencies was not reanalyzed and therefore data in this field were not reliable (Knapp et al., 2010). The cyclone eye further describes a region of relatively less intense activity in the storm path surrounded by a much more active weather system (Moran, 2012). Measuring only the eye can thus miss areas that are much more severely affected. Therefore, the most useful fields to study human-scale storm impacts are the fields which describe the extent of gale-force, storm-force, and hurricane-force winds.

Table 5 Fields describing various storm radii from the IBTRaCS dataset

Field Endings	***Field Definition***
_RMW	Mean radius from the system centre of maximum mean winds, 0 - 999 n mi.
_R34	Mean radius from the system centre of winds at gale-force (17m/s) or above
_R50	Mean radius from the system centre of winds at storm-force (25m/s) or above
_R64	Mean radius from the system centre of winds at hurricane-force (33m/s) or above
_EYE	Mean radius of the cyclone eye

The next step of this exploration is visualizing the radii for each wind speed category. Each of the R34, R50, and R64 fields provide the radius in four directional quadrants from the center of the storm system. First, the distribution of these radii were visualized to identify if there are any outlier observations. This step is particularly important as outlier radii will translate to implausibly large spatial extents of storms, and lead to downstream issues in generated shapefiles due to the global extent of the dataset. 119 observations were found with radii above 1000 nautical miles, a plausible limit based on the distribution of radii in the data as shown in Figure 8. With these observations removed, the average radius of each windspeed extent across directional quadrants was calculated for each of the three windspeeds for each available time point, and converted to distance in meters. The unprojected line dataset was then projected to the World Equidistant Conic projected coordinate system. This coordinate system was chosen to preserve

the distance property for the global dataset and to avoid an origin point near populated areas along the equator and the prime meridian.

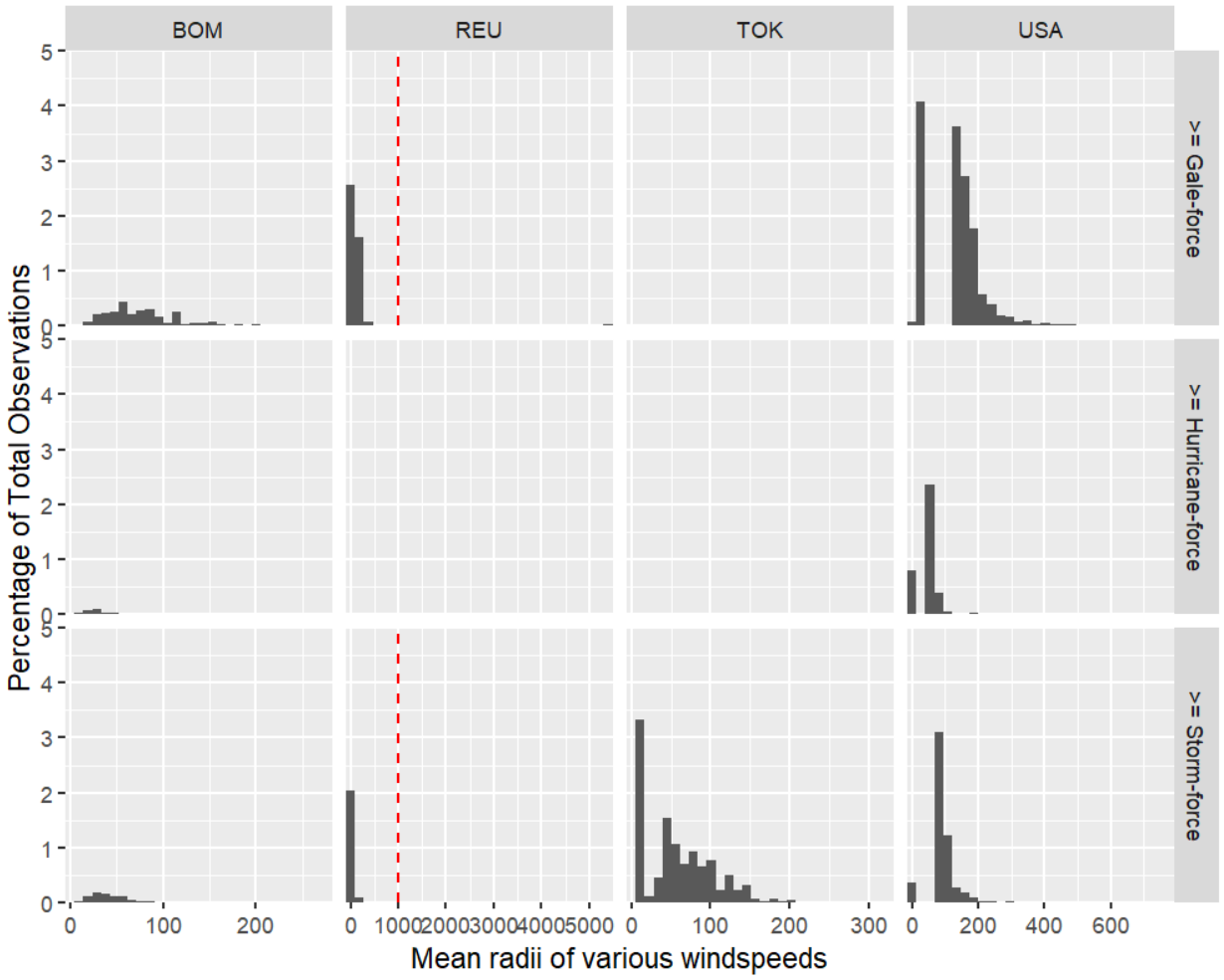

Figure 8 Distribution of the mean radii of gale-force, storm-force, and hurricane-force winds by World Meteorological Organization reporting agencies in the IBTrACS dataset. BOM refers to Australian Tropical Cyclone Warning Centres, REU refers to Regional Specialized Meteorological Center (RSMC) La Reunion, TOK refers to RSMC Tokyo, and USA refers to the National Oceanic and Atmospheric Administration National Hurricane Center. Due to outliers in the Reunion dataset, radii above 1000 nautical miles were ignored.

To visualize a range of storms, a subset of the IBTrACS dataset was created by selecting storm tracks with data available for all three windspeed thresholds—in effect a subset of quite severe storms. Five storm IDs were randomly selected from each of the North Atlantic, North Indian, Southern Pacific, and Eastern North Pacific basins. Storms which achieved landfall in populated places were then selected for visualization, and resulting maps of tropical cyclones Matthew

(2016), Durian (2006), and Fani (2019) are shown in Figure 9. The continental area affected by each of the three radii is shown in Figure 10.

Based on Figure 9 and Figure 10, the land area affected by the most severe hurricane-force winds is much smaller than the extent of gale-force winds. Gale-force winds are not as intense as storm and hurricane-force winds, and we can assume that individuals living in areas prone to storms have a baseline extent of coping measures for periods of high winds and storm surges accompanying gales. Focusing instead on the extent of storm-force and higher winds can mean a more focused damage extent, and therefore sharpened effect estimates. The storm-force wind definition further approximates when the storm reaches Category 3 or higher on the Saffir-Sampson scale, corresponding to wind speeds of at least 178 km/h or 49 m/s or 96 knots (Bell et al., 2000). These major hurricanes have comparatively higher damage potential and pose a greater threat to human lives.

Figure 10 points to several potential analytical caveats. South America and Europe do not experience as many storms as the other continents, as indicated by the lower land area affected by these events. Asia, North America, and Oceania are much better represented, and Africa indicates moderate land area covered by storms. Increasing the windspeed threshold also significant lowers the land area covered by each phenomenon, which may present sample size issues due to low co-occurrence of both extreme event and outcomes of interest. In the temporal domain, storm seasons are concentrated variably across the continents; most storms in Africa occur during November – May, whereas storms in Asia and Oceania have much more year-round coverage. These limitations may affect the observed results.

Based on this exploration, we decide to use the average radius of storm-force winds (25 m/s) or higher to define the damage extent of a storm in the IBTRaCS dataset. A point or polygon was classified as having experienced a storm or tropical cyclone in a month if the spatial intersection of the polygon with the storm-force radius extent during the target month yielded a non-empty

shapefile. The sum of impacted area during each month was also utilized as a proxy indicator of storm activity magnitude.

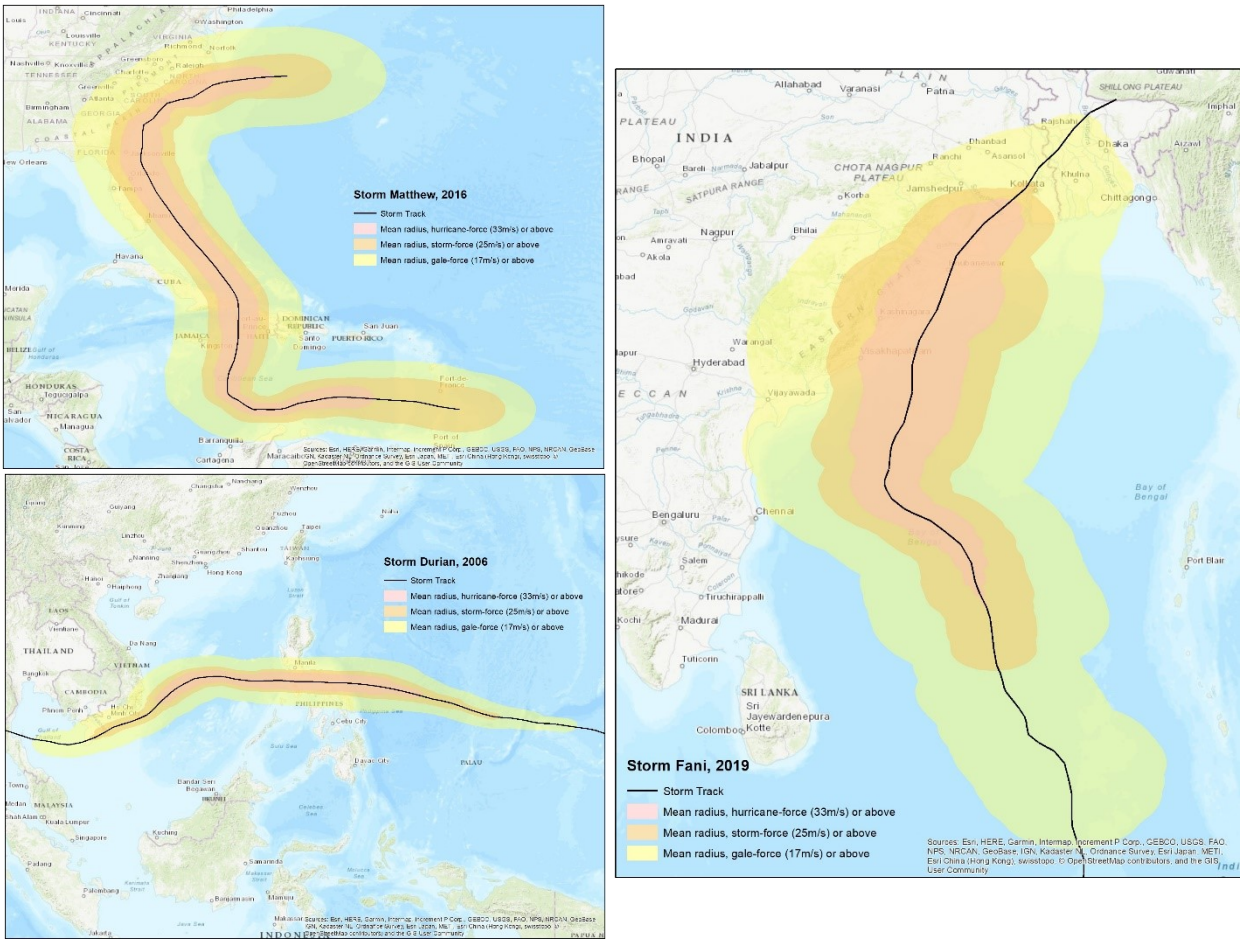

Figure 9 Exploration of the radii of various windspeeds during hurricanes Matthew (2016), Durian (2006), and Fani (2019). Black line indicates storm track, yellow indicates boundary of gale-force winds or above (17m/s), orange indicates boundary of storm-force winds (25 m/s) or above, and red indicates boundary of hurricane-force winds (33 m/s) or above.

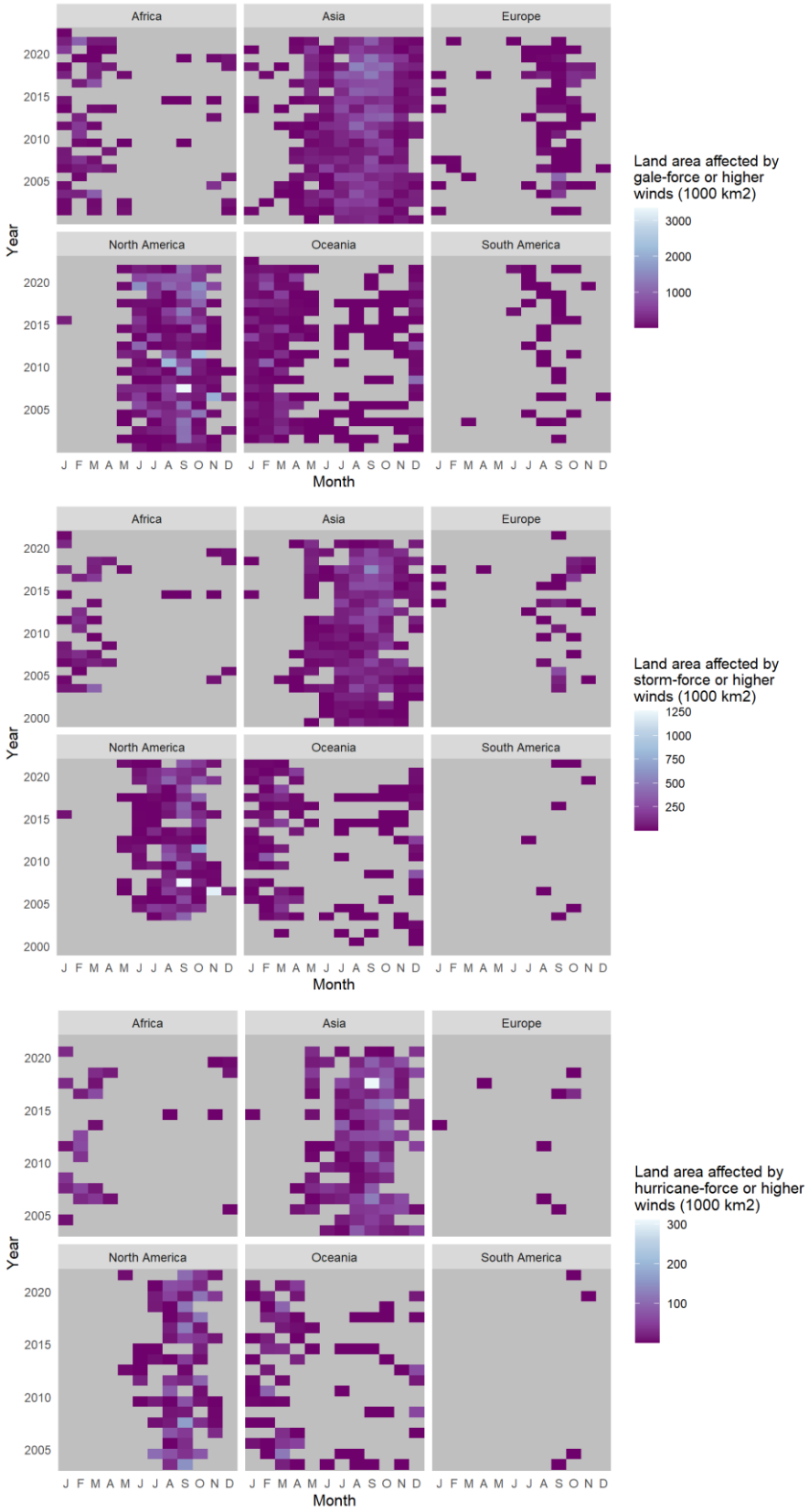

Figure 10 Land area affected by gale, storm, and hurricane force winds or above by year and month.

Floods and Droughts

Consistent with the literature review, precipitation indices were chosen to best represent floods and droughts. Monthly average temperature values for each location was extracted from the MODIS MOD11C3 MODIS/Terra Land Surface Temperature/Emissivity Level 3 product (Wan, Hook, & Hulley, 2015). Monthly average precipitation values were extracted from the Climate Hazards Group InfraRed Precipitation with Station data (CHIRPS) dataset (C. Funk et al., 2015). Both temperature and precipitation averages were used to calculate the location-specific time series of the 1-, 2-, and 3-month Standardized Precipitation Index (SPI) to characterize floods , and the 1-, 6-, 12-, and 24-month Standardized Evapotranspiration Index (SPEI) values to characterize droughts (Beguería, Vicente-Serrano, & Angulo-Martínez, 2010; Beguería, Vicente-Serrano, Reig, & Latorre, 2014). SPEI was calculated using the common temporal extents of both the MODIS and CHIRPS datasets (2002 – 2023) whereas SPI was calculated using the complete available CHIRPS monthly dataset (1981 – 2023).

The determination of whether a flood or drought occurred can be made using several methods. Thresholds of SPI and SPEI have been used to characterize gradients of dryness and wetness for the study of floods and droughts (Bischiniotis et al., 2018). Thus, one definition of each phenomenon utilized in this analysis classifies 1-month SPEI values less than or equal to -1.5 were classified as having experienced Droughts, and 6-month SPEI values greater than or equal to 1.5 were classified as having experienced Flood conditions (Bischiniotis et al., 2018). These thresholds correspond to Severe or Extreme dryness and wetness conditions respectively. However, the generalizability of these thresholds across spatial and temporal scales remains unclear. Therefore, we apply a more general definition based on the distribution of monthly SPI and SPEI values at a particular location during the study period. SPI values greater than the 90^{th}, 95^{th}, and 99^{th} percentile were utilized to define floods, and SPEI values

less than the first, fifth, and 10th percentile were utilized to define droughts. Extremely arid areas where yearly average precipitation is less than 73 mm (0.2mm per day*365 days) were excluded from the drought analysis—this functions as a spatial dry mask.

To test the utility of these definitions we apply them to three cities with vastly different climate dynamics: Dhaka, Bangladesh, N'djamena, Chad, and Mexico City, Mexico. The results of the varied definitions to classify one-month SPI into Floods, and the 12-month SPEI into Droughts, are shown in Figure 11. We see that the 1st/95th percentile provides the most narrow measure of event occurrence and the 10th/90th percentile provides the most frequent measure. The distribution of event occurrence is concentrated around particular years for droughts and is more disperse in the case of floods. This is expected as drought is often a result of prolonged periods of anomalously dry conditions. The diversity of extremely wet months (floods) during the study period across all three cities indicates that extreme events are difficult to predict even in areas with clear monsoon patterns such as Dhaka.

Contrasting the threshold and percentile-based definitions, we observe that the 95th percentile definition most closely matches the extremes identified by SPI and SPEI threshold, albeit with some differences. For Floods, the 1.5 SPI cutoff appears to classify a small fraction of months with SPI values around the threshold as extreme ($n = 3, \mu = 1.549$ in Dhaka; $n = 3, \mu = 1.547$ in Mexico City; $n = 4, \mu = 1.593$ in N'Djamena), disagreeing with the 95th percentile definition. The 1.5 SPI threshold is therefore a more 'generous' definition that identifies more flood events . A similar comparison for the SPEI uncovers some heterogeneity between cities. In Dhaka, the 5th percentile definition classified seven instances as Droughts which were not identified using the -1.5 SPEI cutoff ($n = 7, \mu = -1.460$). In Mexico City ($n = 5, \mu = -1.663$) and N'Djamena ($n = 11, \mu = -1.575$), the -1.5 SPEI cutoff led to identification of more droughts than the 5th percentile

definition. Therefore, we conclude that the SPEI cutoff is similarly a more generous definition that identifies more droughts in these time series.

Based on these differences, we suspect that a larger sample of locations might lead to a larger fraction of values near the 1.5 SPI and -1.5 SPEI thresholds being classified as ‘extremes’. Therefore, we opt for a narrower percentile-based definition of extreme values which utilizes the 95^{th} percentile of the SPI and the 5^{th} percentile of SPEI values to identify floods and droughts respectively in further analyses.

Figure 11 Distribution of droughts (top row) and floods (bottom row) as defined by varied measures of the 12-month SPEI and the one-month SPI respectively for Dhaka, Mexico City, and N'Djamena.

Heatwaves and Coldwaves

Maximum and minimum temperature values were extracted from two datasets: the Climatic Research Unit Timeseries (CRUTS) (Harris, Osborn, Jones, & Lister, 2020) and Terraclimate (Abatzoglou, Dobrowski, Parks, & Hegewisch, 2018). Both datasets present particular processing decisions that may affect this analysis. CRUTS utilizes a long-term record (1901 – present) of ten climatological variables collected from over 4,000 stations and adjusted using angular distance weighting. The underlying CRU dataset serves as input for various global climatological models, and provides temperature data at 0.5° resolution or approximately 50 km^2 (Harris et al., 2020). Terraclimate, on the other hand, utilizes the WorldClim dataset in conjunction with CRU and the Japanese 55-year Reanalysis to generate a high-resolution (1/24°, or approximately 4 km) monthly dataset of climate averages from 1985 - 2022. This increased resolution is valuable for our analysis; however, specific in the distribution of temperatures may affect which months are classified as extreme events such as heatwaves or coldwaves.

As before, we focus our exploration of these datasets to the cities of Dhaka, Bangladesh, N'djamena, Chad, and Mexico City, Mexico. Figure 12 provides a comparison of the distribution of minimum and maximum temperature values in these locations, and Figure 13 compares heatwave and coldwave occurrence between the two datasets. Maximum temperature values greater than the 90^{th}, 95^{th}, and 99^{th} percentile were classified as heatwaves, and minimum temperature values less than the first, fifth, and 10^{th} percentile were classified as coldwaves across both datasets. These comparisons can help illustrate key differences between these datasets.

Comparing the range and shape of distributions in Figure 12, we observe broad similarity between the datasets in Dhaka and N'Djamena. However, in Mexico City, the Terraclimate dataset indicates a larger range of both maximum and minimum temperature compared to

CRUTS. Comparing extreme event occurrence in Figure 13, we see that the different temperature distributions of the two datasets yield slightly different heatwave and coldwave occurrence calendars. In all three cities, coldwaves consistently occur in December – February and heatwaves consistently occur in March – May. Higher percentile thresholds yield a wider temporal distribution of coldwaves while the inverse is true for heatwaves. Due to different underlying value distributions, months classified as extremes are often different between CRUTS and Terraclimate. Given the consistency of identified extreme months between the datasets, we conclude that the Terraclimate dataset should be used for temperature analysis due to its higher spatial resolution. We further conclude that the 95th percentile threshold for heatwaves and the 5th percentile threshold for coldwaves provides a sufficient compromise between occurrence and non-occurrence of extreme events across calendar months for further analysis.

Environmental Covariates

Several analyses in this dissertation explore the influence of continuous environmental covariates in parallel with food systems outcomes. These estimates utilize monthly average temperature, precipitation, and greenness as measured by normalized differenced vegetation index (NDVI). Monthly average temperature values for each location was extracted from the MODIS MOD11C3 MODIS/Terra Land Surface Temperature/Emissivity Level 3 product (Wan et al., 2015). Monthly average precipitation values were extracted from the Climate Hazards Group InfraRed Precipitation with Station data (CHIRPS) dataset (C. Funk et al., 2015). Monthly average NDVI was extracted from the MOD13A3 MODIS/Terra Vegetation Indices Level 3 product (Didan, 2021). These measures were treated as raw averages and hence were not anomalized or standardized over any reference period.

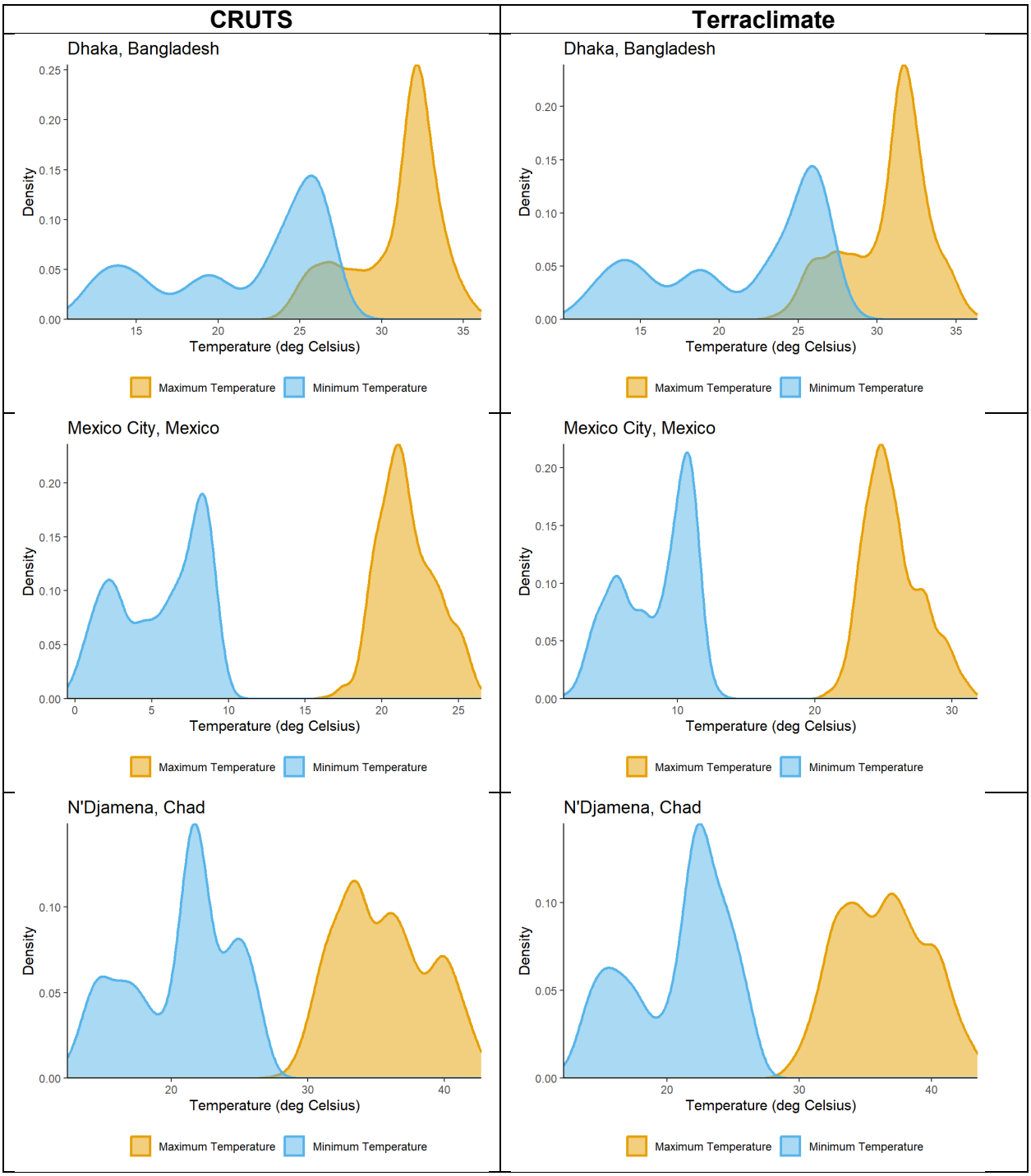

Figure 12 Comparison of minimum and maximum temperature distribution in Dhaka, Mexico City, and N'Djamena according to CRUTS and Terraclimate datasets

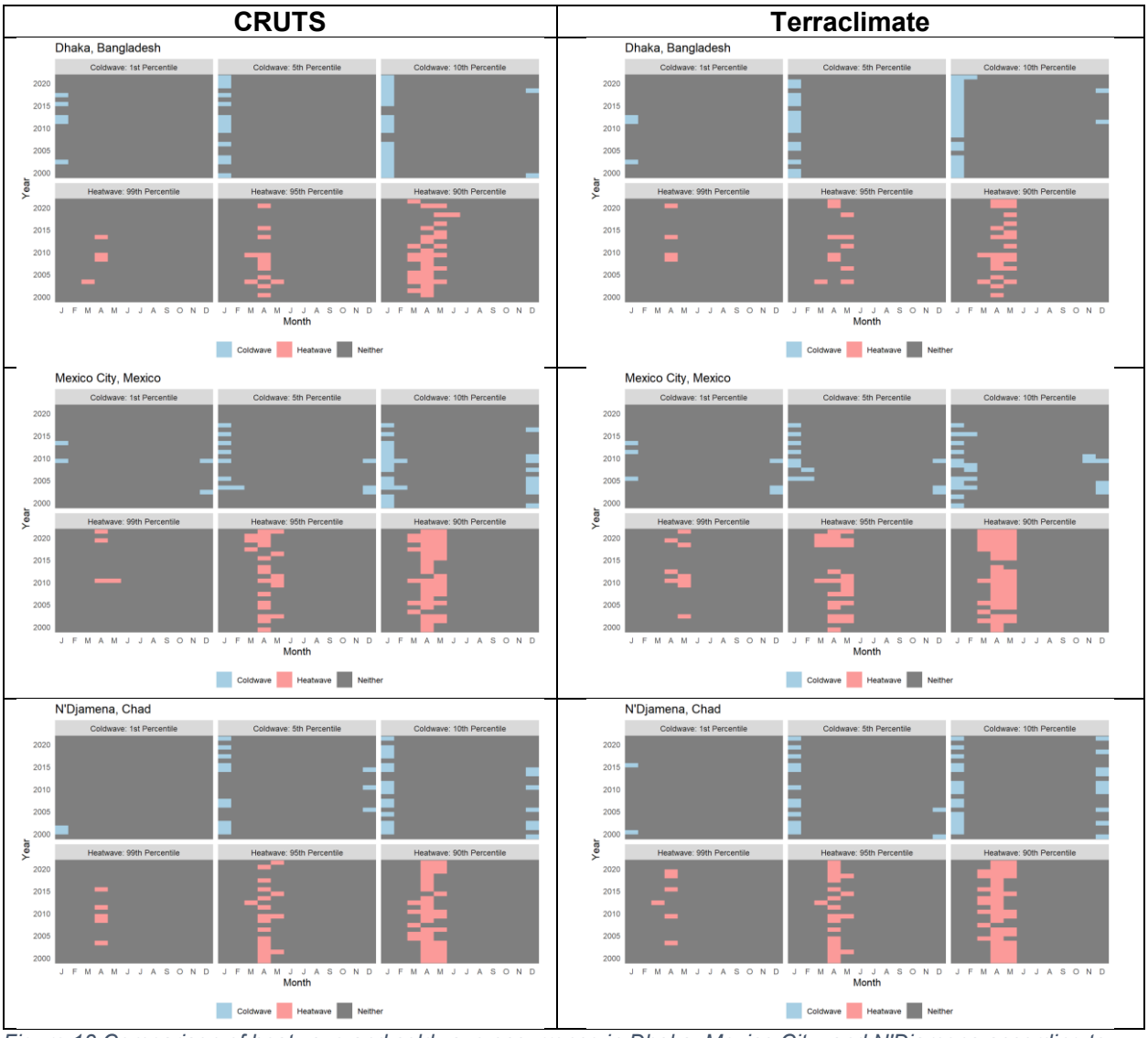

Figure 13 Comparison of heatwave and coldwave occurrence in Dhaka, Mexico City, and N'Djamena according to CRUTS and Terraclimate datasets. Panels represent events defined at the 1st/99th percentile, 5th/95th percentile, and 10th/90th percentile from left to right.

Chapter 4: Retail Food Price Vulnerability to Extreme Weather

Abstract

Anthropogenic climate change has accelerated the frequency and variability of extreme weather events. The impacts of these extreme weather events on food production systems are well documented; however, evidence regarding downstream impacts on transportation, storage, and markets, remains missing. Retail food prices provide a critical indicator of food system performance at the consumer end of supply chains. Quantification of the net welfare impacts of extreme weather events on bulky perishable foods can guide nutrition-sensitive interventions for climate adaptation and resilience planning. We utilize a novel global retail price dataset by combining monthly retail price observations from three early warning systems: FAO GIEWS, USAID FEWSNET, and WFP VAM. We then utilize market locations to extract dichotomous and continuous measures of heatwave, coldwave, flood, drought, and storm events using gridded data for study period of 2000 – 2022.

Key words: Retail food prices, extreme weather events, diet quality, nutrition

Introduction

Weather extremes present critical threats to global food security and nutrition. Disaster-related losses in the agricultural sector totaled USD 280 billion between 2008 – 2018 with significant recent increases due to Covid-19 (FAO, 2021c). Rainfall shocks, droughts, and temperature extremes have been associated with substantial yield anomalies of major cereal crops (Lobell & Gourdji, 2012; Schlenker & Lobell, 2010; Ubilava & Abdolrahimi, 2019; Vogel et al., 2019). These production shortfalls strain households through direct damage to crops and assets as well as indirect pathways such as lost incomes, lowered household budgets, and impaired health (Green et al., 2013; Hallegatte et al., 2016). Greater frequency and variability of climate extremes in upcoming decades are expected to increase poverty rates, endangering global progress towards the Zero Hunger Sustainable Development Goal (FAO, IFAD, UNICEF, WFP, & WHO, 2021; Hertel, Burke, & Lobell, 2010).

Extreme weather is frequently associated with increased or more volatile food prices. Global analyses have demonstrated the heterogeneity of price responses to weather shocks, particularly for maize, rice, wheat, and soybean (Chatzopoulos, Pérez Domínguez, Zampieri, & Toreti, 2020; Peri, 2017; Ubilava & Abdolrahimi, 2019). However, much of the research on food price volatility focuses on commodity price movements during crisis periods such as the 2008 global financial crisis (Cohen & Garrett, 2010; Headey & Fan, 2008), the 2011/12 food price crisis (Cuesta, Htenas, & Tiwari, 2014; FAO et al., 2011), and more recently the Covid-19 pandemic (Akter, 2020; Narayanan & Saha, 2021). Another strand of literature has focused on individual and household responses to weather shocks with price shocks as intermediate determinants of consumption, expenditure, and/or diets (Amare, Jensen, Shiferaw, & Cissé, 2018; Arndt, Hussain, Salvucci, & Osterdal, 2016; Grace, Brown, & McNally, 2014; Hill & Porter, 2017; Kaminski, Christiaensen, & Gilbert, 2016; Lawlor, Handa, Seidenfeld, & Zambia Cash Transfer Evaluation, 2019; Lazzaroni & Wagner, 2016; Porter, 2012). However, few analyses explicitly study the relationship

between weather and food price using long time series of prices with multiple markets and commodities (Cai, Chang, Chang, Țăran, & Pirtea, 2023; Kakpo, Mills, & Brunelin, 2022).

Research bias towards commodity prices as opposed to retail prices is notable. This distinction may be due to greater availability of international price data and historic emphasis on calorie provisioning through trade. However, retail prices provide valuable information about availability, accessibility, utilization, and stability of food supply at local and regional scales. Retail food prices better represent the additional cost paid by the consumer for transportation and storage and can therefore measure the real impact of rising food prices (Takayama, 1971). Retail food prices are often more responsive to local weather shocks and shocks at central wholesale markets than international price volatility (Brown & Kshirsagar, 2015; Minot, 2014). Small demand and supply elasticities also allow retail prices to be highly sensitive to supply shocks (FAO et al., 2011) and therefore incorporated in a wide variety of early warning systems (EWSs). Recent literature on the Covid-19 pandemic demonstrates this sensitivity as retail prices across various food groups were observed to be higher in countries with more stringent mobility restrictions and higher Covid-related morbidity and mortality (Akter, 2020; Imai, Kaicker, & Gaiha, 2021; Narayanan & Saha, 2021). Therefore, retail price monitoring is fundamental for monitoring of diet costs and affordability. Previous studies investigating retail food prices and extreme events have been spatially and temporally limited to particular geographies, record-breaking climate events, or particular humanitarian crises (Klomp & Bulte, 2013; Lawlor et al., 2019; Lazzaroni & Wagner, 2016; Mawejje, 2016; Daniel Maxwell & Fitzpatrick, 2012).

Prices of staple grains and cereals are more studied than any other food group (Kyle Frankel Davis, Downs, & Gephart, 2020). This focus is driven by the primacy of grains and cereals to the diets of poor people, as well as established global trade networks in non-perishable agricultural commodities (Moltedo, Troubat, Lokshin, & Sajaia, 2014). Since poorer households spend a larger fraction of their budget on food, they are more acutely affected by both reduced budgets and price shocks (Green et al.,

2013; Ivanic & Martin, 2014). Low-income households rapidly respond to high prices or low incomes by adjusting consumption through reduced intake and substitution of expensive nutrient-rich foods with staple foods (Dercon, Hoddinott, & Woldehanna, 2005; Gibson & Kim, 2019). However, to the extent possible, diets do not comprise exclusively of staple grains, and price movements in other food groups are relevant to poor peoples' health and nutrition status. Bulky, perishable food items are more expensive due to additional costs for transportation and storage (Takayama, 1971), particularly due to refrigeration. The evolution of the Cost of Healthy Diet metric has also demonstrated the need to consider costs of the whole diet, including food groups such as fruits and vegetables and animal source foods (Herforth et al., 2020). Lack of localized or global research on price trends of food groups such as animal source foods and fruits and vegetables presents a critical gap in price literature (Hasegawa et al., 2021).

EWSs provide a valuable data source to address the dual limitations of retail price availability and bias towards staple foods. Food price monitoring systems such as the Food and Agriculture Organization (FAO) Global Information and Early Warning System (GIEWS) (FAO, 2021b), the World Food Programme (WFP) Vulnerability Analysis and Mapping (VAM) (WFP, 2021), and the US Agency for International Development (USAID) Famine Early Warning Systems Network (FEWSNET) provide valuable data on retail food prices and can enable such analysis. Price observations from these sources are often used in localized predictive models of fragility and food insecurity; however, structural analyses of retail price time series from these sources are notably lacking. Two existing studies have utilized early warning datasets to study price effects. Cedrez et al (2020) provide a time series analysis of compiled data to measure spatial and temporal price variation in 168 markets (Cedrez, Chamberlin, & Hijmans, 2020). Brown and Kshirsagar (2015) utilize a similar combined dataset of early warning systems market prices to investigate differential effects of weather in 2008 – 2012 using the Normalized Differenced

Vegetation Index (NDVI) (Brown & Kshirsagar, 2015). Neither analysis specifically investigates extreme weather events.

In this paper, we aim to describe retail price changes by food group and urbanicity as they respond to a suite of five contemporaneous and recent extreme weather events: heatwaves, coldwaves, storms, floods, and droughts. We focus on net price changes as our outcome of interest rather than market efficiencies to exploit a global dataset of market-level price observations derived from early warning systems. The magnitude and direction of retail price changes are affected by the disruption itself, the impacted supply chain, and the mechanism of downstream impacts throughout the food system. Market locations allow us to utilize the quasi-random nature of extreme events for this analysis. We further disaggregate this study by food groups to identify differential impacts of these hazards on perishable and nonperishable food groups. For example, upward price shifts for perishable and nutrient-dense foods such as dairy and meats may indicate supply constrictions due to shocks impacting a supply chain with higher storage and transportation costs. Alternatively, downward price shifts for the same food group would indicate demand reduction potentially due to widespread loss of income across a region (Y. Bai, Alemu, Block, Headey, & Masters, 2021). These correlations are further distinguished by markets' classification as rural, urban, or peri- and sub-urban to better represent global variability in market connectivity, integration, and population density (Minten, Koru, & Stifel, 2013; G. Shively & Thapa, 2016; Thapa & Shively, 2018).

Quantification of these heterogenous impacts can inform long-term climate adaptation as well as rapid interventions to mitigate diet disruptions due to extreme weather events. This analysis also provides a critical input for simulation studies of global food insecurity and climate which are constrained by limited data about price impacts on livestock, fruits, and vegetables (Hasegawa et al., 2021; Mbow et al., 2019). As the food system intensifies to feed 9.7 billion people by 2050 despite higher likelihood of weather-related disasters (FAO et al., 2021), understanding the impacts of extreme weather events on

various food groups is critical to building resilience in the food system and protecting affordability of healthy diets.

Data Sources and Processing

Retail food prices

Monthly retail food item prices were obtained from early warning system (EWS) databases published by three different international agencies: the Global Information and Early Warning System (GIEWS) by the Food and Agriculture Organization (FAO) of the United Nations (UN); the Famine Early Warning System Network (FEWSNET) produced by USAID; and the Vulnerability Analysis and Mapping (VAM) system from the World Food Programme (WFP). All available data were extracted, and a continuous study period of 2000 – 2020 was utilized for this analysis. Each price observation was then adjusted for its country's inflation using a combined database of monthly consumer price indices for food items from the IMF (IMF, 2021) and the FAO (FAOSTAT, 2021). All prices in local currency units were then adjusted for international comparisons using purchasing power parity prices to a reference period of June 2017 using the World Bank's purchasing power parity (PPP) conversion factor for private consumption (International Comparison Program & World Bank, 2021).

All retail price data were then cleaned to remove outliers. Plausible errors in data entry were defined as values of each market-item time series greater than or less than 3 standard deviations in units of 2017 USD/kCal which could be corrected to fall within the time series range by multiplying or dividing by a power of 10. These *order of magnitude outliers* were corrected to restore the price value to within plausible range. A total of 104 (0.08% of the dataset) order of magnitude outliers were corrected. The winsor2 Stata package was then used to trim the top and bottom 0.5% of price observations within each food group category to remove extreme values most likely due to data entry errors. After trimming, a total of 2,172,210 price observation were available from 3,053 markets in 78 countries.

Food group classification and food composition

All food items in the combined EWS dataset were classified into eight categories and two groups. The *Non-Perishable* category includes the following food groups: Breads and Cereals; Legumes, Nuts, Seeds; Oils and Fats; and Sugar and Confectionary. The *Perishable* category included: Dairy and Eggs; Fish and Seafood; Fruits and Vegetables; and Meat food groups. This classification is based on the UN Classification of Individual Consumption According to Purpose (COICOP) system (Bai et al., 2021a, 2021b).

To allow for comparison across food groups, each food item was also matched to the USDA Standard Reference 28 Food Composition Table (US Department of Agriculture Agricultural Research Service, 2016) or the West African Food Composition Table where appropriate (Vincent et al., 2020). 98% of all items in the larger dataset were successfully matched, and kilocalories in each item as purchased was calculated using the edible fraction of the matched item. Any prices for live animals were dropped due to the lack of food composition data. EWS retail prices were thus standardized to two outcomes as purchased: 2017 USD/kg and 2017 USD/kcal of item.

Extreme Weather Events

Data on tropical cyclones and storms were extracted from the International Best Track Archive for Climate Stewardship (IBTrACS) storm track database (Knapp et al., 2010). Consistent with the exploration detailed in Technique 3: Extraction of Weather Extremes from Gridded Data, the average radius of storm-force winds (25 m/s) or higher was used to determine if a market suffered from a storm.

Both temperature and precipitation averages were used to calculate the location-specific time series of the 6-month Standardized Evapotranspiration Index (SPEI) values to characterize droughts (Beguería et al., 2010; Beguería et al., 2014). SPEI was calculated using monthly

average temperature values from the MODIS MOD11C3 MODIS/Terra Land Surface Temperature/Emissivity Level 3 product (Wan et al., 2015) dataset and the monthly average precipitation values from the Climate Hazards Group InfraRed Precipitation with Station data (CHIRPS) dataset (C. Funk et al., 2015). The CHIRPS dataset was used to calculate the 1-month Standardized Precipitation Index (SPI) to characterize floods. Values above the 95th percentile of SPI were classified as floods, and values below the 5th percentile of SPEI were classified as droughts in each market location.

Maximum and minimum temperature values were extracted from the Terraclimate (Abatzoglou et al., 2018). Maximum temperature values above the 95th percentile were classified as heatwaves, and minimum temperature values below the 5th percentile were classified as coldwaves in each market location.

Global Prices

The FAO monthly food price index (FPI) for the commodity group corresponding to each food item was utilized as a proxy of average global price levels during each month (FAO, 2021a). These FAO commodity groups include: Cereals, Vegetable Oils, Dairy, Meat, and Sugar. These commodity groups correspond to the modified COICOP categories of Breads and Cereals, Fats and Oils, Dairy and Eggs, Meats, and Sugar and Confectionery respectively. Two food groups (legumes, nuts, and seeds; fruits and vegetables) lack a comparable FPI category and are therefore omitted from specifications including the FPI variable.

Urbanization

Each market was assigned an urban classification corresponding to the Global Human Settlement Layer (GHSL) Degree of Urbanization classification in the years 2000 and 2015 (Florczyk A.J., 2019; Pesaresi, Florczyk, Schiavina, Melchiorri, & Maffenini, 2019). Classification for both years derives from the GHSL Settlement Model Grid (SMOD), and the high-level

categories of Urban, Suburban, and Rural were used. Changes in urbanization classification over time were examined to identify urbanization dynamics during the study period. Markets classified as Urban in 2000 and Rural in 2015 were dropped from the analysis[1]. Based on combinations of remaining transitions, all markets were initially classified into typologies of Urban, Rural, Suburban, and Transitional. A balance table comparing characteristics of sample markets to rest of world allowed for merging of the latter two categories to generate the final typology of Urban, Rural, and Peri- and Sub-Urban markets.

Table 6 Urbanization categories of EWS markets per DEGURBA classification

Class in 2000	***Class in 2015***	***Typology***	***% of Markets***
Urban (any density)	Urban (any density)	Urban	64.4%
Rural (any density)	Rural (any density)	Rural	28%
Suburban	Suburban	Suburban	1.4%
Suburban	Urban (any density)	Intensifying Suburb	1.2%
Rural (any density)	Urban (any density) Suburban	Urbanizing Rural	4.6%
Urban (any density)	Suburban Rural	De-Urbanizing City	0.4%
Suburban	Rural	-	0%

Estimation Strategy

We begin by studying dichotomized extreme events defined per various thresholds discussed above. The association between retail food prices and each of the five extreme events were examined using a baseline ordinary least squares (OLS) regression specification shown in Equation 2.

$$\ln(P_{ijt}) = \beta_0 + \beta_1 \text{Extreme Event}_{j,t-n} + \gamma_j + \lambda_{jm} + \theta_{jy} + \tau_i + \varepsilon$$ *Equation 2*

[1] Dropped markets experienced significant conflict or migration during the study period. The14 markets comprising this category are located in northern Sri Lanka, parts of Rwanda, central Mali, southern Malawi, and one market in Mozambique. Two non-conflict related examples were found in Nepal and Cambodia, potentially driven by migration or sprawl.

In this equation, *i* refers to food item, *j* refers to market location, *t* refers to continuous time, *n* refers to lagged month, *m* refers to month, and *y* refers to year of price observation. P_{ijt} indicates one of two outcomes: the natural log of retail price in 2017 USD/1000 kCal, and the difference from the average price of each food group during each market and month of analysis. $\text{Extreme Event}_{\text{j,t}-\text{n}}$ is a dummy variable which represents one of Flood, Drought, Storm, Heatwave, or Coldwave. Each extreme event was lagged by up to three months prior to the month of price observation (*n* = 1, 2, 3) to test for potential persistence. We also include market location fixed effects γ_j to account for unobserved heterogeneity over space, market-month fixed effects λ_{jm} to account for seasonal price fluctuations, market-year fixed effects θ_{jy} to account for year-to-year changes, and item fixed effects τ_i to account for differences in product characteristics such as item packaging and storage requirements. Equation 2 was sequentially applied to the pool of available retail prices, and subsequent subsets by food group, urban category (rural, urban), and both food group and urban category respectively.

Alternate specifications of Equation 2 explore the robustness of observed coefficients to the inclusion of differentially lagged retail food prices and covariates representing average weather including average temperature and precipitation at location *j* and time *t*. The effect of world retail prices was also explored through the inclusion of the FAO commodity group price index for the food category corresponding to retail item *i* of interest during time *t*.

To address spurious significance deriving from multiple comparisons, the Bonferroni correction was applied by dividing standard p value thresholds of 1%, 5%, and 10% by the total number of partitions

(7 food groups x 3 urban categories x 5 extreme weather events = 105 partitions) (Vickerstaff, Omar, & Ambler, 2019). This correction ensures that only the most precise associations are interpreted.

Results

Summary statistics

A summary of dataset characteristics is provided in Table 7. A grand total of 2,172,210 observations are utilized, with 69.1% of observations in Urban markets, 20.0% in Rural markets, and 10.8% in Peri- and Sub-Urban markets. Approximately 59% of the EWS data is sourced from WFP VAM, with GIEWS contributing 36% of the dataset and FEWS contributing approximately 5%. Food price monitoring has improved steadily during the study period; the first decade of the study period contributed only 2.8% of the complete dataset, and the share of observations grew to 25.5% in 2010 – 2014. Food price monitoring has also improved during the Covid-19 pandemic of 2020 – 2022; the greater share of observations during these years comprises approximately 23.1% of the dataset. To account for this improvement in price monitoring during the study period, we utilize market-month and market-year fixed effects to further absorb any seasonality in the retail price signal.

The geographic distribution of market locations in EWS is heavily skewed towards low and middle income countries (LMICs) in the global south. Price observations in Sub-Saharan African markets represent 58.6% of the dataset, and the East Asia & Pacific, Latin America & Caribbean, and South Asia regions represent 9-10% each. Along the income dimension, 91% of price observations in the EWS dataset are collected from markets in Low and Lower Middle income categories per the World Bank's country classification by income group during the year of price observation.

Table 8 presents summary statistics by food group and market type. Prices in weight (2017 USD/kg) and caloric units (2017 USD/1000 kCal) are presented for the purpose of discussion; however, the remainder of the paper discusses only outcome units of 2017 USD/kCal. Breads and Cereals comprise the largest food group for which retail prices are observed (53.0%), followed by Fruits and Vegetables (18.0%) and Pulses, Nuts, and Seeds

(9.9%). There is considerable diversity in food items within these food groups as well; a list of unique items by food group is provided in Appendix 1: Retail Items Included in Early Warning Systems. Breads and Cereals are the cheapest food group at USD 1.59/kg. This food group is USD 0.13 cheaper per kg in rural markets compared to urban markets. Fruits and Vegetables are the next cheapest food group at an average price of USD 1.91/kg, followed by Sugar and Confectionary at USD 2.53 on average. The urban-rural gradient is particularly stark for Sugar and Confectionery, as average prices in rural markets are USD 1.06 higher per kg compared to Urban markets. Rural markets are also observed to have cheaper prices on a weight basis for perishable food groups compared to urban markets, with an average difference of USD 0.85/kg.

As indicated by Table 8, the vast difference in food composition across groups necessitates caloric adjustment for comparison across food groups. On a weight basis, Dairy and Eggs is only 3.7x as expensive as Breads and Cereals; however in calorie terms, the Dairy and Eggs and Fruits and Vegetables food groups are approximately 10x more expensive than Breads and Cereals. Within perishable food groups, rural markets on average appear to be more effective at provisioning Dairy and Eggs and Fish and Seafood whereas urban markets appear to be more effective at provisioning Fruits and Vegetables and Meat, as evidenced by comparatively lower prices per kilocalorie. Retail prices of perishable food groups are also poorly represented and monitored in EWS, with the exception of Fruits and Vegetables. Perishable food groups represent less than 30% of the complete dataset, indicating a critical gap in price monitoring of foods needed for a balanced and healthy diet.

Table 7 Summary of dataset characteristics by data source, year, and World Bank Region, across market urbanization typologies

	Pooled	*Urban*	*Rural*	*Peri- and Sub-Urban*
Total Observations	2,172,210	1,500,656	435,022	236,532
Total Items	105	105	97	98
Total Unique Products	141	141	117	112
Total Countries	78	76	57	51
Total Markets	3053	1742	933	378
% of Observations by Data Source				
FEWS	4.88	5.38	5.56	0.47
GIEWS	36.13	41.84	22.1	25.71
VAM	58.99	52.78	72.34	73.81
% of Observations by Year				
2000 - 2004	2.82	3.19	1.67	2.64
2005 - 2009	11.05	11.96	8.69	9.63
2010 - 2014	25.53	25.22	25.97	26.65
2015 - 2019	37.48	36.99	38.58	38.56
2020 - 2022	23.12	22.64	25.1	22.51
% of Observations by WB Region				
East Asia & Pacific	9.59	10.14	7.88	9.27
Europe & Central Asia	7.75	8.8	1.44	12.69
Latin America & Caribbean	9.96	13.78	1.4	1.45
Middle-East & North Africa	4.29	4.28	4.46	4.03
South Asia	9.77	12.38	5.76	0.59
Sub-Saharan Africa	58.64	50.63	79.05	71.97
% of Observations by WB Income Group				
High Income	0.54	0.78		
Upper Middle Income	8.45	9.2	5.23	9.59
Lower Middle Income	42.29	44.09	42.29	30.86
Low Income	48.72	45.93	52.47	59.56

Table 8 Share of observations, average price per kg, and average price per kCal by food group across market typologies

	Pooled			*Urban*		
	%	*Avg. Price (2017 USD/kg)*	*Avg. Price (2017 USD/kCal)*	*%*	*Avg. Price (2017 USD/kg)*	*Avg. Price (2017 USD/kCal)*
Breads & Cereals	53.0	1.59	0.23	52.5	1.61 *(t = 15.01, p = 0)*	0.23 *(t = 16.78, p = 0)*
Fats & Oils	6.0	4.83	0.27	6.2	4.72 *(t = -7.55, p = 0)*	0.27 *(t = -7.74, p = 0)*
Pulses, Nuts, & Seeds	9.9	3.12	0.46	9.6	3.15 *(t = 4.61, p = 0)*	0.46 *(t = -2.11, p = 0.04)*
Sugar & Confectionery	1.3	2.53	0.33	1.6	2.37 *(t = -13.53, p = 0)*	0.30 *(t = -13.53, p = 0)*
Dairy & Eggs	3.1	5.84	2.35	3.3	5.83 *(t = -0.14, p = 0.89)*	2.42 *(t = 3.32, p = 0)*
Fish & Seafoods	2.1	10.96	5.01	2.0	11.00 *(t = 0.45, p = 0.65)*	5.03 *(t = 0.48, p = 0.63)*
Fruits & Vegetables	18.0	1.91	2.25	17.9	1.91 *(t = -0.82, p = 0.41)*	2.15 *(t = -14.27, p = 0)*
Meats	6.6	11.60	3.05	6.8	11.67 *(t = 3.30, p = 0)*	2.96 *(t = -13.36, p = 0)*
	Rural			*Transitional*		
	%	*Avg. Price (2017 USD/kg)*	*Avg. Price (2017 USD/kCal)*	*%*	*Avg. Price (2017 USD/kg)*	*Avg. Price (2017 USD/kCal)*
Breads & Cereals	54.9	1.48 *(t = -49.46, p = 0)*	0.21 *(t = -54.43, p = 0)*	52.1	1.66 *(t = 26.71, p = 0)*	0.24 *(t = 25.81, p = 0)*
Fats & Oils	6.0	5.04 *(t = 7.87, p = 0)*	0.28 *(t = 6.92, p = 0)*	5.0	5.20 *(t = 8.23, p = 0)*	0.30 *(t = 9.87, p = 0)*
Pulses, Nuts, & Seeds	11.2	3.08 *(t = -4.75, p = 0)*	0.45 *(t = -8.16, p = 0)*	9.0	3.02 *(t = -7.11, p = 0)*	0.51 *(t = 12.65, p = 0)*
Sugar & Confectionery	1.0	3.43 *(t = 22.78, p = 0)*	0.44 *(t = 22.85, p = 0)*	0.0	2.55 *(t = 0.24, p = 0.82)*	0.33 *(t = 0.24, p = 0.82)*
Dairy & Eggs	2.3	4.74 *(t = -15.43, p = 0)*	1.98 *(t = -11.85, p = 0)*	2.8	7.54 *(t = 9.92, p = 0)*	2.45 *(t = 2.22, p = 0.03)*
Fish & Seafoods	2.5	9.81 *(t = -12.33, p = 0)*	4.25 *(t = -14.13, p = 0)*	2.4	12.91 *(t = 13.07, p = 0)*	6.31 *(t = 14.66, p = 0)*
Fruits & Vegetables	16.4	1.88 *(t = -3.92, p = 0)*	2.49 *(t = 21.38, p = 0)*	21.7	1.98 *(t = 6.04, p = 0)*	2.41 *(t = 12.27, p = 0)*
Meats	5.8	10.59 *(t = -21.89, p = 0)*	3.29 *(t = 17.15, p = 0)*	6.9	12.64 *(t = 22.37, p = 0)*	3.30 *(t = 19.09, p = 0)*

Frequency of Extreme Events

Figure 14 presents the frequency of extreme event occurrence by month and year in the study period, for the complete panel of market-months in this dataset. Extreme temperature deviations from normal occur commonly throughout the world, whereas tropical regions are particularly prone to seasonal flooding and storm events. Due to the extremely different climatologies of markets in the EWS sample, the timing of each event within a calendar year holds little meaning; however, event frequencies can still be analyzed. Heatwaves are the most frequently occurring event during the study period (4.3% of market-months), followed by floods (2.99%) and droughts (1.98%). Coldwaves (0.35%) and storms (0.31%) occur least frequently, and storm occurrence is limited to 38.7% of study markets. While floods occur consistently during the study period, increasing occurrence of heatwaves and droughts are observed in the recent decade.

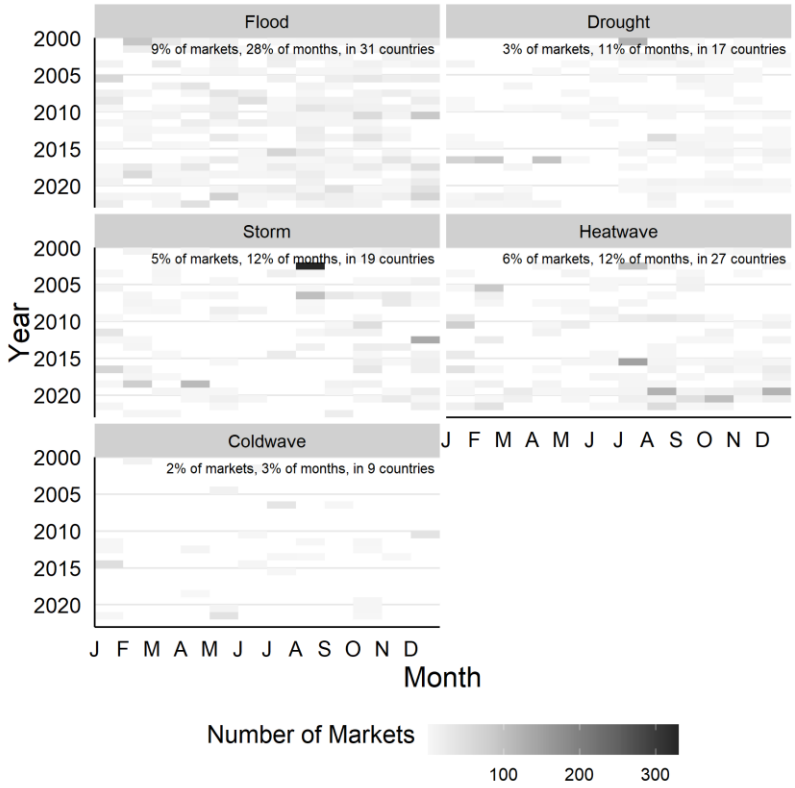

Figure 14 Number of markets affected by extreme events (flood, drought, storm, heatwave, and coldwave) by month and year, 2000 – 2022

Contemporaneous Extreme Events

Figure 15 presents estimated coefficients per Equation 2 applied to split samples by extreme event and food groups for both price by weight and price by calorie outcomes. On average, Heatwaves and Coldwaves are associated with net reductions in retail prices, whereas Storms and Droughts are associated with net increases in retail prices. Statistically significant effects are similar across both weight (Panel A) and calorie (Panel B) price outcomes; therefore, focusing on only statistically significant effects paints a clearer picture of these relationships. Heatwaves and Floods are associated with a less than 1.3% reduction in retail prices, indicating

net demand reduction. Coldwaves, Droughts, and Storms are conversely associated with a 3.7 – 5.0% increase in retail prices, indicating net supply constriction.

Differential responses are observed between food groups in response to extreme events. Although no clear pattern is discernible across non-perishable and perishable food groups, food group-level responses are notable. Storms are associated with a 7% increase in price per 1000 kilocalories of Fruits and Vegetables (β_1 = 0.068 ± 0.016) and Droughts are associated with a 5.2% increase in prices of Breads and Cereals (β_1 = 0.051 ± 0.008). The magnitude of most effects is similar across price outcomes in weight and calorie units; therefore, the remainder of this paper reports coefficients of price in calorie units (USD 2017/1000 kCal). Although Fats and Oils and Fish and Seafoods food groups appear to respond to Coldwaves, the small sample sizes of this category and lack of plausible physical mechanism for this effect call into question the observed effects.

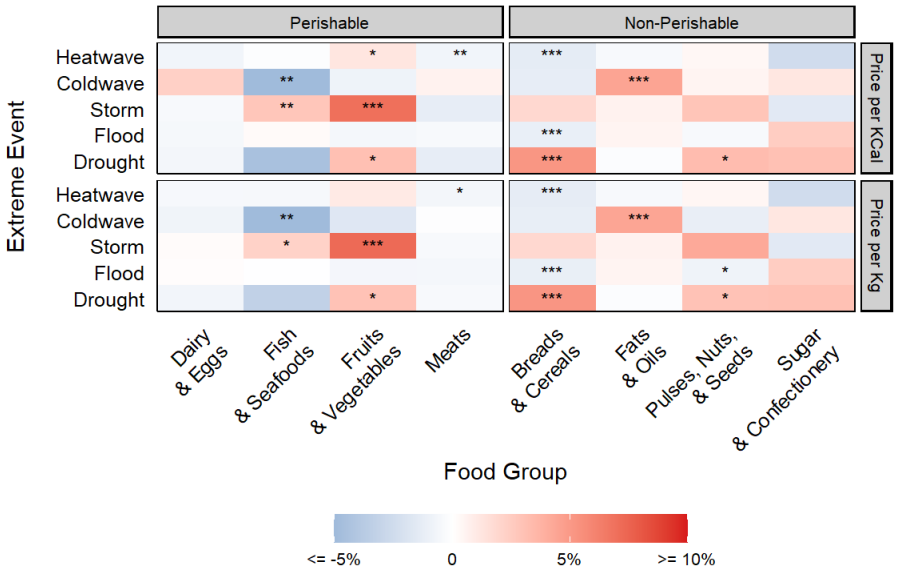

Figure 15 Change in retail price (%) during extreme events (flood, drought, storm, heatwave, and coldwave) by price type (price per kg and price per 1000 kCal).

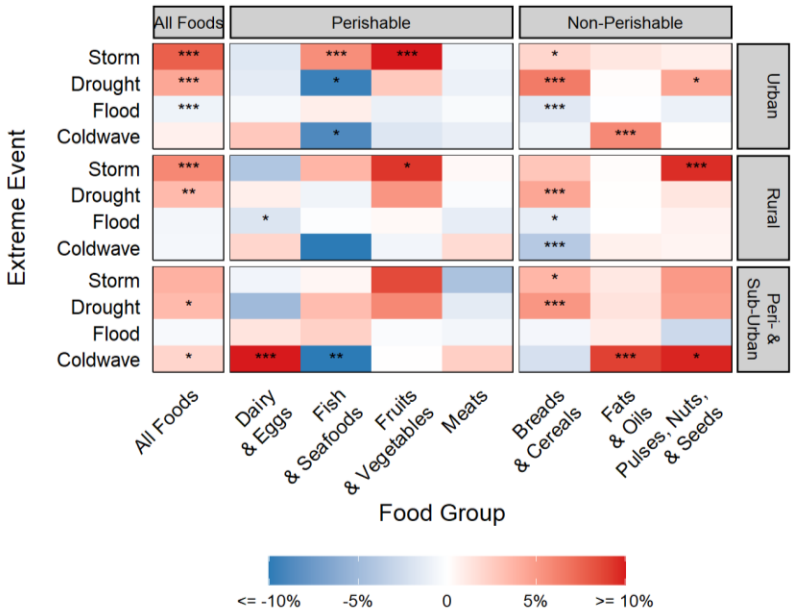

Figure 16 Change in retail price per 1000 kCal (%) by market typology (urban, rural, peri- & sub-urban) during extreme events (flood, drought, storm, heatwave, and coldwave). Note: Sugar and Confectionery food group is excluded from this graph due to data sparsity across most partitions.

Differential impacts are observed across different types of markets for various food groups. For example, months with storm events are associated with an average 3.2-3.8% increase in retail prices in urban and rural markets and 2.1-2.7% increase in Peri- and Sub-Urban markets. However, these effects represent varied magnitudes of changes in the Breads and Cereals (β_{urban} = 2.1%, 0.02 ± 0.009; $\beta_{Peri\ \&\ Suburban}$ = 3.6%, 0.036 ± 0.018), Fruits and Vegetables (β_{urban} = 14.2%, 0.133 ± 0.017; β_{rural} = 9.3%, 0.089 ± 0.034), Fish and Seafood (β_{urban} = 5.2%, 0.054 ± 0.013), and Pulses, Nuts, and Seeds (β_{rural} = 9.5%, 0.091 ± 0.027) food groups. The large magnitudes of price changes for Fruits and Vegetables in both urban and rural markets in conjunction with rising prices for Pulses, Nuts, and Seeds in only rural markets, indicate significant supply reductions.

Droughts present different mechanisms for retail price fluctuations, concentrated mainly in non-perishable food groups. Months with a 6-month SPEI deficit are associated with supply constriction of Breads and Cereals across all market types (β_{urban} = 6.4%, 0.0625 ± 0.0117;

β_{rural} = 4.4%, 0.043 ± 0.012 ; $\beta_{Peri\ \&\ Suburban}$ = 4.2%, 0.051 ± 0.014), and a slight increase in prices of Pulses, Nuts, and Seeds in urban markets (β_{urban} = 4.5%, 0.044 ± 0.017).

Demand reduction is observed less frequently than supply constriction, and is most often a response to floods and coldwaves. Urban markets appear slightly affected by this price reduction in Breads and Cereals (β_{urban} = -1.6%, -0.016 ± 0.003), and Dairy and Eggs prices in rural markets are also slightly affected (β_{rural} = -1.9%, -0.019 ± 0.008) during floods. Demand-side forces also appear to affect Fish and Seafoods during extremely cold months (β_{urban} = -8.9%, -0.093 ± 0.036; $\beta_{Peri\ \&\ Suburban}$ = -18.1%, -0.2 ± 0.076). This may be consistent with individuals reducing consumption of expensive, protein-rich foods and prioritizing staple food consumption when diets are strained. However, we observe a non-significant demand reduction in Breads and Cereals, and a significant increase in retail prices of Fats and Oils in urban markets ($\beta_{uburban}$ = 5.8%, 0.056 ± 0.008) . Due to the trio of constrained sample sizes for Coldwave events, Fish and Seafood items, and Peri- and Sub-Urban regions, the effects in the latter region are not interpreted further.

Effect of Covariates and Lagged Extreme Events

Detailed comparisons of coefficients across models including environmental covariates (temperature, precipitation, and interaction), lagged prices by 1, 2, and 3 months, and world prices per the FAO Food Price Commodity Group Index, are presented in Appendix 2: Sensitivity Analysis of Retail Prices. Presented coefficients are stable to the inclusion most covariates. One exception is observed in retail price changes to Fruits and Vegetables during Storm months. This regression specification is sensitive to lagged prices with potential persistence in the month following a storm. This deviation is interpreted as indicating potential unobserved variables or highly variable seasonal production cycles which mediate observed price changes. In general, coefficients observed in contemporaneous specifications do not change significantly in the following month, but the precision of estimated effects often improves

in the latter specification. This observation provides preliminary evidence of limited persistence effects.

Regional Patterns

Figure 17 presents coefficients estimated for the baseline regression across event, food group, market type, and analytical regions as defined by the World Bank. Widespread heterogeneity is observed across partitions and even among regions experiencing the same event. This finding underlines the limited generalizability of global results and the importance of local context while assessing localized effects.

In East Asia and Pacific (EAP), perishable food groups appear to be most significantly affected by heatwaves, storms, and floods. Synchronized demand reduction is observed for Dairy and Eggs (-42.2%, -0.548 ± 0.079) and Fish and Seafoods (-15.7%, -0.171 ± 0.057) in rural markets, whereas in urban markets, modest increases are observed in retail prices of Fruits and Vegetables (6.8%, 0.065 ± 0.015) and Meats (2.9%, 0.029 ± 0.01). Rural consumers similarly shift consumption away from Dairy and Eggs during flood months (-15.5%, -0.168 ± 0.047), pointing to a pattern of smoothing caloric consumption after water-related extreme events.

In Europe and Central Asia, heatwaves are associated with significant urban demand reduction away from Fish and Seafoods (-22.9%, -0.26 ± 0.032) and Fruit sand Vegetables (-3.9 -0.04 ± 0.01). Both coldwaves and droughts are associated with significantly higher retail prices of Fats and Oils (17.6 0.162 ± 0.024; 10.0 0.095 ± 0.024).

The Latin America and Caribbean region provides the largest magnitudes of price movements observed in this analysis. During storm months, rural demand reduction of dairy and eggs (-22% -0.248 ± 0.066) and fruits and vegetables (-31.1%, -0.373 ± 0.118) in parallel with extremely high retail prices of Breads and Cereals (67.9%, 0.518 ± 0.122) indicates potentially severe impacts to rural diets. A similar pattern is observed after floods, with rural demand

reduction of Dairy and Eggs (-18.9 -0.209 ± 0.064) and supply constriction and therefore higher prices of Breads and Cereals (26.2%, 0.233 ± 0.066). Urban markets appear more resilient to storms than rural ones as they face the issue of net supply constriction for Dairy and Eggs (21.2 0.192 ± 0.06) and Meats (6.2 0.06 ± 0.016). Finally, heatwaves present a unique challenge for LAC as Breads and Cereals, Dairy and Eggs, Fats and Oils, and Fruits and Vegetables all experience a price increase of 5-9%. These concurrent increases may make it difficult for the poorest individuals to adequately smooth diets.

The Middle East and North Africa region faces comparably large magnitudes of retail price changes during months of concurrent extreme events. Demand reduction of Dairy and Eggs in rural markets is observed during drought (-27.7 -0.324 ± 0.12) and flood (-26.0 -0.301 ± 0.084) months. During flood months, supply constriction is also observed for Pulses, Nuts, and Seeds in rural areas (12.4 0.117 ± 0.027). Urban markets also significantly reduce demand for Fish and Seafoods by 22-57% across all studied extreme events. Both Urban and rural markets compensate similarly by reducing demand for Fruits and Vegetables by approximately 4.5% during heatwave months.

The South Asia region presents two trends that are inconsistent with the other regions. During storm months, rural retail prices of Fruits and Vegetables increase by 28% (0.247 ± 0.028) in conjunction with a 3.8% reduction in Breads and Cereals prices (-0.039 ± 0.015) and a 11.4% decrease in Fats and Oils prices (-0.121 ± 0.033). During flood months, urban retail prices experience a smaller increase of 4.7% (0.046 ± 0.013) for Fruits and Vegetables, and a demand reduction of 2.3% for Pulses, Nuts, and Seeds (-0.024 ± 0.005). Both trends indicate that the fruits and vegetables food group provides a critical means to smooth consumption when grains and pulses become difficult to obtain or the quality of these items may be affected. Rural areas also experience a supply constriction of 8.4% (0.081 ± 0.028) for Dairy and Eggs prices

during heatwave months, indicating potential impacts to poultry and livestock during productivity during these periods.

Finally, in Sub-Saharan Africa, demand reduction of Breads and Cereals is observed in rural markets during heatwaves (-2.4%, -0.024 ± 0.005) and in both urban and rural markets during coldwave months (-3.9%, -0.04 ± 0.01; -3.3 -0.034 ± 0.013. Droughts and storms are inversely associated with supply reductions of 4.4-6.4% for Breads and Cereals and 9.0-10.5% for Pulses, Nuts,a and Seeds in urban markets.

Non-Crisis Period Subset

Due to the occurrence of three major economic crises during the study period, a subset was created by removing years with potential global impacts on retail prices (2008, 2010, 2011, and 2020-2022). We acknowledge the global heterogeneity of experiences during and after these crises and excluded the above years as an approximation of times where most markets in our dataset might have been affected. Although most lockdowns related to the Covid-19 pandemic ended in 2021, we completely exclude 2020-2022 in this subset due to potential bias from incomplete reporting and global supply chain effects on retail prices in 2021 and 2022 in the combined EWS dataset.

Application of the baseline regression specification to this subset generates effect estimates higher than those generated from the pooled sample, indicating that extreme weather events' association with retail prices is often more pronounced in non-crisis years. The difference may be due to greater frequency of non-extreme price observations during crisis periods in the EWS dataset, or potentially due to local and regional price regulation policies to curb inflation during periods of global crisis. Subsample estimates indicate a 15.1% increase in retail prices of Fruits and Vegetables during storm months, along with a 3.5% increase in Breads and Cereals and a 3.2% increase in Fats and Oils prices. Heatwaves and floods are

associated with net demand reduction, and floods in particular are associated with 2-3% lower demand for Breads and Cereals and Pulses Nuts and Seeds in urban areas.

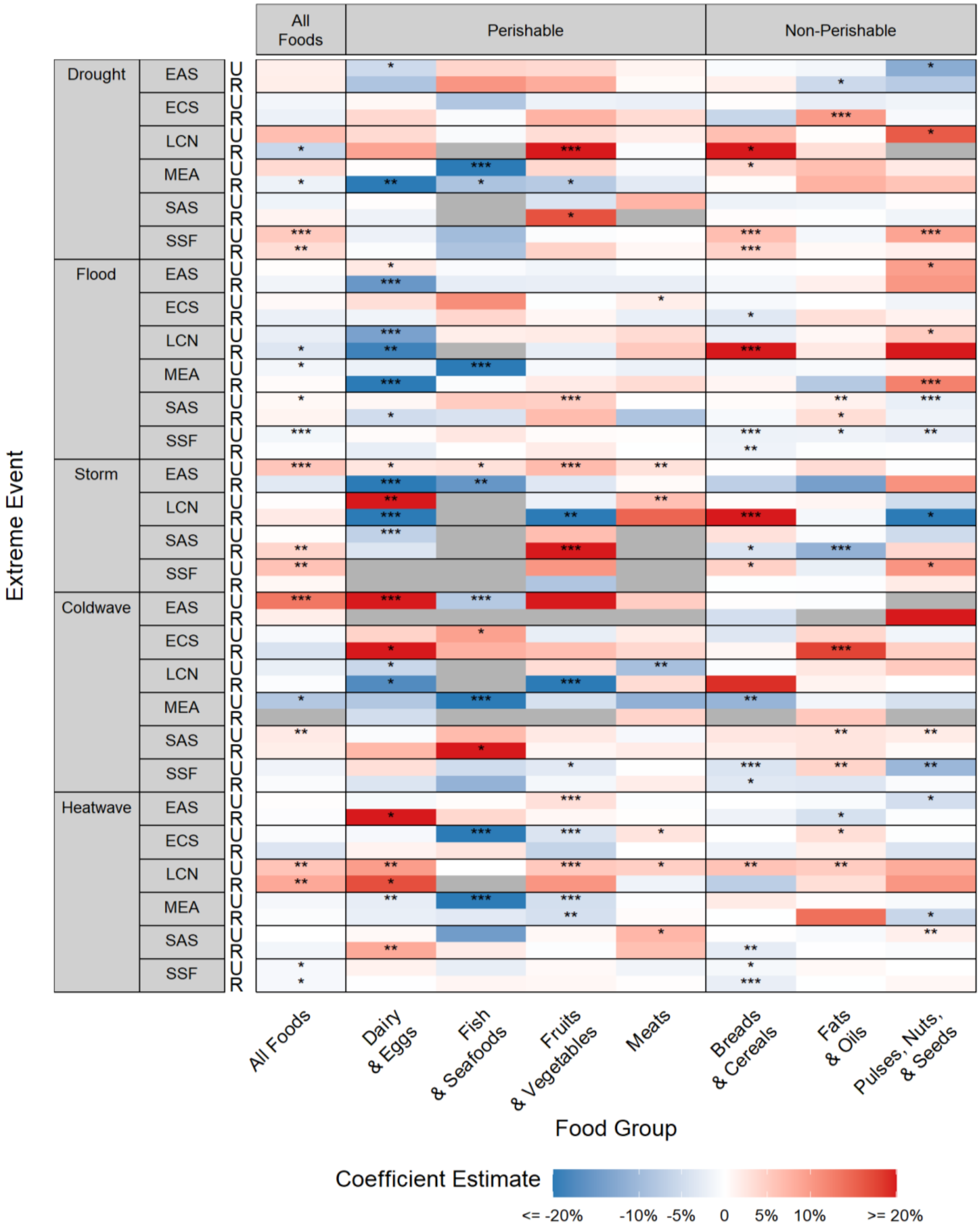

EAS: East Asia & Pacific, ECS: Europe & Central Asia, LCN: Latin America & Caribbean, MEA: Middle East & North Africa
SAS: South Asia, SSF: Sub-Saharan Africa. * p < 0.05, ** p < 0.01, *** p < 0.001.

Figure 17 Changes in retail price per 1000 kCal (%) by extreme events in the contemporaneous month, World Bank regional unit, market type (urban, and rural), and food group. Note: Sugar and Confectionery food group and Peri- and Sub-Urban market type are excluded due to data sparsity across most partitions.

Discussion and Limitations

This paper presents a novel database of retail prices from early waring systems (EWS) to test the relationship between extreme. We find significant heterogeneity in price changes across food groups, market types, and geographic regions. Due to relatively small magnitudes of fluctuations, we conclude that retail price are very resilient to extreme weather.

Several limitations affect presented results. Firstly, spatial resolution of both markets and source weather data influence our results. High resolution datasets were chosen to derive covariates, but pixel-level inconsistencies may have been abstracted into this analysis. Source earth observation datasets are also subject to error from variables such as cloud cover and smoke. The NASA Level 3 products utilized in this analyses are already corrected for common issues, but available percent accuracy fields for each source raster were not examined. This may be particularly challenging during periods of greater storm activity or flooding when cloud cover is more likely to introduce error in earth observation. The accuracy of market GPS locations may also contribute to spatial error. GPS points were validated to ensure points are located on land, but no further corrections were made to coordinates obtained from the EWS databases.

Temporal resolution is another key limitation. The GIEWS and FEWS databases provide weekly time series of retail price data from a subset of markets which were not utilized here; instead, we use monthly average retail prices to match the temporal scale of chosen earth observation data. This decision is associated with loss of precision (T. M. Alarcon Falconi, Estrella, Sempertegui, & Naumova, 2020) and limited ability to support early warning. Analysis of earth observation data at the weekly scale is also computationally intensive, and more readily

realized at smaller spatial scales. However, the monthly time scale provides a more representative time interval to measure net outcomes of complex supply and demand forcings on retail prices. The monthly time scale is more commonly used in literature as well (Brown & Kshirsagar, 2015; Cedrez et al., 2020; Letta, Montalbano, & Pierre, 2021). However, as computational capacities improve, future work can study weekly time series to generate more precise estimates of extreme weather and its effects on retail prices.

The constructed market categories (urban, rural, peri- and sub-urban) utilized in this analysis can also bias effect estimates. The DEGURBA classification from which our typology was derived, faces several limitations including discrepancies in official population statistics, distinctions between adjacent conurbations, and somewhat arbitrary population thresholds to distinguish between categories (Dijkstra, Brandmüller, Kemper, Khan, & Veneri, 2020; Dijkstra, Poelman, & Veneri, 2019) An inverse source of error is also identified, whereby destruction of built-up area from natural disasters may affect input datasets used to derive the DEGURBA classification. Despite these limitations, this dataset was developed specifically for the purpose of facilitating international comparisons, and is thus extremely pertinent to the scope of our analysis. Despite the small sample size of Peri- and Sub-Urban markets (12.4%), we retain this category to demonstrate the gradient of climate impacts across our analysis. Future work can utilize more detailed DEGURBA classifications which can be used for identifying particular trends among subsamples of urban areas such as intensifying suburbs, urbanizing rural areas, and de-urbanizing cities (Table 6). The latter category is particularly relevant for investigations on the feedback loops between violence and retail prices of food and fuel as leading indicators of food insecurity (Raleigh, Choi, & Kniveton, 2015).

Human error in price data collection also impacts our analysis. All EWS databases collect retail prices from various national agencies and institutions and are thus subject to errors in the process of recording, reporting, and curating price data. We utilize a simple order of

magnitude correction to identify and correct obviously egregious outliers; however, limited means are available to validate each data point. We further recognize that many critical data points may be collected during periods of social distress such as hyperinflationary periods, extreme food insecurity, and/or prolonged violent conflict. Given this context, we advocate for robust post-processing methods to help identify and resolve these errors. Sufficiently long time series data can allow for reasonable imputation of values, which further facilitates scenario development and forecasting of extreme weather impacts. Further standardization of ambiguous unit measures such as loaf, sack, and packets can help reduce human error and allow analysts to retain more data for downstream analysis and early warning.

Conclusions

This observational study quantifies the association between various extreme weather events and anomalies and retail food price changes. We discover heterogenous impacts across food groups, underscoring the importance of monitoring retail prices of a diverse range of foods to sustain healthy and affordable diets. Our results suggest that extreme events differentially affect retail food prices across low and middle income countries. Perishable food groups such as Fruits and Vegetables and Dairy and Eggs are most significantly impacted by moisture-related extreme events such as Storms, Floods, and Droughts.

Chapter 5: Acute Malnutrition Seasonality in Cross-Sectional Data

Introduction

Reduction of wasting or low weight-for-height is a key target towards the Zero Hunger Sustainable Development Goal. In 2022, approximately 45 million children under five suffered from wasting, with 93% of the global burden in low- or lower-middle-income countries [REF: SOFI 2022]. Despite the recognition of this inter-sectoral priority, accounting for locally specific seasonal patterns of wasting remains a “missing piece” of the nutrition puzzle (Baye & Hirvonen, 2020; UNICEF, WHO, & IBRD/WB, 2020). Short-term fluctuations in weight and weight-for-height measures render nutrition surveillance of relevant indicators particularly challenging (Chotard, Mason, Oliphant, Mebrahtu, & Hailey, 2010; Vaitla, Devereux, & Swan, 2009).

Existing measures of wasting seasonality are limited by the low frequency and incompatible goals of source surveys, invariant survey timings, and survey designs which reduce the complexity of overlapping agroecologies and livelihoods. Estimates of wasting prevalence most frequently derive from national household surveys which aim to study incomes and expenditures rather than fluctuating anthropometries. Surveys therefore prioritize access to respondents during economically significant periods of pre- and post-harvest among agricultural households, rather than collecting data year-round. Economists’ goal of measuring large-scale changes in incomes and expenditures is also reflected in the measurement frequency of 3-5 years, which is functionally meaningless for monitoring short-term fluctuations in wasting. Enumerators’ access to surveyed communities is also governed by seasonal phenomena such as flooding and extreme heat; therefore, national household surveys may be repeated during convenient times of the year and during the same seasons rather than being staggered throughout the calendar year (Baye & Hirvonen, 2020; UNICEF et al., 2020). Finally, survey designs which stratify the sample across administrative boundaries in place of climatic or livelihood

aggregations can mask variabilities across these domains. Extensive qualitive research demonstrates that households with varying livelihoods often coexist in close proximity and may often pool resources. Point estimates of wasting prevalence obtained from cross-sectional surveys can therefore not be utilized to study meaningful trends due to limited representativeness and repeat observations during a calendar year (Baye & Hirvonen, 2020).

In the temporal domain, current knowledge about wasting seasonality is limited by the practice of constructed temporal groupings such as seasons, which obscure continuous variation within the calendar year. We demonstrate this limitation using data from rapid assessment surveys conducted in arid regions of Sub-Saharan Africa in a previous study (Venkat, Marshak, Young, & Naumova, 2023). Qualitative studies further indicate that these categories are often not aligned with local seasonal calendars (FAO and Tufts University, 2019), and likely emerged from disciplinary foci on production-oriented agricultural calendars. Although previous literature has suggested linkages between seasonal wasting and rainy and/or agricultural lean seasons (Chambers, 2007), these associations are difficult to validate or quantify in the absence of disaggregated data which studies phenomena at higher temporal resolutions (Marshak, Venkat, Young, & Naumova, 2021). Limited availability of global agricultural calendars further limits the application of such categories at large spatial scales, and serves as an important limitation in the utility of existing cross-sectional datasets for seasonality analysis.

These data limitations can be overcome by pooling data from existing cross-sectional domain and aligning spatial and temporal boundaries to facilitate seasonality analysis. Survey data provide a long-term record of frequent cross-sectional observations in multiple locations to effectively analyze seasonality. One valuable secondary dataset to study nutrition seasonality is the 15-year compilation of child-level anthropometry from Standardized Monitoring and Assessment of Relief and Transition (SMART) surveys (Isanaka, Boundy, Grais, Myatt, & Briend, 2016). The compiled SMART dataset has previously been used to study the relationship

between stunting and wasting in emergency contexts (Isanaka et al., 2016), as well as seasonal differences between agricultural and agro-pastoral communities in sub-Saharan drylands (Venkat et al., 2023). Other valuable datasets include the USAID Demographic and Health Surveys (DHS), which has been collecting household data in 90 countries for over 30 years, as well as the UNICEF Multiple Indicator Cluster Survey, which has been collecting a slate of public health indicators from households in 120 countries for 29 years. Pooling data from all three sources can provide a valuable database of anthropometry with potentially overlapping observations to sufficiently characterize wasting seasonality where present.

This chapter extends previous work on the topic of seasonal patterns of wasting through several key improvements. We improve the underlying seasonality methodology of multiple harmonic regression to sharpen the precision of estimated seasonal features. We also expand the source data to include anthropometry measurements from SMART, DHS, and MICS databases. Finally, we further add resolution to the analysis by utilizing Koppen climate classifications as opposed to general aridity classes, and partition the data by dominant precipitation modality to account for varied livelihoods, resource use patterns, and resultant pathways to undernutrition. The spatial scope of this study is limited to the continent of Africa. This approach underlines environmental variability as a basic driver of acute malnutrition and further enriches current knowledge on the linkages between wasting and the environment.

Data Sources

The anthropometric outcomes utilized in this dataset derive from three main data sources. The first is a compilation of anthropometry from Standardized Monitoring and Assessment of Relief and Transition (SMART) surveys originally implemented by non-governmental organizations and United Nations organizations for nutrition assessment in emergency and development settings (Myatt et al., 2018). The source dataset was provided to authors upon request by Mark Myatt in September 2017 (Myatt et al., 2018). This dataset has been previously analyzed as part of initial SMART assessments for each county, and collectively to investigate global patterns of stunting and wasting (Isanaka et al., 2016; Myatt et al., 2018). The SMART dataset contains observations for a total of 1,886,293 children from 52 countries during 2000 – 2015. The SMART survey methodology utilizes standardized survey questionnaires to measure nutritional status of children under age five (SMART, 2017). SMART surveys also utilize a reliable cluster sample size of at least 900 children from 30 households in 30 clusters (SMART, 2017). SMART surveys are intended for rapid assessment of acute malnutrition, and the comparable survey methodology allows for reasonable time series analysis. Although this dataset is biased towards rural populations facing complex crises (FAO and Tufts University, 2019), it provides valuable data on extreme wasting in critical populations.

The second dataset derives from IFPRI's Advancing Research on Nutrition and Agriculture (AReNA) GIS dataset. This is a convenient compilation of USAID Demographic Health Surveys (DHS) spatially matched to geo-referenced data on various factors including agricultural production, agroecology, climate, demography, and infrastructure. The complete AReNA-DHS dataset includes DHS data from 184 demographic health surveys (DHS) surveys implemented in in 60 countries. These data provide observations for a total of 1,919,707 children from 82 countries during 1986 - 2022. AReNA-GIS also provides the GPS coordinates of the DHS survey clusters where available with urban clusters displaced by up to 2 kilometers and rural

cluster locations displaced by up to 5 kilometers with a further 1% of the rural clusters displaced by up to 10 kilometers (Burgert, Zachary, & Colston, 2013) This jittering is implemented by USAID to preserve anonymity. The spatial scale of displacement distances are unlikely to cause drastic differences in climatology.

The final dataset derives from a compilation of Multiple Indicator Cluster Surveys implemented by the United Nations International Children's Emergency Fund. A total of 185 completed surveys were identified, and data from 1,588,171 children were identified as containing data on both subnational geography, survey month, as well as anthropometry for children under age five. The compiled MICS dataset contains observations for a total of 1,298,979 children from 125 countries during 1999 – 2022.

Methods

Data Cleaning and Verification

No data cleaning was performed for the AReNA-GIS dataset as this has already been processed and standardized by USAID and IFPRI. The SMART dataset has been cleaned and standardized for several previous publications (Isanaka et al., 2016; Myatt et al., 2018; Venkat et al., 2023).

To generate the combined MICS dataset, all publicly accessible survey datasets were downloaded from the MICS website on November 18, 2018 and updated on April 15, 2023. The following fields were extracted from each survey where available: survey timing fields (year, month, day, and date of interview), surveyed location fields (administrative levels 1 – 3 indicating where survey was implemented), raw child anthropometry, sex, age in months, calculated Z scores for weight-for-height (WHZ) and height-for-age (HAZ), and fields flagging implausible values in these calculated indices (WHZFLAG, HAZFLAG). If WHZ and HAZ fields were not available but raw anthropometry fields were, WHZ and HAZ were calculated based on

established WHO anthropometric and clinical cutoffs (WHO, 2000; WHO & UNICEF, 2009). Extracted data were then coalesced into standardized fields and duplicate values were removed. Observations missing subnational location information or at least the month and year of interview were removed. If the survey was conducted in an IDP or refugee camp based on the reported administrative regions, collected observations were flagged and subsequently removed since individuals in these settings rely on humanitarian aid and may thus be subject to different seasonal patterns (Darrouzet-Nardi & Masters, 2017; Kim, Humphrey, Marshak, Gathuoy, & Krishnan, 2020) . Observed GAM may also be artificially high in these settings due to population displacement and extreme asset depletion. Observations flagged as biologically implausible according to the WHO reference standards, defined as defined as WHZ>5 or WHZ<-5, were also removed.

Location matching

No location matching was performed for the AReNA-GIS dataset as approximate GPS points of survey clusters were already provided.

For the SMART and MICS datasets, location fields from each survey were cleaned to remove duplicate information and ensure that the matched spatial boundary accurately represents the narrowest administrative level in which the survey was implemented (e.g. district, town, or village). The matching itself was implemented using fuzzy string matching between the text describing the complete survey location and a list of administrative divisions compiled from the FAO Global Administrative Unit Layers (GAUL) dataset (FAO, 2015), Global Administrative Boundary Database (GADM) (Global Administrative Areas (GADM), 2012), and the United States Agency for International Development (USAID) Demographic and Health Survey (DHS) Spatial Data Repository (ICF, 2019). These three datasets combined include the majority of enumerated subnational administrative boundaries around the world.

Fuzzy string matching was utilized to compare the target survey location to the list of reference administrative boundaries within the survey country, and extract the most likely match based on the Levenshtein distance between strings [REF]. A combination of country name and increasingly higher level administrative boundaries were tested for string matching, and the most accurate match was retained. If multiple matches were found, the smallest administrative boundary that most accurately represents the spatial extent of the survey was selected. A GADM boundary was prioritized over a DHS boundary, and a DHS boundary was preferred to the GAUL matched boundary. All matching was done using the fuzzywuzzy package in R, and all results were manually reviewed and iteratively corrected. The only country that could not be matched to spatial data was Trinidad and Tobago (MICS 2006 and 2011) due to lack of reference data matching appropriate survey administrative boundaries. Details about this matching process are provided in Technique 2: Matching Surveys to Spatial Boundaries with Fuzzy Matching.

Covariate Extraction

Text matching allows for the extraction of a spatial boundary for each surveyed location. However, due to vast differences in population densities across the study region, a further layer of spatial subsetting was applied to subset the most likely surveyed areas within each administrative unit, and thereby match observed populations to the environment to which they were most likely exposed.

Each survey extent feature was intersected with the Global Human Settlement Layer (GHSL) Degree of Urbanization (DEGURBA) classification (Florczyk A.J., 2019; Pesaresi et al., 2019). The 2023 DEGURBA dataset is available for the years 2000, 2005, 2010, 2015, and 2020; the classification closest to the survey year was chosen as most appropriate. Within each survey feature, pixels classified as Very Low Density were removed from the matched survey. This classification corresponds to over 99% of the study area as shown in Figure 18. Very Low

Density pixels correspond with sparse and distant human settlements which may be difficult to access as part of national surveys such as the MICS and DHS. Inclusion of these areas may also distort the extracted climate exposures due to the independent and dependent variables not sharing a common spatial extent. Therefore, Very Low Density pixels were excluded and the remaining areas were utilized for further analysis.

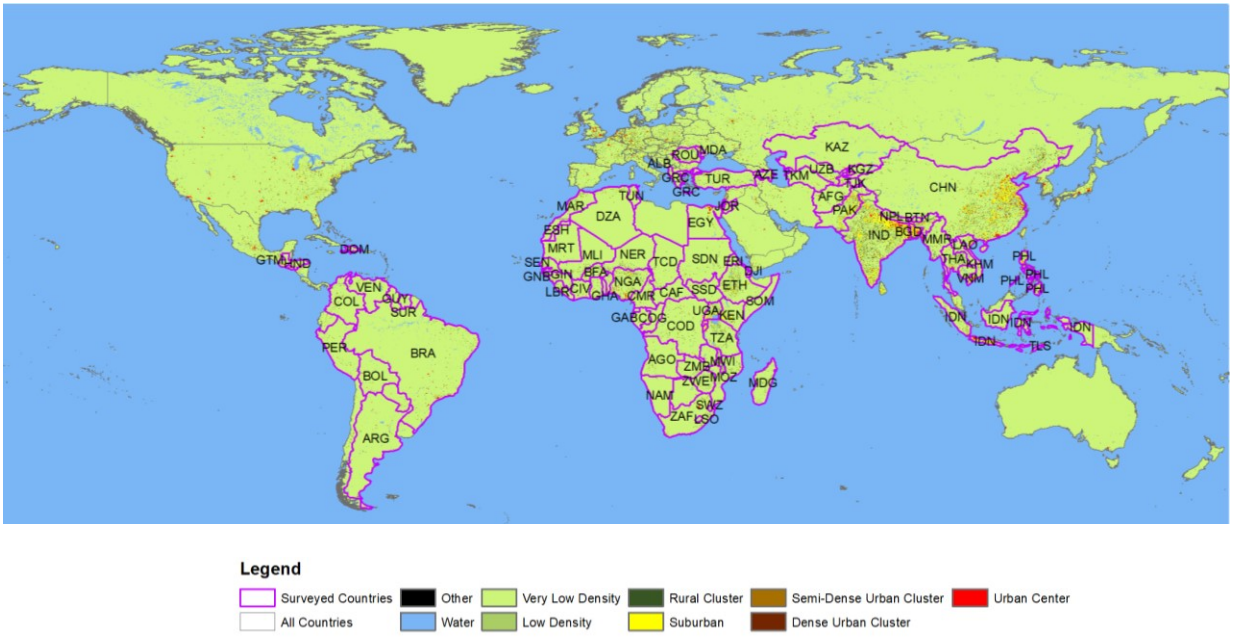

Figure 18 Global Human Settlement Layer (GHSL) Degree of Urbanization (DEGURBA) classifications in countries common to DHS, MICS, and SMART datasets. Very Low Density pixels comprise a majority of the analysis and are therefore excluded.

Each survey boundary feature classified as low or higher population density based on the DEGURBA classification was then spatially intersected with two global shapefile comprising dominant rainfall patterns (Knoben, Woods, & Freer, 2019) and levels 1 – 3 Koppen-Geiger classifications (Beck et al., 2018) respectively. Therefore, if a survey region includes multiple Koppen classes, only the classification which applies to the largest area was retained. The distribution of these features are shown in Figure 19.

The following R packages were utilized for spatial analysis: rgdal (R. Bivand, Keitt, & Rowlingson, 2019), rgeos (R. Bivand & Rundel, 2018), raster (Hijmans, 2019), tmap (M, 2018), spdep (R. S. Bivand, Pebesma, & Gomez-Rubio, 2013), and sf (Pebesma, 2018).

Dataset	Dominant Precipitation Pattern	Koppen Climate Classificatio
SMART	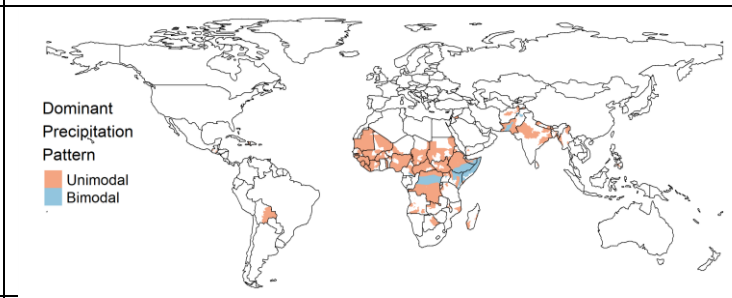	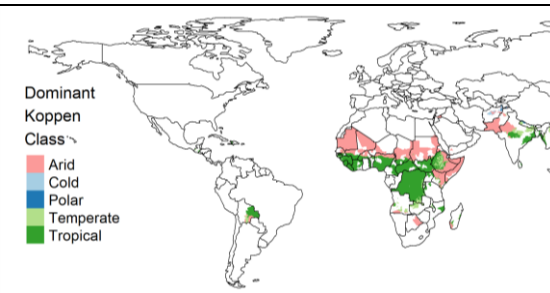
MICS	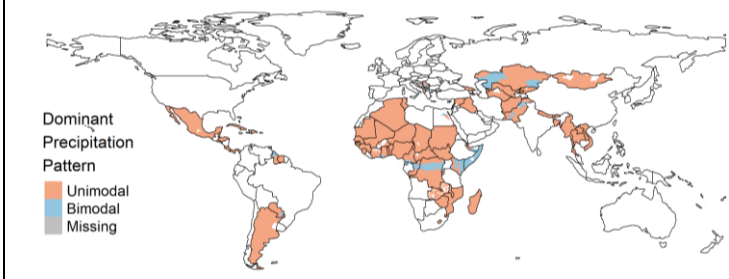	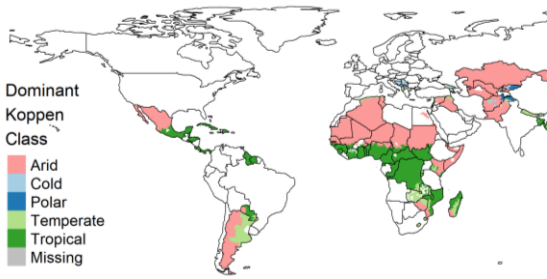
DHS	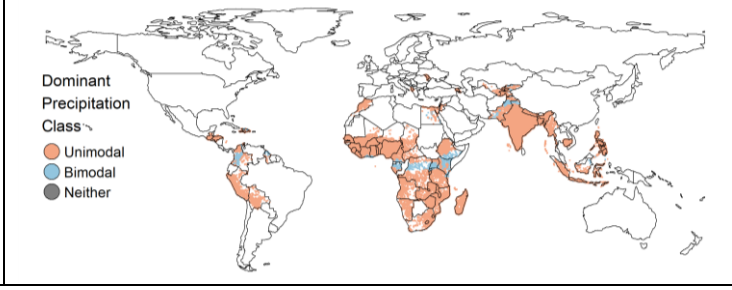	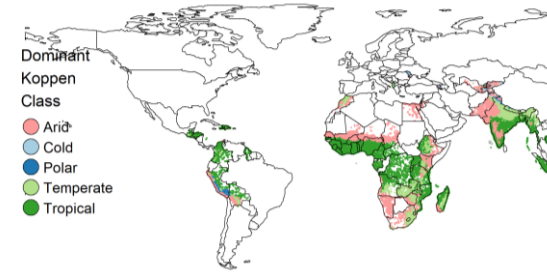

Figure 19 Maps of spatial extent of SMART, MICS, and DHS survey data, classified by (left) rainfall patterns and (right) Koppen level one climate classifications

Extreme Weather

Data on tropical cyclones and storms were extracted from the International Best Track Archive for Climate Stewardship (IBTrACS) storm track database (Knapp et al., 2010). Consistent with the exploration detailed in Technique 3: Extraction of Weather Extremes from Gridded Data, the average radius of storm-force winds (25 m/s) or higher was used to determine if a survey region suffered from a storm.

Both temperature and precipitation averages were used to calculate the location-specific time series of the 6-month Standardized Evapotranspiration Index (SPEI) values to characterize droughts (Beguería et al., 2010; Beguería et al., 2014). SPEI was calculated using monthly average temperature values from the MODIS MOD11C3 MODIS/Terra Land Surface Temperature/Emissivity Level 3 product (Wan et al., 2015) dataset and the monthly average precipitation values from the Climate Hazards Group InfraRed Precipitation with Station data (CHIRPS) dataset (C. Funk et al., 2015). The CHIRPS dataset was used to calculate the 1-month Standardized Precipitation Index (SPI) to characterize floods. Values above the 95th percentile of SPI were classified as floods, and values below the 5th percentile of SPEI were classified as droughts. If at least 10% of the survey area experienced a flood or drought during the survey month, it was classified as such.

Maximum and minimum temperature values were extracted from the Terraclimate (Abatzoglou et al., 2018). Maximum temperature values above the 95th percentile were classified as heatwaves, and minimum temperature values below the 5th percentile were classified as coldwaves. If at least 10% of the survey area experienced a heatwave or coldwave during the survey month, it was classified as such.

Based on the above minimal definitions, only 21 instances of extreme events were observed within the joint survey dataset. This limited sample size was insufficient to run further analyses to investigate extreme weather effects. Therefore only seasonal wasting was explored further.

Estimation Strategy

Seasonality Analysis

The choice of regression model to be implemented depends in large part on the distribution of the outcome of interest. Child-level wasting and regional average GAM can be modeled in many ways; previous analyses have compared child-level logit regression and population-level beta regression and found that seasonal characteristics derived from both formulations are sufficiently similar (Venkat et al., 2023). Although previous studies have applied logistic regression to study associations between wasting and various independent variables, an analysis of seasonality can be implemented across various functional forms. The distribution of binary wasting across the defined Koppen and precipitation partitions presents another challenge for seasonality modeling. Figure 20 provides a visual summary of the survey characteristics using L-moments, or unbiased normally distributed measures of distribution parameters (Hosking, 1990). Positive L-Skewness values indicate a long right tail, and large values of L-skewness values generally suggest high volatility in wasting outcomes. Overall positive L-Kurtosis values indicate a more peaked distribution on average, although a wide range of sample characteristics are noted. The overall bow shape of the L-moment diagram indicates that based on distribution characteristics, any univariate distribution in the Generalized Gamma or Beta families could potentially fit this data (Vargo, Pasupathy, & Leemis, 2010). However, the goal of this analysis is not to extract a model of best fit, as we have very limited knowledge about the functional form of the processes by which wasting is observed in any of these cases. Since the goal is extraction of seasonal characteristics, we decide to test three

regression formulations in each partition: the child-level logit regression of wasting outcomes, the Poisson regression of wasting counts, and the beta regression of GAM rates.

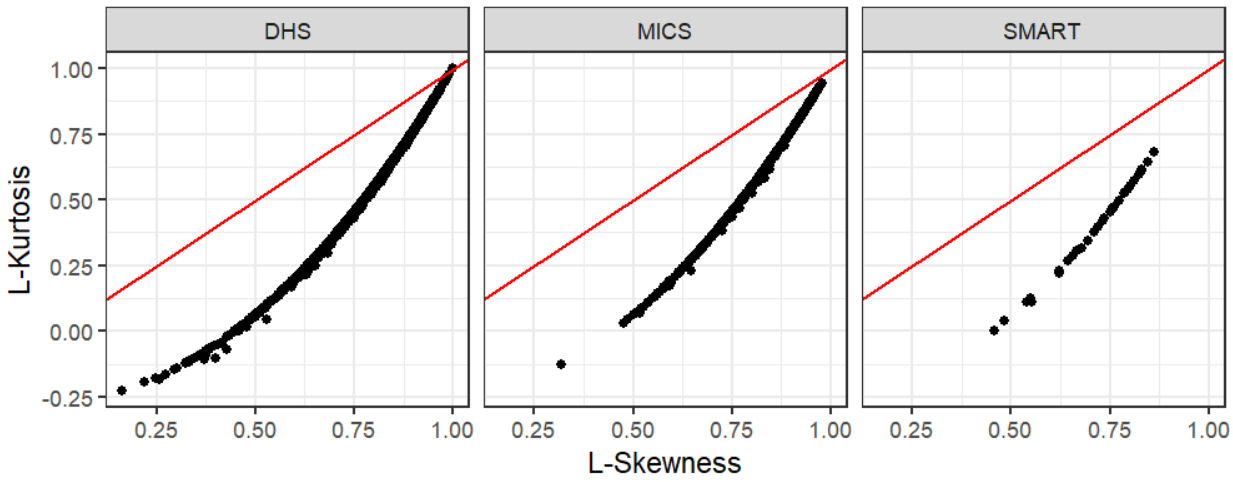

Figure 20 L-moment diagram for DHS, MICS, and SMART datasets. Each dot represents a set of sample L-moments derived from survey data partitioned by level one Koppen climate class and precipitation mode.

Multiple harmonic seasonality was tested with three specifications of the canonical regression where the outcome *O* is observed at Koppen class K, dominant precipitation type P, and continuous time *t* which is recorded as a continuous sequence of days or months in the study period. Assuming an annual cycle, ω refers to a constant cycle duration of 12 months or 365.25 days which constitutes the calendar year. *T(t)* is a cubic polynomial of to accommodate nonlinear fluctuations and long-term trends. The first specification tested child-level wasting using a logit regression (Equation 3), the second specification used a Poisson regression of counts of wasted children (Equation 4), and the third specification tested GAM prevalence using a beta regression (Equation 5). Given that the underlying factors generating these outcomes are the same, we expect similar seasonal characteristics identified from each model.

Complete details regarding the harmonic regression methodology are presented in Chapter 3: Techniques and Workflows for Spatial and Temporal Alignment in the Technique 1: Multiple Harmonic Regression section. The particular features of interest in this analysis is the peak timing of wasting and its confidence interval, which indicates the duration of greatest expected

wasting in each partition. To assess the reliability of the peak timing estimate, we also utilize the calculated peak value of wasting, which provides estimated likelihood of wasting or GAM prevalence depending on the specification.

$logit(Wasting)_{K,P,t} = \beta_0 + \beta_1 \sin(2\pi\omega t) + \beta_2 \cos(2\pi\omega t) + \beta_3 \sin(4\pi\omega t) + \beta_4 \sin(4\pi\omega t) + \beta_5 T(t)$	*3*
$Poisson(Wasted\ Children)_{K,P,t} = \beta_0 + \beta_1 \sin(2\pi\omega t) + \beta_2 \cos(2\pi\omega t) + \beta_3 \sin(4\pi\omega t) + \beta_4 \sin(4\pi\omega t) + \beta_5 T(t)$	*4*
$GAM_{K,P,t} = \beta_0 + \beta_1 \sin(2\pi\omega t) + \beta_2 \cos(2\pi\omega t) + \beta_3 \sin(4\pi\omega t) + \beta_4 \sin(4\pi\omega t) + \beta_5 T(t)$	*5*

Sensitivity Analyses

Several alternate specifications were tested to examine the stability of calculated seasonal characteristics. The cycle duration of 12 months was tested by using survey dates standardized to the first of the month, whereas a cycle duration of 365.25 days served as a comparison by using the exact survey date. This comparison studies the effect of aggregation in time series, and the loss of precision when inexact dates are used for calculation of seasonality characteristics. Extracted seasonal features including peak timing and magnitude were compared across model specifications. Results are presented in Appendix 3: Sensitivity Analysis of Seasonal Wasting Curves.

Results

Data Description

Table 9 Characteristics of Source Cross-Sectional Survey Datasets

Characteristics / Dataset	***SMART***	***MICS***	***DHS***
Number of Observations	1,383,463	608,067	600,103
Number of Surveys		78	105
Spatial Resolution	Level 1 Administrative Unit	Level 1 Administrative Unit	Cluster (2-10 km)
Covered Time Period	2000 - 2015	1999 - 2020	1990 - 2020
Observations by Decade			
1990s		1% (n = 5,913)	15% (n = 88,111)
2000s	43.75% (n = 604,245)	24% (n = 145,684)	33% (n = 200,308)
2010s	56.3% (n = 779,218)	72.9% (n = 443,113)	52% (n = 311,640)
2020s		2.2% (n = 13,357)	0%
Survey Frequency			

Percentage of Survey Population by Koppen Classification			
Tropical	64.5% (n = 892,755)	58.0% (n = 352,398)	50.4% (n = 302,525)
Arid	27.1% (n = 374,628)	29.7% (n = 180,724)	33.5% (n = 200,966)
Temperate	8.39% (n = 116,080)	12.2% (n = 74,381)	16.1% (n = 96,584)
Cold		0.1% (n = 564)	
Percentage of Survey Area by Precipitation Mode			
Unimodal	81.6% (n = 1,128,746)	94.5% (n = 574,638)	90.2% (n = 541,050)
Bimodal	18.4% (n = 254,717)	5.5% (n = 33,429)	9.8% (n = 59,053)

Spatial Distribution of Surveyed Populations

The spatial distribution of sample sizes across each of the studied dataset is shown in Figure 21. The SMART dataset contains the most repeat observations, particularly in Oromiya and Amhara states of Ethiopia, and parts of the Democratic Republic of Congo. The MICS dataset has fewer repeat observations, with the highest sample sizes in West Africa (Sierra Leone, Gambia, and parts of Mali). A large area of large sample size is also observed in Algeria in the MICS dataset; however, this region encompasses a large portion of the Sahara desert with small pockets of settlements which were likely surveyed as part of one sampling area comprising several similar administrative regions. Finally, the DHS dataset provides the highest spatial resolution of sampled areas at the community level. As with the MICS dataset, large sample sizes are observed in southern Mali, Gambia, Sierra Leone, and parts of Benin and Nigeria. In both cases, areas with large sample sizes and lighter colors indicate locations where the survey has been established for a sufficiently long time, and likely yields multiple observations for a more reliable estimate of seasonality. On the other hand, map regions with darker colors indicate fewer samples and therefore less confidence in derived seasonality estimates.

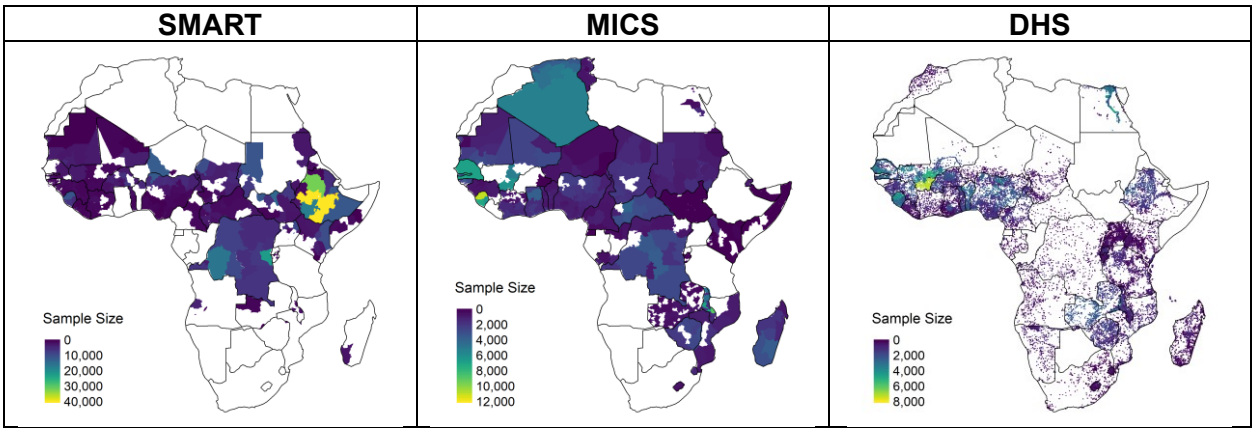

Figure 21 Maps of subnational sample sizes within each of SMART, MICS, and DHS datasets.

Temporal Distribution and Survey Completeness

The temporal distribution of survey observations across all three datasets is shown in Figure 22. The MICS dataset contributes the least number of surveyed children (n=594,791; 31.3%) to the overall analysis, followed by DHS (n=600,122; 31.3%) and then SMART (n=720,434; 37.6%). In general, the large areas of grey indicate that most partitions are sparse—i.e. surveys are conducted at particular times and in particular regions, and results are therefore unlikely to be spatially or temporally representative. The biased sampling is evident in the Temperate, Bimodal partition, where data is only available from the DHS dataset in seven countries. Sparse partitions are also observed in the MICS dataset in Arid, Bimodal regions, and in the SMART dataset in Temperate, Unimodal and Tropical, Bimodal regions. It is also notable that surveys in the study region are generally never implemented in December or January, indicating a critical data gap. This likely reflects social, administrative, and/or logistical challenges to survey implementation during these months across the region.

Temporal completeness presents yet another challenge to seasonality analysis. Complete stretches of data availability are common, but data are not uniformly distributed across calendar months. The DHS dataset exhibits lots of variability in monthly sample sizes, and the variability of the SMART dataset is somewhat masked in Figure 22 due to larger overall sample sizes. The

MICS dataset indicates the lowest completeness of the three datasets, with comparatively fewer monthly sample sizes distributed across a more years compared to the SMART dataset which ends in 2015. Although no clear patterns are apparent, Figure 22 allows us to conclude that these time series are likely not stationary and a flexible harmonic specification might be valuable for seasonality analysis.

Figure 23 demonstrates the distribution of GAM prevalence by each partition. No clear evidence of seasonality is present across any partition. The SMART dataset seems to provide a slightly higher average GAM estimate of 12.1% compared to MICS (8.29%) or DHS (8.27%). In the Arid, Unimodal partition the months of May – July appear to generally have higher GAM compared to the rest of the year; however this pattern requires statistical validation.

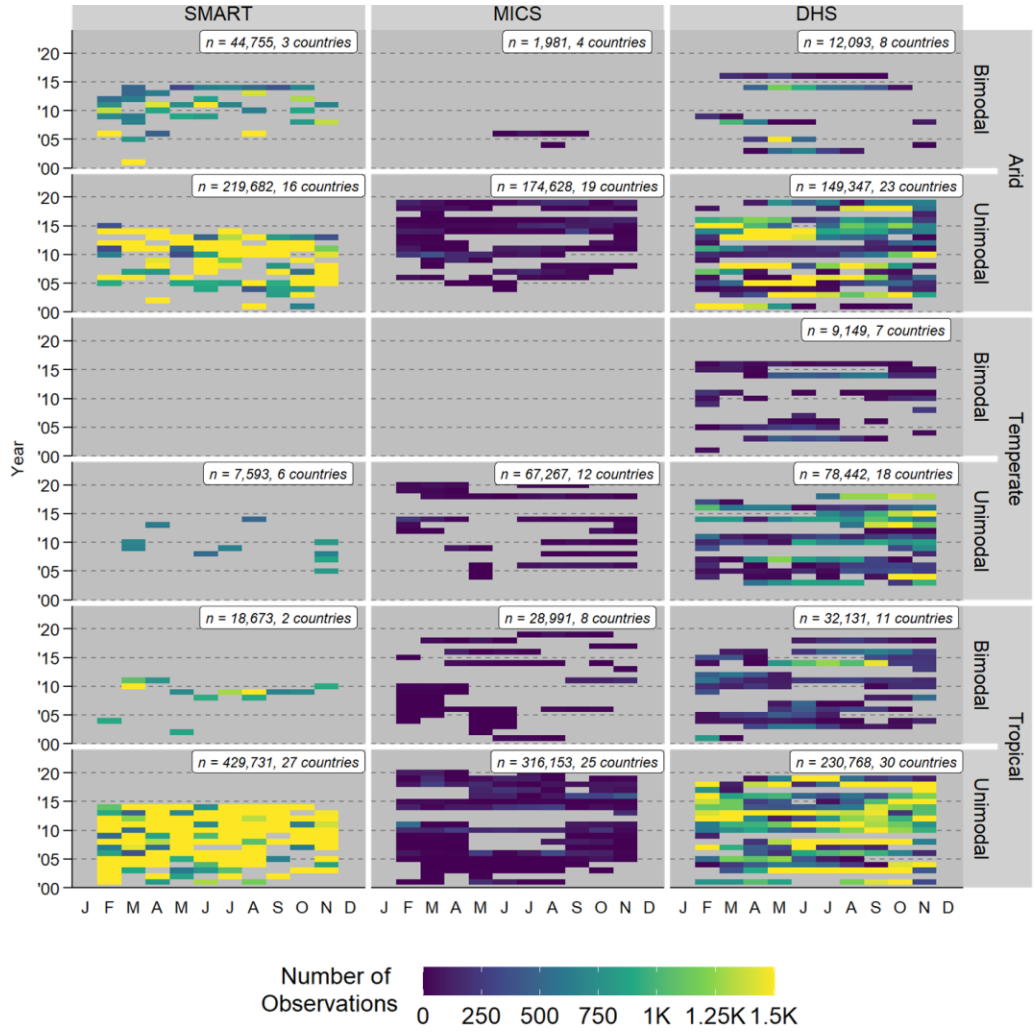

Figure 22 Heatmap of the number of observations and surveyed countries by month and year across SMART, MICS, and DHS datasets. Subplots indicate partitions by Koppen Level 1 class and precipitation modality.

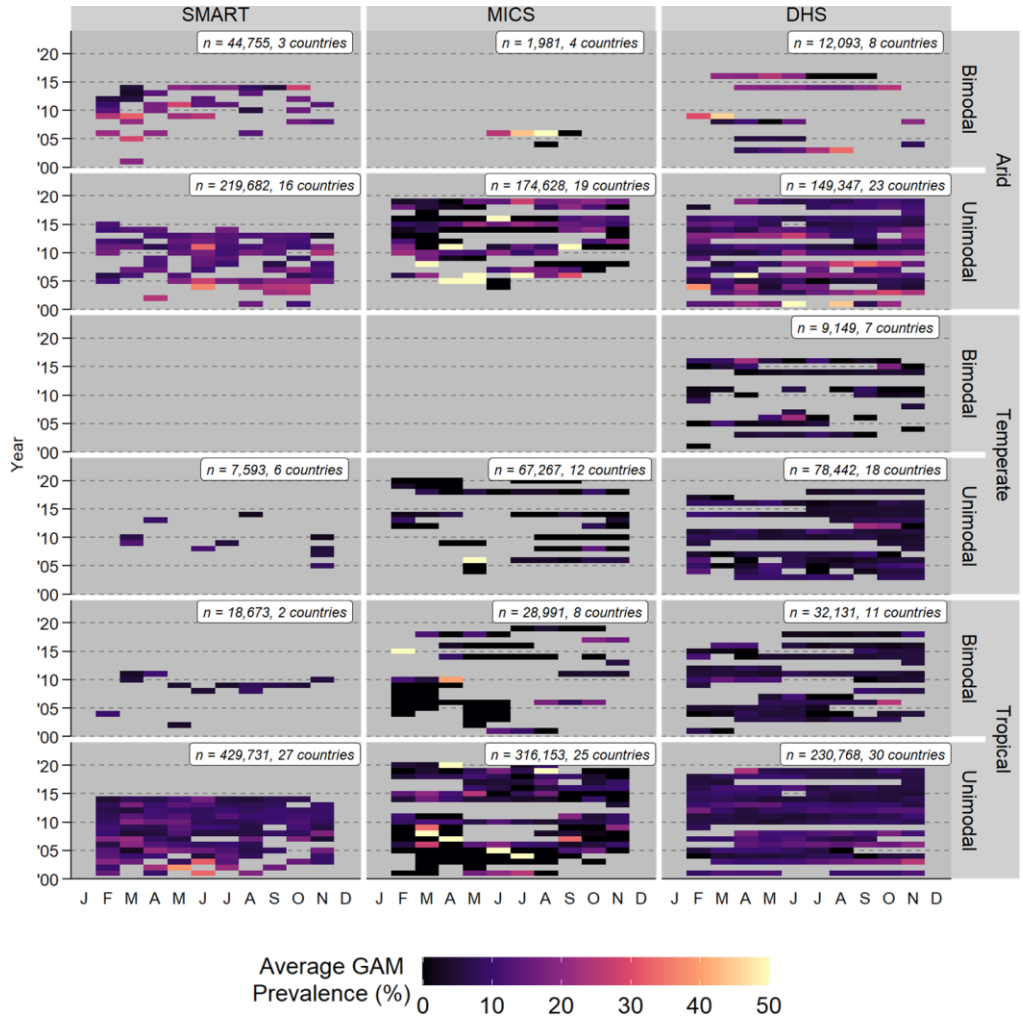

Figure 23 Heatmap of the prevalence of GAM and surveyed countries by month and year across SMART, MICS, and DHS datasets. Subplots indicate partitions by Koppen Level 1 class and precipitation modality.

Seasonality Analysis

Country-Level Patterns

Figure 24 provides a simple visualization of the peak timings identified by multiple subregions within each country and partition. Wider portions of each violin indicate greater probability of peak timing occurring during this time. In general, Unimodal Temperate and Tropical regions exhibit extensive variability in peaks, as evidenced by narrow bands that extend throughout the year. In contrast, some countries provide preliminary evidence of two peaks in some regions; e.g. bimodal Tropical regions of Zambia, and Arid Unimodal Ethiopia and Algeria. Particularly

narrow periods of peak timings are also observed, for example in Temperate Unimodal Tanzania and Tropical Unimodal Liberia.

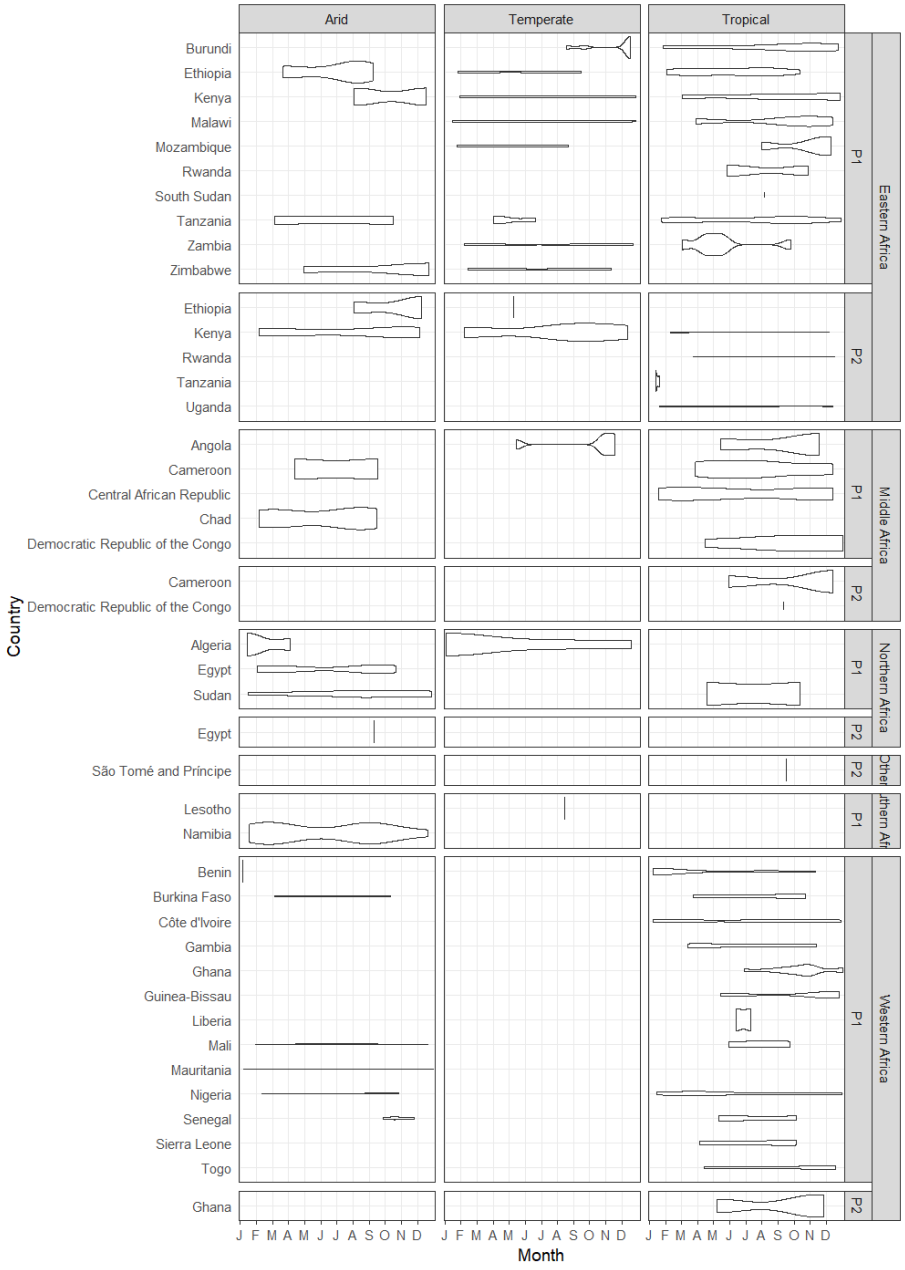

Figure 24 Violin plots of peak timings by Koppen class (x axis) and precipitation modality (y axis), organized by geographic region and country.

Peak Timings

As tabulated in Appendix 3: Sensitivity Analysis of Seasonal Wasting Curves, a wide distribution of peak timings are observed from models where multiple harmonic regressions identify

statistically significant seasonality. Although few patterns are immediately evident, the widespread heterogeneity is preliminary evidence that seasonal wasting is a localized phenomenon, and requires further investigation and validation using higher resolution data if available.

Although harmonic regression is technically feasible with a sparse dataset, we identify the pitfalls of using this method with exceedingly spare data in Appendix 3: Sensitivity Analysis of Seasonal Wasting Curves. Temporal completeness of less than roughly 7% is associated with implausible and potentially erroneous values of peak timings and estimated peak values, thereby providing an approximate ex-post diagnostic of model reliability. We conclude that a minimum threshold of 7% temporal completeness is required to obtain plausible values of seasonal characteristics. Therefore, seasonality results from partitions with less than 7% completeness and/or implausibly high peak values of wasting are not interpreted further.

Subnational Patterns

Figure 25 demonstrates a map of harmonic patterns of wasting using pooled data across the three datasets modelled using a beta regression (5). The SMART dataset points to a clear belt of unimodal wasting in the Sahel region. Just below this belt, a region of bimodal wasting is observed in Somalia, southern Ethiopia, and northern Kenya. Comparing this region against the MICS dataset reveals some differences since MICS surveys often have higher spatial resolution than the SMART dataset. The Sahelian belt identified from the SMART analysis is observed to have some localized variations at the Eastern and Western extremes in the MICS dataset. This variation is noticeable particularly around the Kassala region of Sudan and the Dakhlet-Nouadhibou region of Mauritania. At the highest spatial resolution, the DHS dataset confirms this localized variability and potential overlap in unimodal and bimodal wasting patterns by Koppen regions. The variability of neighboring regions is particularly noticeable in Ghana and Nigeria. Although spatial overlap are limited across the three datasets, Nigeria presents

somewhat different harmonic patterns between DHS and MICS datasets, and Ethiopia presents different regional patterns between SMART and DHS datasets. These differences may indicate that patterns of wasting seasonality must be validated across all available data for researchers to derive robust conclusions around seasonal wasting.

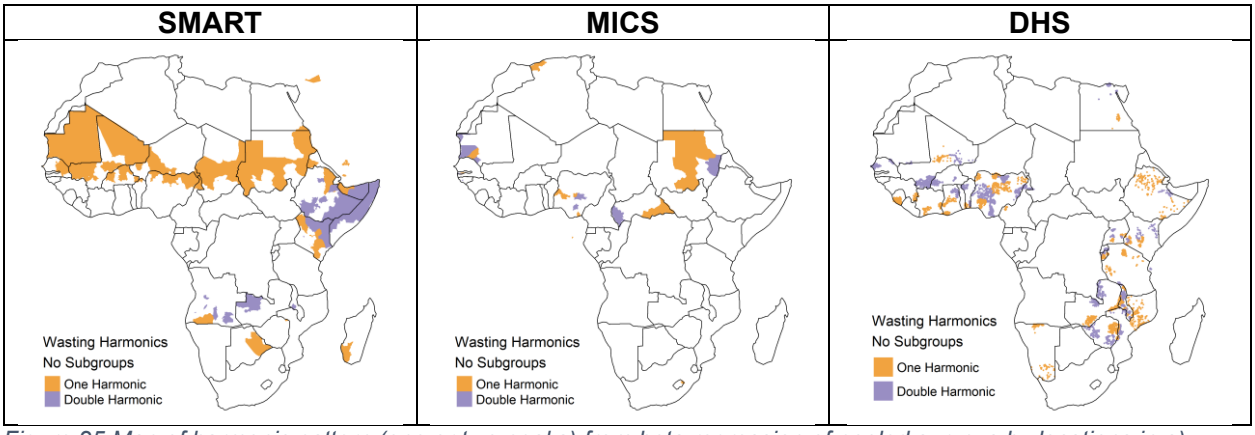

Figure 25 Map of harmonic pattern (one or two peaks) from beta regression of pooled surveys by locations in a) SMART, b) MICS, and c) DHS datasets

Peak Timing of Wasting

Figure 26 presents visualizations of the peak timing of wasting modeled using a beta regression (5) using pooled data across the three datasets. As with harmonic patterns, the SMART dataset indicates a clear belt of September – October peaks in the Sahel region with a similar belt of August peaks just to the south. This gradient is called to question by peak timings derived from MICS dataset, which indicate greater variability in northern Somalia and western Mauritania. This variability is particularly noticeable in the DHS dataset in the southern Sahel's dry subhumid belt, where a wide range of seasonal peaks of wasting are observed. Some alignment is notable across datasets, particularly in northern Nigeria (SMART, DHS) and central Nigeria (MICS, DHS). However, spatial overlap of statistically significant harmonic patterns is extremely limited across datasets.

SMART	MICS	DHS

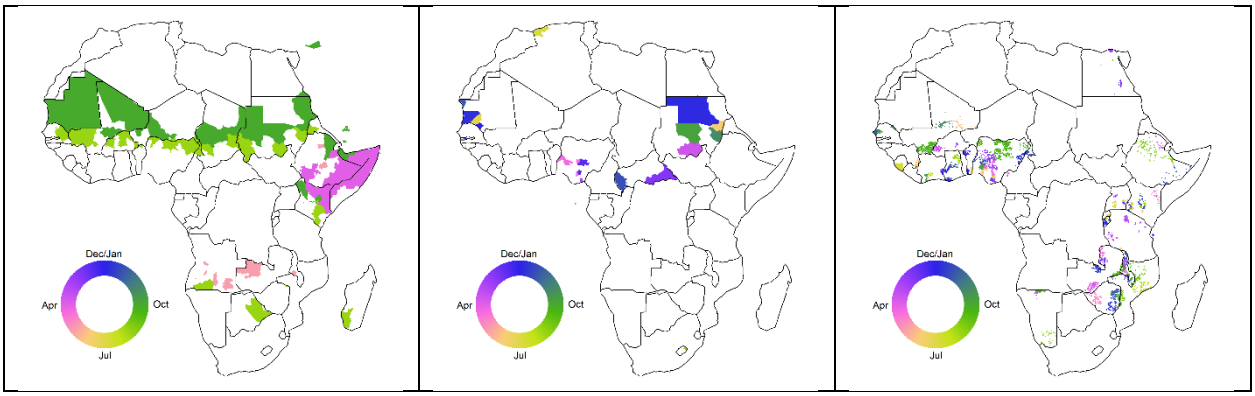

Figure 26 Map of peak timing of wasting by survey locations derived from multiple harmonic regression of wasting prevalence using beta specification in a) SMART, b) MICS, and c) DHS datasets

Sensitivity Analysis

Model Choice

The unit of the dependent variable and the choice of model used to evaluate seasonality effectively determine the observed result. Testing three models allows us to investigate if different specifications are more or less sensitive to the harmonic formulation. The time-variant outcome of interest, i.e. wasting or GAM, can be modeled in many ways: as a logit regression of child-level binary outcome, as a Poisson regression of counts of wasted children, or as a beta regression of average prevalence of wasting (GAM). Since the goal of this analysis is not identifying the model of best fit, one methodology is not necessarily more reliable or valid than another. All the above transformations of a binary outcome are essentially different ways of contextualizing the data; thus, each of the above models can be compared to investigate model sensitivity and validate calculated seasonal features.

We test all three models and find several differences in each models' sensitivity to seasonal characteristics in the outcome. The Logistic specification emerged as the most conservative formulation, with no statistically significant seasonal curves identified after removal of implausible values. The Poisson model identifies the next highest fraction of seasonality models, particularly in Tropical Unimodal areas. Finally, the beta regression also identifies a considerable fraction of seasonal characteristics. Few areas of spatial overlap are observed

across model specifications; in other words, the regions identified as having statistically significant seasonality in the Logit model are frequently different from the regions identified as having statistically significant seasonality in either Poisson or Beta regression specifications.

The regions of overlapping statistically significant seasonality across model specifications are presented in Figure 27, alongside their completeness and sample size measures. Overlapping confidence intervals of peak timing estimates indicates convergence across models. We observe limited overlap in peak timings across specifications in Arid regions, where data primarily derives from the MICS dataset. In Temperate regions, models with the Beta specification appear to have larger confidence intervals compared to Poisson models, whereas wider confidence intervals from Poisson models appear to dominate in Tropical regions. Alignment between Beta and Logistic peak timing estimates is often up to one month apart, and peak timings derived from Poisson models often overlap with confidence intervals from Beta regression models.

Figure 27 points to key strengths of different model formulations. Firstly, confidence intervals of estimated peak timings have broad overlap, indicating broad convergence of estimated seasonal characteristics across model specifications. In temperate regions, Poisson and Beta models appear to be quite sensitive to seasonal wasting, whereas in coastal Tropical countries such as Guinea Bissau and Benin, beta regressions appear to be more adept at identifying two distinct peaks within a wide peak timing window calculated from Poisson specifications. Based on these results, we outline a hierarchy of confidence in estimated peak timings based on convergence across model specifications. In this hierarchy, High Confidence indicates overlapping confidence intervals of peak timing with, Medium Confidence indicates non-overlapping confidence intervals but seasonality identified across multiple specifications, and Low Confidence indicates only one estimate of seasonal characteristics, often derived from the beta specification. Across models, the presented peak timing is the estimate with narrowest

confidence interval. This diagnostic would be useful in most areas except for Arid regions, where the harmonic cycle appears to be off by exactly half a cycle across models. Tabular details of differences are provided in Appendix 3: Sensitivity Analysis of Seasonal Wasting Curves.

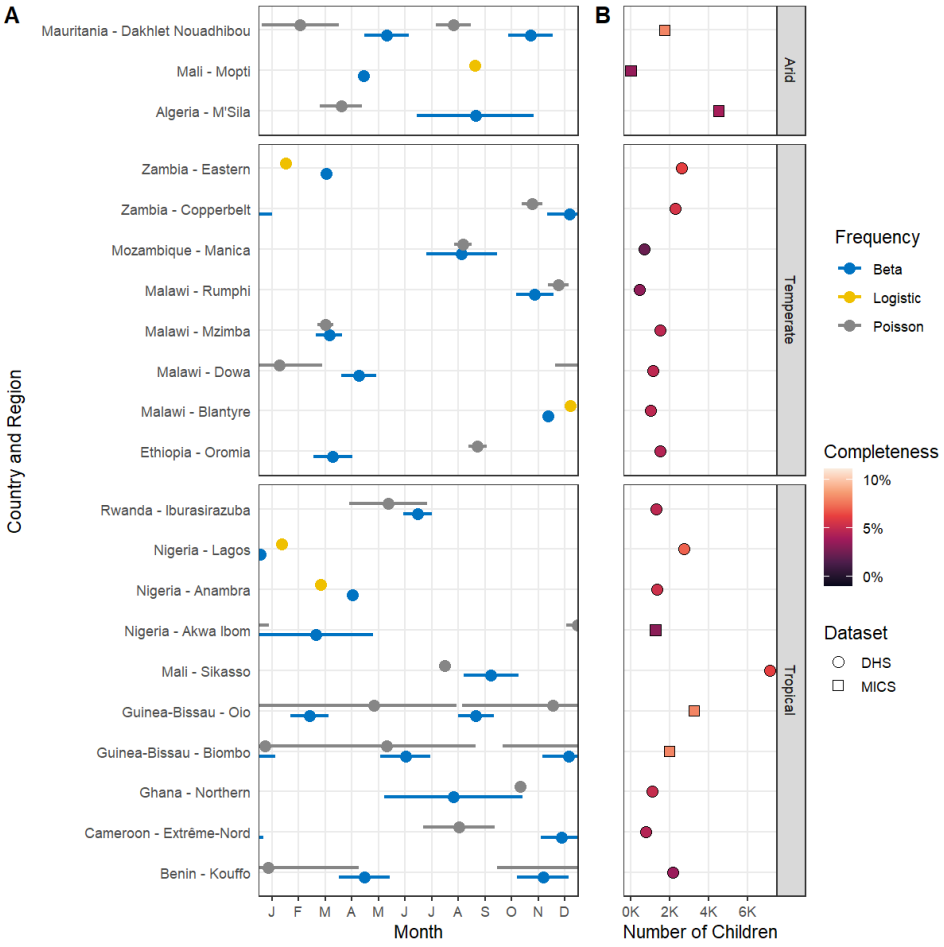

Figure 27 Comparison of peak timing among administrative regions with statistically significant seasonality across multiple specifications. Panel A presents peak timings across regions, and Panel B presents sample size and completeness.

Frequency and Temporal Aggregation

The choice of frequency used and the level of temporal aggregation undoubtedly affects model results. The analyses presented above use a frequency of 12 and round dates to the first of the month to allow us to utilize the SMART dataset, which does not provide the exact dates of survey implementation. However, exact survey dates are available in the MICS and DHS

datasets, and thus can be utilized to cross-validate the effect of temporal rounding. We find that in areas with overlapping statistically significant seasonality across both frequencies, temporal aggregation to the month of survey alters the estimated peak timings by up to two weeks (Figure 28). In rare occasions, estimates of peak timings can differ by up to two months, as in the example of Jigawa in Nigeria. This finding reinforces our conclusion that precision matters, and the exact date of survey should be used with a frequency of 365.25 days in harmonic regression where possible. Tabular results from this exploration are presented in Appendix 3: Sensitivity Analysis of Seasonal Wasting Curves.

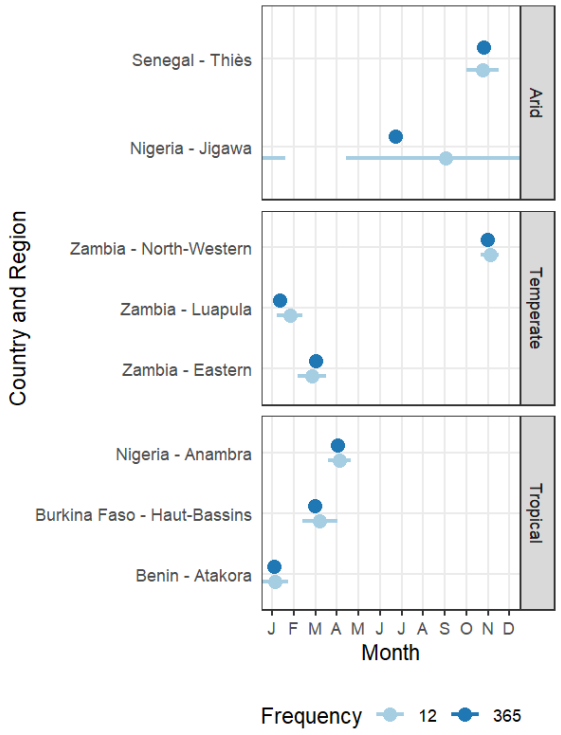

Figure 28 Comparison of peak timings across countries and regions where multiple harmonic regression models with both monthly (frequency = 12) and daily (frequency = 365) were statistically significant.

Discussion

This analysis demonstrates the utility of data fusion across multiple cross-sectional databases to derive and validate seasonal characteristics of wasting. We extract preliminary evidence of highly variable seasonal wasting, and calculate periods of acute distress at high spatial and

temporal resolution. Similar methods have been applied previously to African drylands, where climate and the environment are emerging as “basic and systemic drivers of acute malnutrition” (FAO and Tufts University, 2019; Young, 2020). We further update previous methodologies and findings around acute malnutrition seasonality to uncover a more complex picture. These findings can be utilized to improve existing monitoring systems to reduce acute malnutrition, and to temporally target interventions for sustained progress towards the Zero Hunger Sustainable Development Goal.

This chapter further presents a critical update and application of multiple harmonic regression. Commonly used seasonality methodologies often aggregate continuous time into discrete categories or seasons structured around the agricultural calendar (Marshak et al., 2021). Such categories may be useful for economic analysis of farm incomes or production, but they often fail to capture intra-seasonal fluctuations in acute malnutrition. Treating time as a continuous variable in multiple harmonic regression allows us to utilize established delta methods and flexible arithmetic extensions to reliably derive seasonality characteristics such as peak timing, peak values, and corresponding confidence intervals. In combination with data fusion, this technique can help generate vital baselines to monitor human health impacts of the changing climate.

All three datasets in this analysis are subject to unique strengths and limitations. The SMART dataset provides critical information in fragile settings and likely surveys more vulnerable populations than either MICS or DHS. However, older surveys fail to include key details such as the date of survey implementation, and the dataset lacks information on household-level characteristics such as family size, maternal health, household construction, and access to sanitation infrastructure that are known to affect health and nutrition outcomes. Such data are routinely collected in DHS and MICS surveys. MICS in particular collects data from biological mothers or primary caregivers of children under five years of age, thereby collecting more

information about caregiving behaviors, food consumption, and vaccination status. However, MICS does not provide georeferenced data to accompany its surveys; therefore, researchers need to perform several more steps to derive spatial insights. DHS provides the highest resolution, cluster-level data in this analysis, along with information on family and household-level characteristics. However, the computational demands of using this large dataset are significant and may hinder widespread use of this valuable dataset.

Despite these limitations, uniting these datasets allows us to cross-verify the calculated seasonal characteristics using best available data, and test hypotheses around model choice and frequency. The belt of October peaks in Sahel countries identified in the SMART dataset serves as an important reminder to seek verification; since this phenomenon is not corroborated by either MICS or DHS, we approach it with more caution than certainty. Pooling data also attenuates the effect of survey-specific idiosyncrasies in an already noisy dataset, for greater precision in statistical analyses and potentially greater generalizability beyond the individual survey. However, we underscore that few truly generalizable findings can be extracted from this work. The spatial scale of analysis remains large still, and any calculated peak timings must be validated with higher resolution data where available. These findings would be best used as a high-level indicator to monitor progress towards SDG 2, and as a starting point for discussions around scaleable public health strategies around peak wasting periods.

The spatial matching methods utilized in this analysis present several unique challenges and limitations. Firstly, spatial information in shapefile format was not available for either MICS or SMART, necessitating manual matching to known spatial boundaries. Despite best efforts, we acknowledge that errors in this process were possible, particularly in regions whose boundaries have changed over time. It is also difficult to retroactively verify the spatial extents of the original survey beyond the subnational unit information provided. Secondly, the attempt to account for population density using the GHSL DEGURBA dataset, may have introduced spatial error in this

process. Although fewer human settlements are known to exist in cells identified as Very Low Density, we cannot be confident that surveyed communities were exclusively located in areas included in this analysis. Further, given that this intersection is the basis of the Koppen and Precipitation classes assigned to each partition, there may be compounded spatial error in the assignment of these partitions, as well as downstream extreme weather event calculations. The latter phenomenon may also be associated with exposure misclassification, whereby a community that did not experience and extreme weather event is incorrectly assigned as having experienced it in this analysis. These errors are unfortunately difficult to correct retrospectively in the absence of the GPS coordinates of survey clusters.

Future research can investigate several rich threads of questioning based on these findings. One critical first step is validating and contextualizing calculated seasonal patterns with information about livelihoods, resource use, and local calendars. Beyond seasonal wasting, the effect of extreme weather events on stunting is also of particular public health interest. These analyses typically control for several individual, household, and community-level factors known to affect long-term health outcomes (Block et al., 2021; Brown et al., 2020). Conceptually, the partition by Koppen climate zones and precipitation modes may also be conflated with concurrent factors which more directly affect wasting. Such intermediates may include conflict, political upheaval, or livelihood changes. Investigations of drivers or concurrent phenomena may benefit from similar applications of multiple harmonic regressions to establish concurrent or sequential periodicity. A simple extension would could also examine connections to the continuous climate such as precipitation, temperature, and NDVI.

Several guidelines for future research agendas also emerge from this work. Synergies across DHS, MICS, and SMART can prioritize a shared goal of developing high confidence seasonality estimates across geographies. One research agenda can focus on improving data collection specifically in areas where current evidence points to Medium Confidence in our estimates of

wasting seasonality. Data from these regions indicate a lack of convergence in the presence of statistically significant seasonality, and thus provide a clear need for better evidence. Below this threshold, areas with Low Confidence in seasonal wasting estimates already meet a minimum quantitative threshold that indicate potential presence of seasonal wasting. Calculated peak timing and prevalence estimates can be utilized to improve nutrition surveillance in these areas. Both categories further provide an avenue for myriad government agencies and non-governmental organizations to contribute valuable data and fill this critical gap in evidence. We further prove that aggregate regression specifications such as the Beta and Poisson models are sensitive to seasonality. These models thus provide an important means for data sharing that respects privacy and anonymity of study populations while allowing for health surveillance data collection and reporting.

This investigation further suggests several recommendations for data collection. Firstly, given the scale of investment mobilized to conduct a round of data collection for DHS or MICS, the limited spatial and temporal coverage across partitions is surprising. Average completeness across partitions was 4.3%, indicating that the average partition only had data available for 11 months of the 264 months in the study period. We recommend that DHS and MICS teams work with national statistical agencies where possible, and invest in monitoring strategies that can help minimize gaps in anthropometry data collection. Potential strategies may include implementing rapid assessments such as the SMART survey for routine monitoring in areas with particularly high rates of wasting, or crowdsourcing platforms to collect self-reported data. We further suggest that future survey designs meaningfully account for climatological representativeness beyond traditional rural/urban partitions. Inclusion of climate zones in the study design phase and in the survey sampling strategy will allow for greater spatial coverage. Routine data collection, warehousing, and provisioning of the spatial data behind MICS and SMART survey can also greatly help researchers conducting similar analyses. The DHS has

implemented a jittering method to reasonably anonymize survey cluster locations, and these methods can be easily extended to the MICS and SMART datasets. Investments in data infrastructure are training on seasonality analysis and spatiotemporal alignment are also recommended. Such techniques can allow researchers to continue applying these methods to extract policy-relevant insights at higher spatial scale to fill in the ‘missing piece’ of the seasonality puzzle (ACF International, 2013).

Conclusions

This analysis demonstrates the existence of heterogenous seasonal patterns of wasting in the study area across the three datasets. Although our findings have limited generalizability, this preliminary evidence of seasonal patterns and peak timings can be utilized for further examinations at higher spatial scales. We also find that some formulations of the outcome variable are particularly useful for identifying seasonal characteristics. Temporal completeness of the input time series also plays a critical role in the precision of calculated seasonal characteristics, and temporal completeness of at least 7% of the study period is recommended for future analyses.

Chapter 6: Probabilistic Applications for Famine Early Warning Systems

Abstract

Early warning systems [EWSs] such as the Famine Early Warning System Network [FEWSNET] reconcile multiple dimensions of food insecurity into discrete predictions of food security status in alignment with the Integrated Phase Classification [IPC]. These predictions aim to mobilize humanitarian action and save lives before onset of emergency conditions. A decade of data availability and computational advances have enabled quantitative analyses of accuracy, skill, and bias in these systems. However, forecast-based methods often fail to incorporate structural knowledge of famine systems or the ordinal nature of the IPC scale. We conceptualize acute food insecurity as a Markov process defined by five distinct states and linked by transition probabilities between each pair of states. The utility of this approach is illustrated using 13 years of FEWSNET current status observations of acute food insecurity comprising subnational data at the level one administrative unit boundary. We demonstrate that most of the study area follows a memoryless stochastic process across IPC phases, otherwise called the Markovian assumption. We then generate maps of transition probabilities, steady state phases, and conditional probabilities across critical phase pairs. We also introduce measures of persistence, volatility, and crisis duration as diagnostic tools for famine surveillance. This analysis presents a novel probabilistic method to quantify acute food insecurity and famine. Findings can be used to better understand famine system dynamics from existing EWSs and improve forecast quality and skill across multiple spatial and temporal scales.

Introduction

Hunger affected approximately 735 million individuals worldwide in 2022 (FAO, IFAD, UNICEF, WFP, & WHO, 2023), of which over 258 million people in 58 countries experienced acute hunger requiring urgent humanitarian assistance (FSIN & Global Network Against Food Crises, 2023). Food security and famine early warning systems [EWSs] are critical tools for monitoring food crises and mobilizing responses to address food insecurity. EWSs of various scales track indicators related to food insecurity, including food prices, food production, consumption and nutrition patterns, livelihoods, and mortality metrics such as the crude death rate (Buchanan-Smith & Davies, 1995). Recent EWSs also incorporate satellite-derived information on climatological phenomena to estimate crop yields and water balance and quantify risk of drought and crop failure (Buchanan-Smith & Davies, 1995; Chris Funk et al., 2019). Various information streams, indicators, and expert opinions are then digested into time- and location-specific projections of food security status, which normatively informs action. EWSs have existed in one form or another since the 1960s, and have often incorporated varied indicators leading to extensive research on food insecurity measurement and famine scales in EWSs (Jones, Ngure, Pelto, & Young, 2013; Leroy, Ruel, Frongillo, Harris, & Ballard, 2015; Young & Jaspars, 2006).

Since the early 2000s, the Integrated Phase Classification [IPC] has emerged as the preferred approach for reconciling data from multiple sources to quantify degrees of food insecurity. The five-phase scale was developed in 2004 by the Somalia Food Security and Nutrition Analysis Unit of the FAO, and has since evolved to incorporate multiple thresholded indicators of diet, hunger, and coping (The Integrated Food Security Phase Classification (IPC) Global Partners, 2019). The IPC scale thus incorporates multiple dimensions and pathways to hunger for an effective assessment of food insecurity, in a logical progression from no risk (Phase 1) to famine (Phase 5) (deWaal, 2017; Lautze, Bell, Alinovi, & Russo, 2012; Daniel Maxwell & Hailey, 2020;

D. G. Maxwell & Majid, 2016). The five-phase IPC scale has been adopted by several formal EWSs, including the US Agency for International Development [USAID]'s Famine Early Warning Systems Network [FEWSNET]. FEWSNET was launched in 1985 with a mandate to provide information to guide USAID programming (FEWSNET, 2018). Since March 2011, FEWSNET has utilized the IPC scale to communicate scales of food insecurity; prior to this, FEWSNET used a five-phase scale similar to the IPC (FEWSNET, 2019). FEWSNET assessments are considered IPC-compatible and not formal IPC analyses due to the absence of a consensus of technicians from key stakeholder agencies. In addition to Current Status (CS) measures of acute food insecurity, FEWSNET also releases predictions of short-term (3-4 months) and long-term (6-8 months) food insecurity based on most-likely scenarios (FEWSNET, 2018)2. The short-term (ML1) and long-term (ML2) projections inform critical humanitarian coordination and resource mobilization decisions at USAID and elsewhere.

The accuracy of FEWSNET's quarterly predictions has received recent attention in the humanitarian landscape. Choularton et al observe a mean accuracy of 78% in Ethiopia (R. J. Choularton & Krishnamurthy, 2019a), and higher average accuracy of 83% in parts of East Africa that experience higher conflict levels (Krishnamurthy, Choularton, & Kareiva, 2020). Backer and Billings further present a range of prediction accuracy at the country level across Africa (Backer & Billing, 2019). These studies so far have focused on the accuracy of FEWSNET forecasts using traditional metrics of forecast accuracy, bias, skill, and error. Analyses of phase transitions primarily consider 'higher than predicted' phase outcomes, indicating Type 2 error where food insecurity, hunger, and/or mortality is worse than predicted. Type 1 error, where observed phases is lower than predicted, are also considered. Such approaches provide necessary measures about the accuracy and reliability of the forecasting

[2] Prior to 2016, assessments were released four times per year—in January, April, July, and October. After 2016, FEWSNET modified this schedule to release assessment three times per year—in February, June, and October.

system; however, they are less useful for developing and examining structural models of the acute food insecurity outcome. Existing approaches further ascribe equal weight to the magnitudes of residuals at the upper end of the scale (i.e. a prediction of Phase 4 and an observed Phase 5) as the lower end of the scale (i.e a prediction of Phase 1 and an observed Phase 2). This issue may be partially circumvented by only studying Type 1 error in critical phases (Phase 3 or higher), but it still fails to provide a structural model of the famine system.

This gap is addressed through a Markovian definition of the famine early warning system. A Markov chain describes an infinite process defined by a limited number of possible states and probabilities of transitions between them. As a process with five distinct phases and a release cycle of approximately four months, IPC phases can be modeled as a discrete time Markov chain. At each time step, IPC phase in a region can change to another phase or remain the same with a particular probability. Although theoretically any pair of transitions is possible, several are infeasible given the nature of the outcome (e.g. Phase 1 to Phase 5 at the extremes of the scale). Humanitarians may be particularly interested in transition probabilities at the higher end of the IPC scale—Phase 2 to 3 (the threshold for mobilizing humanitarian action), Phase 3 to 4, and Phase 4 to 5. These upward transitions which describe worsening food security situations can be mirrored by downward transitions describing improving food security conditions.

A Markov chain approach towards modeling acute food insecurity phase classification provides several advantages to the existing forecast-based approach. Perhaps most importantly, the Markov approach is well-aligned with conceptualizations of famine evolution and drivers from the humanitarian literature. Famine studies has evolved towards a systems dynamics lens in the past decade. Famine systems have been recently conceptualized as comprising drivers of pressure which accumulate over a hold period to induce self-reinforcing dynamics and eventual rebalancing (Paul Howe, 2018). These concepts are efficiently translated to quantitative

transition probabilities between phases or duration spent in one of the critical phases. Secondly, the Markov approach allows for scaling in the spatial and temporal domains; probabilities can be calculated over any spatial, agroecological, or climatological boundary and using any combination of input time series. In its strict definition, a Markov process depends only on its current state and is therefore inherently ‘memoryless’; however, time-dependent Markov models can be deployed to more accurately represent seasonally variant livelihoods and food production cycles closely associated with acute food insecurity. Finally, a probability-driven approach is aligned with established methodologies in risk management and decision theory. Transition and conditional probabilities between phase pairs provide critical information about system performance and can also be used as a time-variant dependent variable to study the influence of various predictors. These measures can be incorporated into surveillance systems to generate more informed Bayesian priors and improve famine early warning through probabilistic approaches.

This study aims to demonstrate Markov applications to study famine systems using a 13-year dataset of acute food insecurity observations and predictions from FEWSNET. First, the Markovianity assumption is tested using a variety of statistical methods. Transition probabilities for all five phase are derived and visualized during three time periods: during the early phase of FEWS with four observations per calendar year (2009 – 2015), subsequent years with only three observations per year (2016 – February 2020), and during and after Covid-19 (June 2020 – present). We further develop and map temporal metrics such as persistence, volatility, and crisis duration to identify regions with acute and chronic food crises. Finally, the conditional probability, or likelihood of predicting and observing particular transitions, using FEWSET ML1 projections. Altogether we present novel quantitative methods for famine systems monitoring.

Methods

Spatial Data Processing

FEWSNET short-term and long-term prediction shapefiles were available at a frequency of 3-4 months starting in July 2009. A total of 59 FEWSNET assessments were available for the study period of 2009 – 2022 (FEWSNET, 2018, 2019). FEWSNET shapefiles since March 2012 include a field indicating the effect of humanitarian assistance; if the HA field across shapefiles is coded as 1, then phase classification would likely be at least one phase worse in the absence of humanitarian assistance. If the HA field was coded as 0, then humanitarian assistance was judged to cause insignificant change in IPC phase outcome (FEWSNET, 2019). The HA column was subtracted from the assigned phase in all datasets to better represent the dynamic effect of humanitarian aid. Each shapefile was rasterized to a raster grid with resolution of 0.05° (approximately 6 km). Pixels containing values for at least 25% of the study period (at least 14 observations) were retained, and each pixel was matched to level one administrative boundary within FEWSNET countries from the FAO Global Administrative Unit Layers (GAUL) dataset (FAO, 2015). Pixel counts were then summarized by phase and observation period for the complete spatial extent of FEWSNET countries.

Estimation of Markov Properties

This analysis begins by representing the IPC phase of a region at time t as the stochastic process X_t. X_t has a finite state space of five possible phases or states, such that $S = \{1, 2, 3, 4, 5\}$. Movement between these phases is unrestricted for each time step such that X can hold any feasible state s at time t (Fewster, 2013; Grimmett & Welsh, 2014). The relevant state-space for this analysis is a matrix of all five possible IPC phases that can be held by each pixel or administrative region.

X_t can be characterized as a classical time series where each observation is dependent on lags, or previous observations with diminishing influence. Alternatively if X_t is memoryless, it satisfies the Markov property and is considered a Markov process. This simplification implies that the probability of state s being held in the subsequent time step is conditional only on the state held in the current time step and not on previously held states. This can be written as:

$$\mathbb{P}(X_{t+1} = \mathrm{s} \mid X_t = s_t, X_{t-1} = \mathrm{s}_{t-1}, \ldots X_0 = s_0) = \mathbb{P}(X_{t+1} = \mathrm{s} \mid X_t = s_t)$$

Movement between states in the state space is unrestricted but the distribution of these movements may not be uniform. With each time step, X can transition between feasible states s_t and s_{t+1}. Transition probabilities describe the likelihood of movements between states during successive time steps. These probabilities can be calculated by tabulating the frequency of pairs $X_{s,t}$, $X_{s,t+1}$for all S in the state space. Probabilities can be arranged in a square transition matrix M (Table 10), where each entry $p_{t,\mathrm{t+1}} = p_{i,j}$ describes the conditional probability that the subsequent state is j given that the current state is i. The rows in matrix M must sum to one to completely describe transition probabilities. In other words:

$$p_{t,\mathrm{t+1}} = p_{i,j} = \mathbb{P}(X_{t+1} = \mathrm{j} \mid X_t = i) \; for \; i, j \in S$$

$$\sum_{j=1}^{5} p_{i,j} = \sum_{j=1}^{5} \mathbb{P}(X_{t+1} = \mathrm{j} \mid X_t = i) = \sum_{j=1}^{5} \mathbb{P}_{\{X_t = i\}}(X_{t+1} = \mathrm{j}) = 1$$

Table 10 Transition Probability Matrix for Markov Process X with five phases

		Xt				
		Phase 1	Phase 2	Phase 3	Phase 4	Phase 5
Xt+1	Phase 1	$p_{1,1}$	$p_{1,2}$	$p_{1,2}$	$p_{1,4}$	$p_{1,5}$
	Phase 2	$p_{2,1}$	$p_{2,2}$	$p_{2,2}$	$p_{2,4}$	$p_{2,5}$
	Phase 3	$p_{3,1}$	$p_{3,2}$	$p_{3,2}$	$p_{3,4}$	$p_{3,5}$
	Phase 4	$p_{4,1}$	$p_{4,2}$	$p_{4,2}$	$p_{4,4}$	$p_{4,5}$
	Phase 5	$p_{5,1}$	$p_{5,2}$	$p_{5,2}$	$p_{5,4}$	$p_{5,5}$

This Markov formulation allows for exploration of several properties of FEWSNET data. Since each X_t is a random variable, the probability of X being state s at time t=0 can be described as $\mathbb{P}(X_0)$. Since there are five states, the probability distribution of X_0 is denoted by matrix π such that:

$$\boldsymbol{\pi} = \begin{bmatrix} \pi_1 \\ \pi_2 \\ \pi_3 \\ \pi_4 \\ \pi_5 \end{bmatrix} = \begin{bmatrix} \mathbb{P}(X_0 = 1) \\ \mathbb{P}(X_0 = 2) \\ \mathbb{P}(X_0 = 3) \\ \mathbb{P}(X_0 = 4) \\ \mathbb{P}(X_0 = 5) \end{bmatrix}$$

Transposing matrix π, we arrive at π^T, which is a row vector describing the probability of X starting at each state. X_1, or the state of X at the next time step, can be described by:

$$\mathbb{P}(X_1 = \mathrm{j}) = \sum_{j=1}^{5} \mathbb{P}(X_1 = \mathrm{j} \mid X_0 = i) * \mathbb{P}(X_0 = i) = \sum_{j=1}^{5} p_{i,j} * \pi_i = (\pi^T M)_j$$

In two time steps, X_2 can be described similarly as:

$$\mathbb{P}(X_2 = \mathrm{j}) = \sum_{j=1}^{5} \mathbb{P}(X_2 = \mathrm{j} \mid X_0 = i) * \mathbb{P}(X_0 = i) = \sum_{j=1}^{5} (M^2)_{i,j} * \pi_i = (\pi^T M^2)_j$$

Thus, the probability distribution of the Markov process X at timestep t can be calculated as the matrix product of the starting state probabilities and multiples of the transition matrix M such that $\boldsymbol{X_t \sim \pi^T * M^t}$. This further allows for calculation of trajectory probabilities by multiplying $\boldsymbol{\pi^T}$ by any sequence of $\boldsymbol{p_{i,j}}$ values from transition matrix M to define the likelihood of particular trajectories between IPC phases. The probability of ever reaching a target state ($\boldsymbol{h_G}$) and the time taken to reach the target state ($\boldsymbol{m_G}$) can both be calculated as the minimal non-negative solution for a given transition matrix and a starting state. Both $\boldsymbol{h_G}$ and $\boldsymbol{m_G}$ can be calculated as:

$$h_G = h_{i,G} \begin{cases} 1 & for\ i \in G \\ \sum_{j \in S} p_{i,j} * h_{j,G} & for\ i \notin G \end{cases}$$

$$m_G = m_{i,G} \begin{cases} 1 & for\ i \in G \\ 1 + \sum_{j \notin G} p_{i,j} * m_{j,G} & for\ i \notin G \end{cases}$$

Several topics routinely addressed in mathematical descriptions of Markov chains are excluded here in favor of simplicity and clarity. Class structure of states is not particularly relevant to this analysis as very few instances of absorbing states and closed classes are observed empirically. We further present a select few phase trajectories with the goal of illustrating the utility of this method rather than completely describing the source dataset.

A series of hypothesis tests were performed to test whether a time series of CS observations are Markovian. First, a classical Chi-square based test was implemented that looks at triplets of successive observations and compares them to a Binomial distribution with similar parameters (Spedicato, 2017). We then extend this test to investigate whether independence and uniformity assumptions are valid over the unit interval using a Ljung-Box test for autocorrelation and a Pearson's chi-squared test for discrete uniform data respectively (Hart & Martínez, 2019). Finally, we compare a multinomial logit regression model with first-order dependency against a model with second-order dependency and derive the Likelihood Ratio Test from this comparison to assess if the augmented model provides better fit and therefore violates the Markovianity assumption.

Transition Probabilities

A time series of FEWSNET Current Status (CS) observations were abstracted for each pixel in the study area. The frequency of unique trajectories over time was tabulated to derive the proportion of each phase transition. These proportions were then transformed into a matrix with the rows representing preceding phases, the columns representing subsequent phases, and the matrix populated with proportion of observations (Table 10). Cells were normalized by the total number of pixels to derive transition probabilities. This process was repeated for the complete study period, as well as three temporal subgroups (Pre-2016, 2016-2020, and 2020-Present).

These temporal groupings were chosen for differences in the FEWS release cycle; prior to 2016, data were released on a quarterly cycle per calendar year, whereas FEWS has provided three data releases per calendar year since. The 2020 – Present subgroup was defined to compare the duration of the global Covid-19 pandemic to previous time periods. Next, the transition probability of Phase 3 to Phase 4, and Phase 4 to Phase 5, were mapped. This calculation also allows us to derive the steady state probability of each phase, or the long-term probability that each phase will be realized independent of initial state. This steady state IPC phase of each pixel was also visualized.

Persistence, Volatility, and Crisis Duration

Pixel-level transition matrices also allow for calculation of persistence, or the continuous time period spent in a particular phase, and volatility, or the continuous time spent transitioning between dissimilar phases. For pixels which had ever experienced Phase 4 or Phase 5, the continuous sequences of transitions from and to the same phase (diagonals) were identified and the time difference between consecutive sequences were summed to derive persistence in each phase. To present a more intuitive timeline of food crisis, we also calculated the crisis duration for each pixel per a naïve definition of the beginning, middle, and end of a crisis period. Consistent with the IPC scale, the start of a food crisis was defined as the time period in which a phase transition from a lower phase to Phase 3 or higher is observed, and the end of the crisis period was defined as a transition from Phases 3, 4, or 5 to Phase 2 or Phase 1. Within this pre-defined consecutive crisis period, volatility was defined as the number of transitions between dissimilar phases. All three measures provide a spatially and temporally variant assessment of famine risk.

Conditional Probabilities

Short-term projections (ML1) from one time period were then matched to observed (CS) phases in the next time period. This matching generated a matrix for each time period populated

by expected and observed phase counts. Similar to Table 10, the conditional probability matrix comprises rows representing predicted phases, the columns representing observed phases, and the matrix populated with proportion of each phase pair. Conditional probabilities were then visualized for critical phases.

Comparison to IPC and Cadre Harmonisee

All available spatial data was extracted from the Famine Early Warning System (FEWSNET) website on June 2, 2022 and updated on April 25, 2023. All available tabular data for Cadre Harmonisee was extracted from Humanitarian Data Exchange on October 8, 2023. All available IPC data was extracted using the IPC API on March 31, 2023 and updated on November 1, 2023.

IPC and FEWSNET provided spatial data in GEOJSON and shapefile formats respectively, which were processed and matched to phase predictions and observations. Cadre Harmonisee was the only dataset for which spatial matching was performed. Subnational administrative fields were matched to reference administrative units from the database of Global Administrative Units (GADM) (Global Administrative Areas (GADM), 2012). Details about the fuzzy matching process are available in Chapter 3: Techniques and Workflows for Spatial and Temporal Alignment Technique 2: Matching Surveys to Spatial Boundaries with Fuzzy Matching.

All spatial data were then rasterized, or converted to gridded format, with each file corresponding to the generated prediction and observation dates. To calculate transition probabilities, current status observations were subset and stacked to generate a matrix of pixel time series for a global extent. Pixels were then summed by phase to generate time-variant counts of phase transitions. To calculate conditional probabilities, pairs of prediction and observation phases were then extracted to generate a matrix of pixel time series for a global extent. Pixels were then summed by phase to generate time-variant counts of matched prediction and observation.

Extreme Event Calculation

Both temperature and precipitation averages were used to calculate the location-specific time series of the 6-month Standardized Evapotranspiration Index (SPEI) values to characterize droughts (Beguería et al., 2010; Beguería et al., 2014). SPEI was calculated using monthly average temperature values from the MODIS MOD11C3 MODIS/Terra Land Surface Temperature/Emissivity Level 3 product (Wan et al., 2015) dataset and the monthly average precipitation values from the Climate Hazards Group InfraRed Precipitation with Station data (CHIRPS) dataset (C. Funk et al., 2015). The CHIRPS dataset was used to calculate the 1-month Standardized Precipitation Index (SPI) to characterize floods. Pixel values above the 95th percentile of SPI were classified as floods, and values below the 5th percentile of SPEI were classified as droughts.

Due to the geographic focus on Africa, only maximum temperature values were extracted for this analysis from the Terraclimate (Abatzoglou et al., 2018). Maximum temperature values above the 95th percentile were classified as heatwaves. Values were calculated for each pixel on a common raster grid to align with FEWS, IPC, and CH phase prediction time series. Details of dataset extraction are provided in Technique 3: Extraction of Weather Extremes from Gridded Data.

Estimation of Extreme Weather Effects

The estimation strategy to study the influence of extreme weather on conditional probabilities is shown in Equation 6, where the outcome is constructed as the conditional probability of predicting phase *ST* in the short term given phase *CS* in pixel *j* and quarter *q* of data release. Although any phase pairs can be studied, the particular research question of interest is the likelihood of underpredicting critical transitions—in other words, failing to predict Phase 3 or higher in the presence of Phase 3 at a particular location. We index dataset *d* due to underlying

differences in the source datasets. To match extreme event occurrence with the quarter of dataset release, we utilize shared time *t*, or the month and year of dataset release, for temporal alignment. To further account for regional differences in administration and context, we include a fixed effect for country γ_j and run split sample regressions by country as well as dataset.

$$P(ST_{j,d,q+1} \perp CS_{j,d,q}) = \beta_0 + \beta_1 Extreme\ Event_{j,t} + \gamma_j + \varepsilon$$	*Equation 6*

Results

Markovianity

Figure 29 presents the result of pixel-level hypothesis testing for Markovianity using Chi2 test of triplets. We find that most pixels in the study area (52.1%) meet the Markovianity assumption that future state depends only on the current state and not on previous states. Two categories of insufficient data are defined, based on the diversity of phases observed (Not Enough Variation) and the availability of sufficient samples to implement the Chi2 test (Insufficient Observations).

The Not Enough Variation category is next most frequently observed and indicates regions that have sufficient sample size but insufficient diversity in phases for a Chi2 test. Pixels in Afghanistan and Haiti are most commonly classified as not having sufficient variation, indicating that these regions often stay in the same phase regardless of the phase identity—a finding echoed by the steady state map in Figure 32. 20% of pixels in Figure 29 are classified as having Insufficient Observations, or sufficient variation but less than the roughly 30 samples required for a Chi2 test. These areas are found primarily in West Africa, the Ethiopian highlands, Tanzania, Madagascar, and Zambia. Non-Markovianity, or potential longer time dependence, is definitively observed for a fraction of pixels (2.6%). Clusters of non-Markovianity are distributed across southern Nigeria, eastern Sudan and South Sudan, southern Ethiopia, and across Zimbabwe. This concentration of non-Markovian pixels may indicate different temporal

dynamics in these regions, perhaps due to trade or high seasonality, which causes longer-term autocorrelation in food security status. We also observe regions with a mix of Markovian and non-Markovian pixels, indicating spatial heterogeneity and potentially localized autocorrelation in food security.

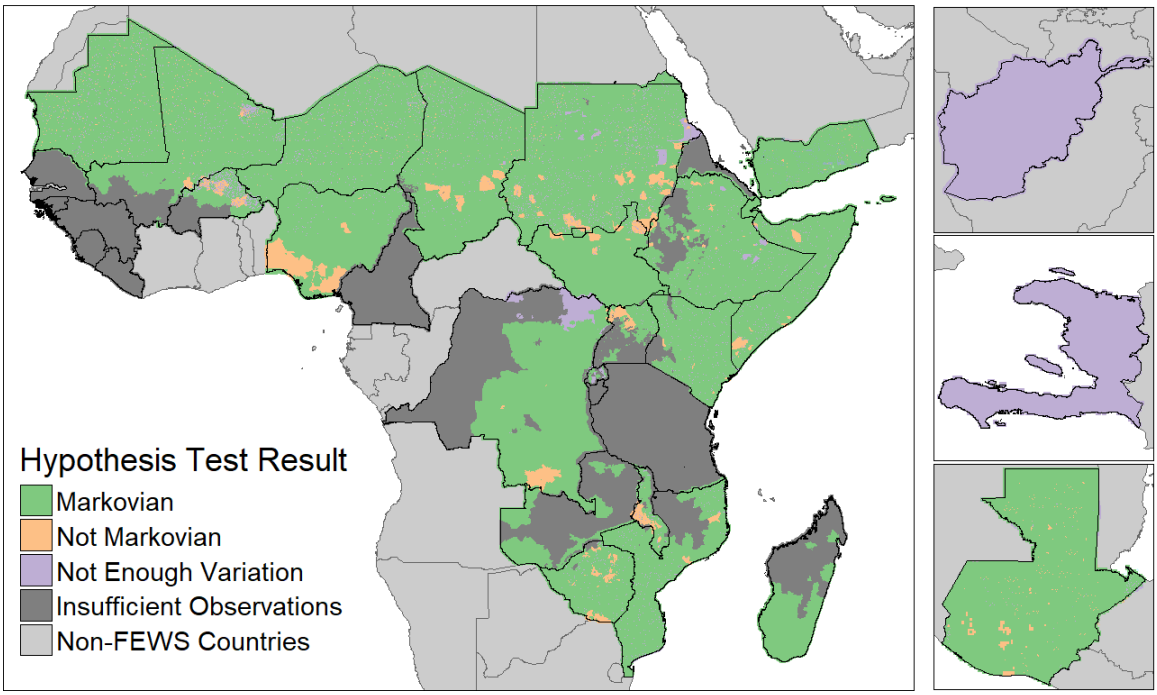

Figure 29 Chi squared test results for time tendency in Markov chain models of pixel-level IPC phase trajectories.

Transition Probabilities

Figure 30 presents heatmaps of transition probabilities from and to each of the five IPC phases. A strong tendency to persist in the same phase as the previous time period is observed, but this periodic persistence has decreased in recent years. We observe that improvements to food insecurity status are becoming less prevalent than in earlier years. For a pixel classified as Phase 4, the likelihood of transitioning to Phase 3 has decreased from 41.6% pre-2016, to 33.4% in 2016-2020, to 17% in 2020-present. Similarly, for a pixel classified as Phase 3, the likelihood of transitioning to Phase 2 has decreased from 33.5% pre-2016 to 24.7% in 2016-2020 and 23.6% in 2020-present. On the other hand, frequency of transitions to the same

phases are increasing. A pixel in Phase 4 was 81.3% likely to stay in Phase 4 in 2020-present, compared to 55.1% in pre-2016. Similarly, a pixel in Phase 3 was 69% likely to stay in Phase 3 in 2020-present, compared to 55.7% pre-2016. In the pre-2016 period, a fraction of transitions from Phase 5 to Phases 2, 3, and 4 are observed as a potential incongruity. Pixels contributing to these cells derive from the October 2011 and January 2012 FEWS CS release, which reflects the effects of humanitarian aid distributed in response to the 2011-2012 drought primarily in Shabelle Dhexe, Shabelle Hoose, Bay, and Bakool regions of Somalia. A smaller fraction of such transitions from Phase 4 have been observed in crisis regions since.

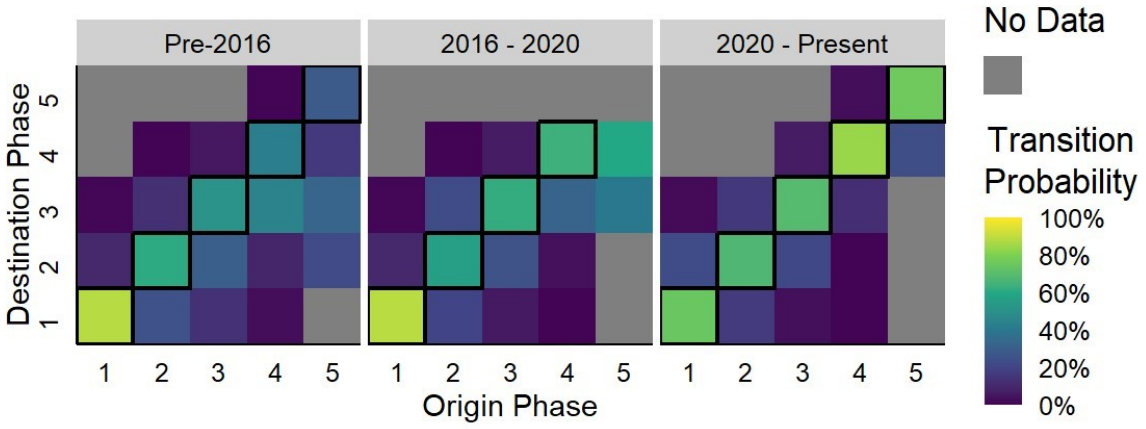

Figure 30 Transition probabilities from origin phase (x axis) to destination phase (y axis) over three time periods (Pre-2016, 2016-2020, and 2020-Present)

Figure 31 provides a map of transition probabilities ($X_{p\to p+1}$) for two critical transitions: Phase 3 to 4 ($X_{3\to4}$) and Phase 4 to 5 ($X_{4\to5}$). As expected, $X_{3\to4}$ and $X_{4\to5}$ are higher in areas known to have experienced famine. Concentrated high values of $X_{4\to5}$ in southern Somalia reflect the observation of famine in the region during the 2011-2012 East Africa drought. The map of $X_{3\to4}$ has more observations, indicating that this transition has been observed more frequently in comparison. Pockets of high $X_{3\to4}$ values in northern Somalia and Ethiopia reflect the effects of sustained droughts in the Horn of Africa in 2016-2017 and 2020-2022. Although these droughts affected larger areas, humanitarian aid abated the risk of worsening food security in other regions.

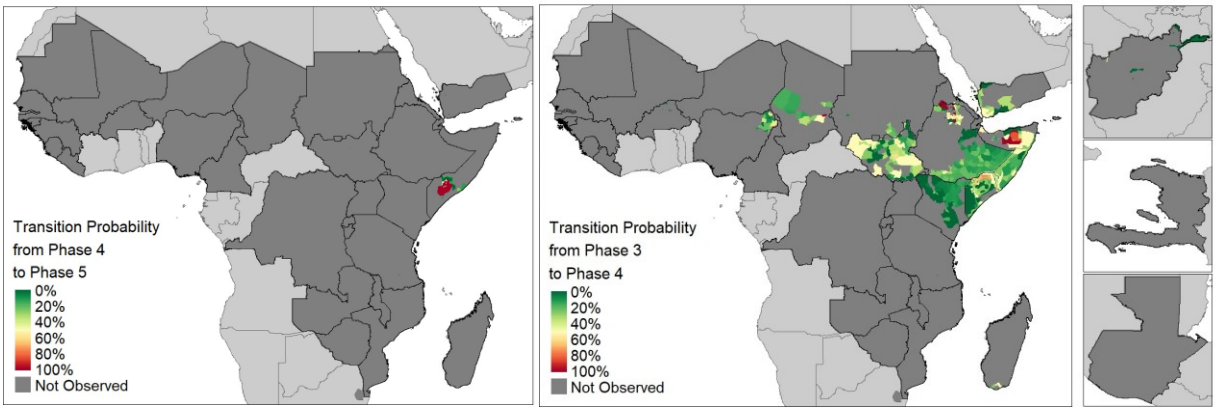

Figure 31 (left) Map of pixel-level transition probabilities; (left) from Phase 4 to Phase 5; and (right) Phase 3 to Phase 4.

Steady State Probabilities

Pixel-level Markov chains yield the steady-state phase as shown in Figure 32. Particular crisis hotspots, or areas with steady states of Phase 3 or higher, are observed in DRC, Ethiopia, South Sudan, Nigeria, and Yemen. Steady state of Phase 4 is observed only in Yemen and northern Nigeria, indicating consistently eroding food security during the study period. Despite the high transition probabilities of Phases 3 and 4 in the Horn of Africa, prevalent steady states of Phase 2 and Phase 3 indicates volatile food security in the region during the study period.

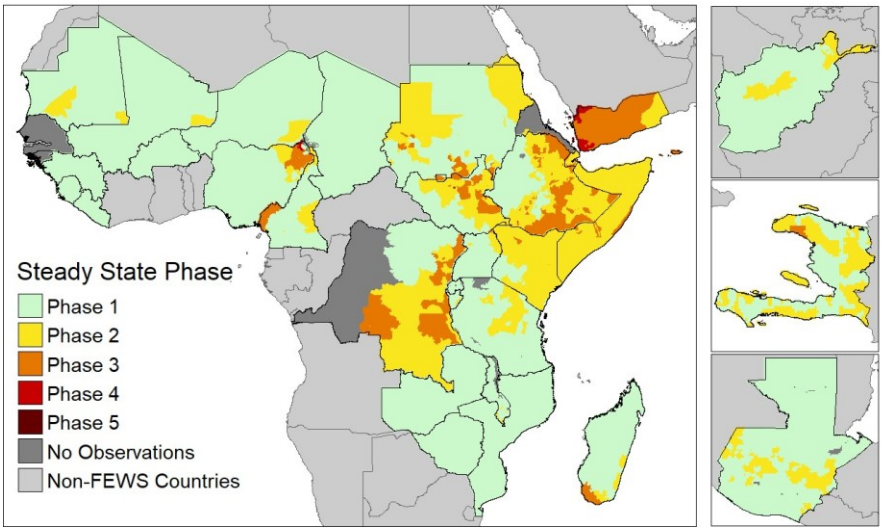

Figure 32 Average steady state phase by pixel calculated from all FEWSNET current status observations over the 13-year study period.

Persistence, Volatility, and Crisis Duration

Figure 33 provides maps of all three temporal metrics using a threshold of IPC Phase 3 to define the start and end of a consecutive crisis period. As expected, Panel A highlights chronic food crises in western Cameroon, northeastern Nigeria, eastern Yemen, and much of South Sudan. The distribution of crisis duration ($\mu = 92.1 \pm 99.5$ weeks, skewness = 3.4 weeks) among pixels which have experienced Phase 3 at any point during the study period, indicates a large number of higher values. Panel B of Figure 33 maps the average volatility, or the number of transitions between dissimilar phases, during a crisis period. The volatility measure ($\mu = 3.1 \pm 2.7$ transitions, skewness = 11 transitions) indicates that regions with protracted crises experience the highest volatility in food security, primarily in Cameroon, Nigeria, and Sudan. Finally, average duration of persistence in Phase 3 across all pixels which have ever experienced Phase 3. Persistence in Phase 3 usually lasts little under one year ($\mu = 40.8 \pm 85.7$ weeks), with high-persistence regions having longer crisis durations and lower volatility.

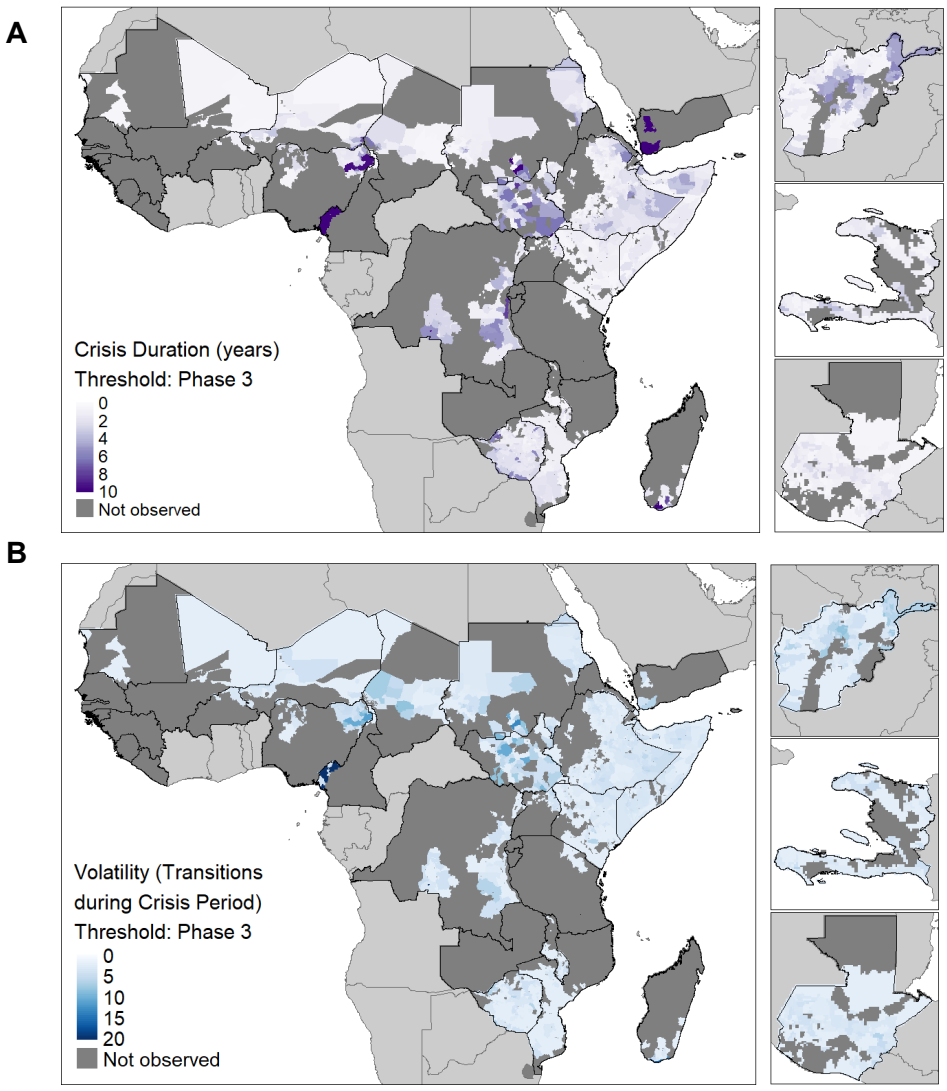

Figure 33 Pixel-level maps of (A) crisis duration, (B) volatility, and (C) persistence in Phase 3. The crisis duration is defined as the consecutive time spent by a pixel in Phase 3 or higher; Persistence refers to the average consecutive duration in Phase 3 for each pixel; and Volatility refers ot the number of transitions between dissimilar phases during a crisis period.

Conditional Probability

Figure 34 presents average conditional probabilities across the three time periods. Clear asymmetric behavior is observed across the diagonal, indicating that the higher the predicted phase, the less likely it is to be observed. This is intuitively consistent, as FEWS long-term projections often have a lead time of 6-8 months and guide humanitarian efforts towards preventing the realization of worse food security outcomes. The lower share of observations above the diagonal compared to below the diagonal indicates that overprediction occurs more

often than underprediction. Underprediction of Phase 4 and 5 occurred in 2011-2012 as before, but is also observed in June 2017 scattered across Ethiopia, South Sudan, and Somalia. As the critical threshold for action, underprediction of Phase 3 is also an important measure of system performance. The conditional probability of predicting Phase 2 and observing Phase 3 has increased from 8.6% pre-2016 to 19.3% in 2016-2020 and 14.2% in 2020-present. The geographic distribution of both phenomena are shown in Figure 35. Panel B indicates that underprediction to Phase 3 is most consistent in North Kanem and Bahr el Ghazal regions of Chad, Tigray and Afar in Ethiopia, and Hajjah, Al Hudaydah, Shabwah, and Abyan governorates of Yemen.

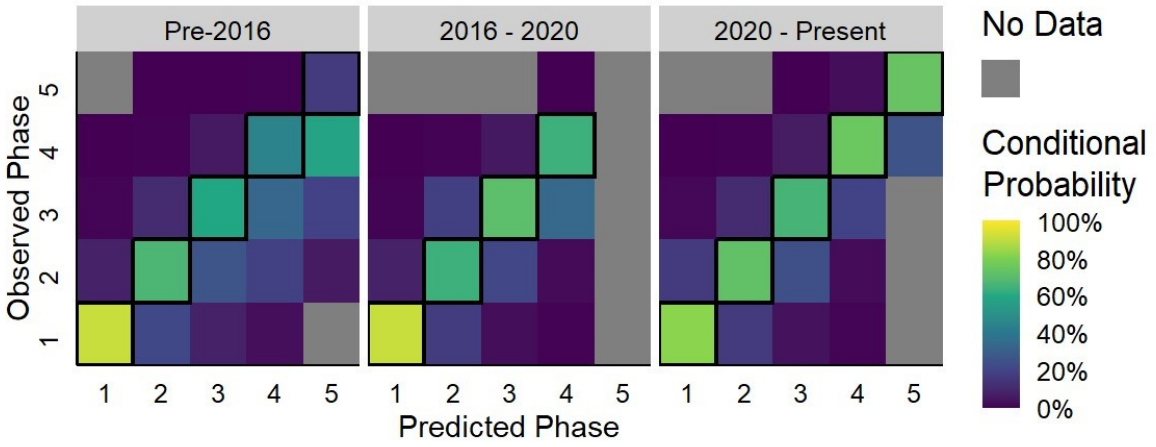

Figure 34 Conditional probabilities from predicted IPC phase (x axis) to observed phase (y axis) during 2007 – 2016, 2016-2020, and 2020-present.

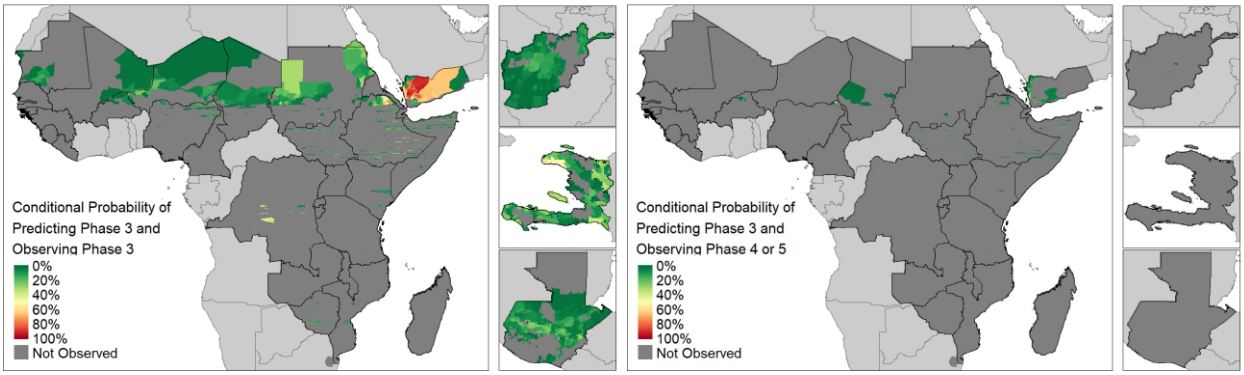

Figure 35 Pixel-level conditional probability maps of: (left) correct prediction of Phase 3 and (right) underprediction of Phase 4 or Phase 5 by predicting Phase 3.

Comparison to Probabilistic Distributions of IPC and Cadre Harmonisee

Table 11 provides a comparison of FEWS, IPC, and Cadre Harmonisee (CH) datasets. Both these data sources are much newer than FEWS, and present significant departures in the spatial and temporal domain. Unlike FEWS, IPC does not have a regular data release schedule for the global dataset; rather, it is a mixed system of some countries with routine monitoring of acute malnutrition and other countries where assessments are implemented as and when crises occur. This often leads to inconsistent temporal extents compared to the FEWS and CH datasets. The CH, which is specific to West Africa, has the fewest number of countries covered, but provides a robust database of short-term projections in the region since 2015 onwards. However, CH does not provide spatial data, and therefore spatial extents needed to be matched manually for further analysis. Finally, neither IPC nor CH provide an assessment of the effect of humanitarian assistance as provided in FEWS; therefore, no further adjustment to a 'true' scale was performed for either dataset.

Table 11 Characteristics of Source Datasets

Characteristics / Dataset	***FEWS***	***IPC***	***CH***
Number of countries covered	62	58	27
Period of data availability	2009 - present	2017 - present	2014 - present
Number of unique observation periods	48	80	19
Number of unique short-term prediction periods	48	80	12
Spatial data available?	Yes	Yes	No
Regular release schedule?	Yes	No	Yes
Information about humanitarian assistance	Yes	No	No

Figure 36 and Figure 37 provide grids of transition and conditional probabilities respectively across all three datasets. Compared to the FEWS dataset, it can be observed that transition probabilities in the IPC dataset take on a narrower range of possible values. The censoring

effect of the consensus mandate is observed in the IPC and CH panels, where Phase 5 is never observed. Conditional probability of higher order phases also indicate that underprediction, or pixels above the diagonal, is more commonly observed in IPC than either FEWS or CH. Given that IPC assessments are implemented as needed instead of an established assessment cycle, the higher probability of underprediction may reflect particularly volatile emergent crises. Probability graphs for the CH dataset are more widespread, and the prevalence of deviations below the diagonal point to general overprediction. Although the conditional probability of correctly predicting phases is improving since 2016, recent overprediction is noted.

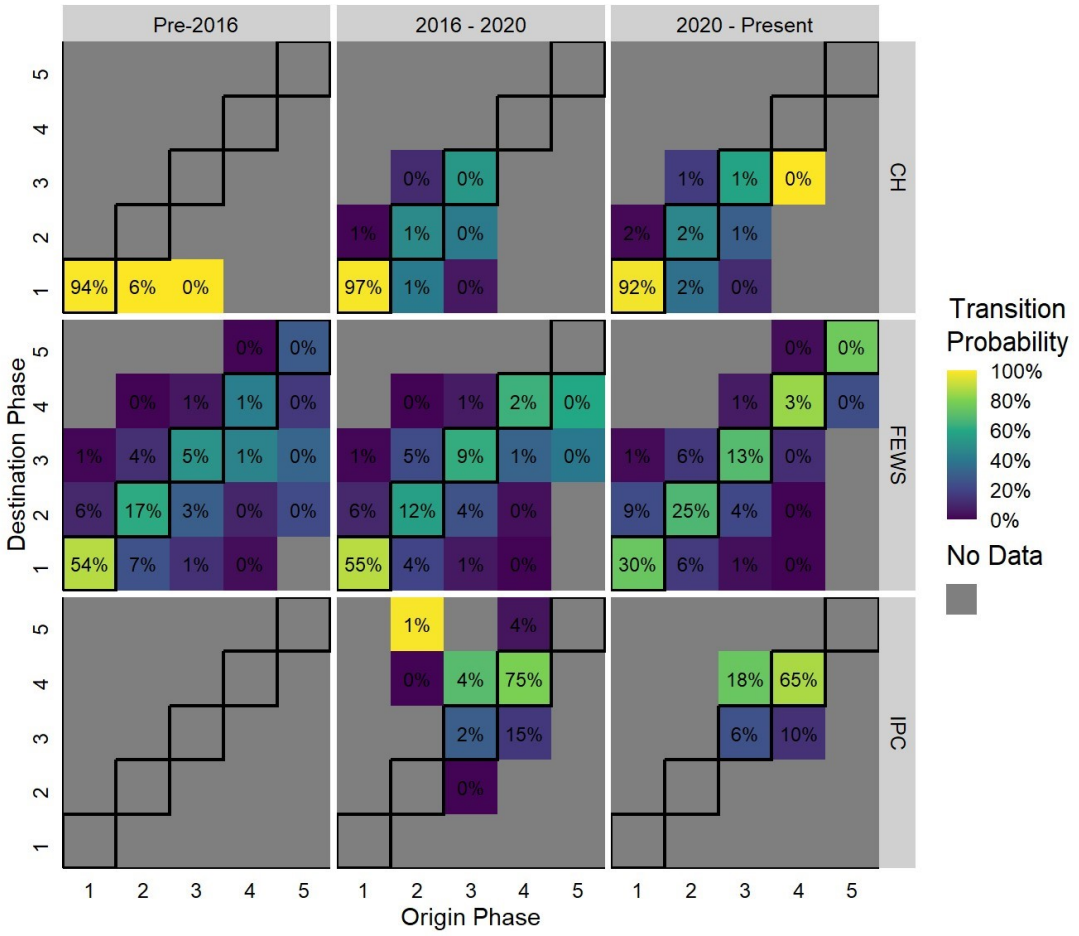

Figure 36 Transition probabilities from and to each of the five phases of acute food insecurity across (top) CH, (middle) FEWS NET, and (bottom) IPC datasets. Colors indicate transitional probabilities and numbers within each cell indicate total fraction of pixels within each time period and dataset partition.

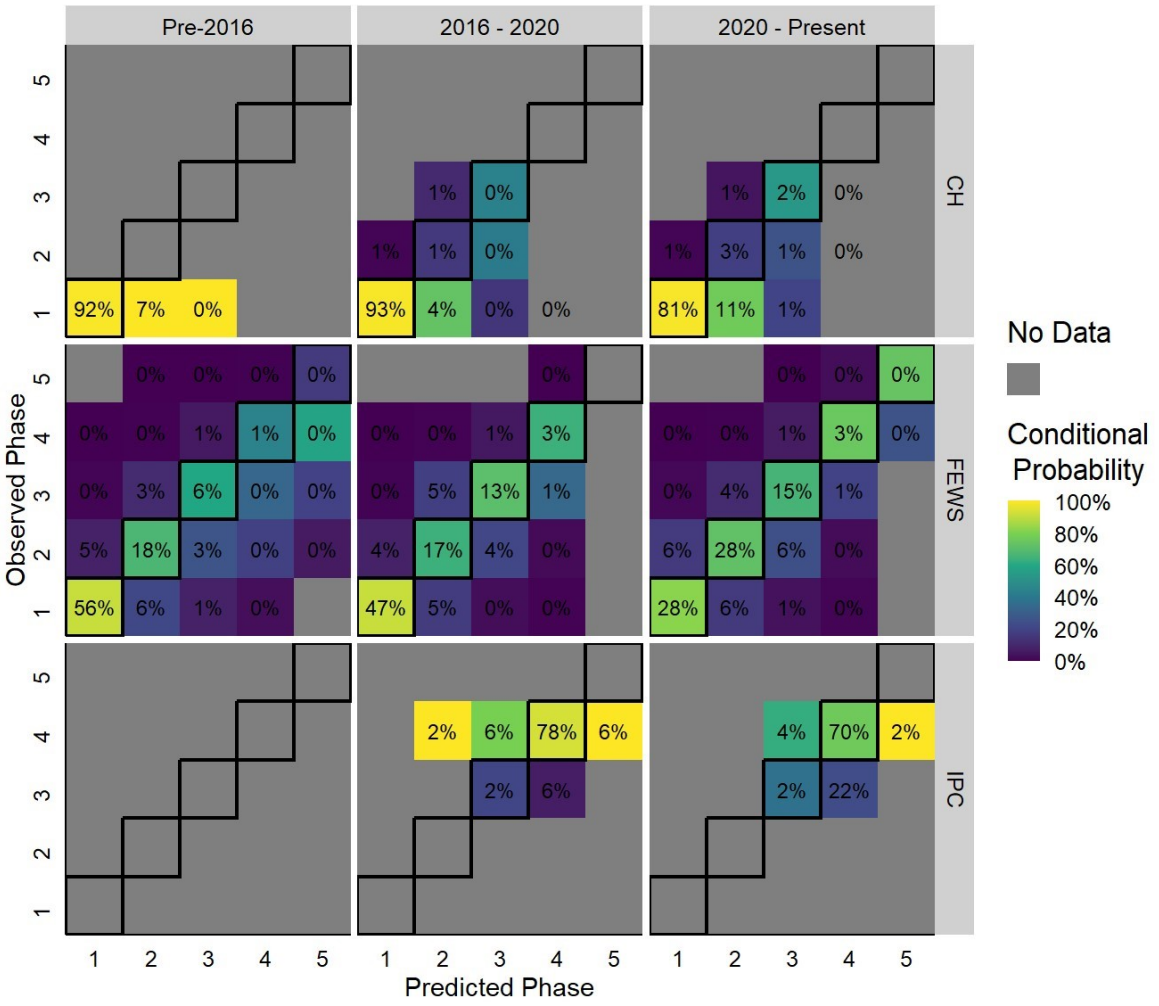

Figure 37 Conditional probabilities from and to each of the five phases of acute food insecurity across (top) CH, (middle) FEWS NET, and (bottom) IPC datasets. Colors indicate conditional probabilities and numbers within each cell indicate total fraction of pixels within each time period and dataset partition.

Associations between Conditional Probability and Extreme Weather

Complete regression results from the estimation are provided in Appendix 4: Extreme Weather and Underprediction of Critical Phase Transitions. A wide range of effects are observed. The CH dataset specifically yields extremely high magnitude coefficients for Heatwaves and Droughts which is not corroborated by FEWS. This indicates that more observations may be required from the CH dataset before interpretation of these results. FEWS is the longest and largest dataset under analysis, and effect sizes are much more muted. We observe 3.4-5.3x

higher likelihood of underprediction during heatwave months in Ethiopia, Eritrea, Somalia, and Mozambique from the FEWS data. The 28.6x underprediction likelihood in Zimbabwe is also particularly surprising. Effect magnitudes for flood events are more consistent between FEWS and CH data, with IPC providing too few observations for analysis. Per FEWS, flood months are associated with a 2.1-3.7x likelihood of Phase 3 underprediction in Chad, South Sudan, and Yemen. Saudi Arabia in particular indicates an 8x underprediction likelihood, which is particularly high. Finally, drought months are associated with a 2.6-8x increase in underprediction likelihood, with significant associations in Burkina Faso, Ethiopia, Mali, and Somalia. In particular, Madagascar indicates a 10x likelihood of underprediction during flood months.

Discussion

This analysis demonstrates the utility of Markovian approaches to famine early warning systems. We determine that majority of the FEWS study region meets Markovian assumptions that current IPC phase depends only on the previous IPC phase, and there is limited evidence for long-term memory in the FEWS study area.

One strength of this probabilistic approach to famine is its alignment with established concepts in famine theory such as pressure, hold, and rebalancing (Paul Howe, 2018; P. W. Howe & Naumova, 2022). Temporal metrics such as persistence and crisis duration in this article are closely related to Howe's conceptualization of hold as the absence of efforts, environments, or institutions to alleviate worsening food insecurity (Paul Howe, 2018). The factors driving persistence in a location and IPC phase remain open to interpretation. In some contexts, persistence may represent recovery from an idiosyncratic shock, whereas in other contexts it may mean successful aid delivery or programming to prevent worsening food security. This analysis presents no assumptions about the sources or underlying drivers; instead we outline quantitative diagnostic tools to investigate these phenomena. One point of departure from

existing literature is the assignment of distinct start and end dates to define a crisis period. We recognize this as a rudimentary characterization of famine, but present it to emphasize the temporal dimension of famine analytics. Despite proof of limited autocorrelation between famine states, phase trajectories and measures such as persistence and crisis duration can assist with classification of emergent crises into famine archetypes and short-term predictions of phase trajectories (P. Howe, 2010). Monitoring temporal dynamics is also particularly important in locations with few observations of rarer phases. In these regions, monitoring adjacent phases can better inform analysts about spatiotemporal variation in crisis patterns to generate more informed null hypotheses about the future. Finally, temporal metrics can also support investigation into longer-term phenomena of interest such as rebalancing and resilience.

The findings presented herein are subject to several limitations. The sample size of 39 observations provides a limited time series, and data for many regions are available for only a fraction of this study period. The 3-4 month duration between FEWS release cycles contributes another constraint. Wasting and acute hunger can occur at a timescale of weeks; therefore, the time period of observation every 3-4 months may be misaligned with the time period in which acute food insecurity unfolds. To address this issue, FEWSNET often publishes more frequent updates to their projections particularly for evolving crises. However, updates are rarely made to the CS release, which provides the best estimate of current acute food insecurity conditions. Despite these limitations, the strength of FEWS and similar EWSs is the detection of population-level experience of acute food insecurity with a lag of a few weeks. Markovian methods such as transition probabilities and conditional persistence help utilize the complete available time series to extract meaningful null hypotheses regarding acute food insecurity prevalence and recurrence in a region.

Improvements to the underlying data can help refine the presented methodology. Shortening the FEWS cycle to generate more frequent observations is the ideal solution to address systematic

limitations. More observations would lengthen the time series and help address the temporal misalignment between survey cycle and acute food insecurity outcomes. In probabilistic terms, improved survey frequency can also improve the likelihood of observing Phase 4 and Phase 5 for improved explanatory and predictive power. Finally, FEWSNET can also improve the quality of this analysis by curating high-frequency updates to the ML1 projections alongside their cyclical CS, ML1, and ML2 products. Although updates are structured to provide stakeholders near real-time projections in rapidly evolving situations, these data are difficult to access post hoc or years after the crisis in question. Systematic curation of these data can help analysts contextualize particular episodes of acute food insecurity, and improve metrics such as transition probabilities and volatility. Many of these limitations can be addressed via scale investments in famine surveillance, which can accelerate Markovian analysis and facilitate rapid humanitarian action.

Spatial and temporal alignment and computational costs are recurring challenges for this analysis. Utilizing high resolution gridded data partly resolves the challenge of changing spatial boundaries across the study period; however, gridded data also present boundary problems. FEWS data is disseminated as polygons, and rasterizing these data to a consistent grid can generate outliers or false transitions at polygon boundaries. Although a minimum threshold of 1% of the study area was used to limit the influence of these pixels across all analyses, it is important to be cognizant of these potential sources of error. In the temporal domain, the pre-defined validity periods for FEWS observations and projections significantly simplifies this analysis. However, our decision to measure the validity period from the start of the month, as opposed to the middle of the month, may affect our estimates of persistence, volatility, and crisis duration (T. M. Alarcon Falconi et al., 2020). Additionally, even though majority of the study region was found to be Markovian, we expect different temporal dynamics in a small fraction of the study area. Collapsing the temporal domain of this data in effect discounts the time

dependence of each transition and the trajectory of food insecurity faced by residents of a particular region. A sensitivity analysis on the temporal dynamics of acute food insecurity in non-Markovian regions would be warranted in the future as longer time series of FEWS observations become available. Computational costs must also be accounted for; pixel-level time series analysis for Markovian applications is more computationally expensive than previous studies on this topic. We thus recommend centralized storage of these workflows and outputs on FEWSNET for dissemination to analysts. This initiative can also facilitate regular generation of a 'famine system diagnostic report' to summarize changes to the presented transition probabilities in high spatial resolution and in near-real time.

Despite the aforementioned concerns, a Markovian analysis of famine early warning provides a missing unit of risk analysis for widespread applications in humanitarian systems. Transition probabilities across critical phases can be utilized to analyze contextual drivers of particular phase transitions, such as extreme weather and conflict. The spatial clustering of these patterns is also relevant and research into this topic can help guide resources across humanitarian and development sectors towards particular 'hotspots' of high risk. These metrics can also be extended to other famine early warning systems such as the IPC and Cadre Harmonisee for systematic comparisons and learning. IPC also provides population estimates by phase, which can be utilized for sharper population-level models of acute food insecurity. Future analyses can also improve efforts to model critical phase transitions by addressing key data gaps. Quantification and spatiotemporal alignment of humanitarian aid disbursement, which is directly linked to improving food security, can improve both explanatory and predictive models of famine risk. Methodological advancements can also include hidden Markov chain models, Markov-Chain Monte Carlo methods to estimate confidence intervals of likely phase trajectories, and Bayesian inference for famine early warning.

Our methodology also highlights the need for more nuanced quantitative methods and associated vocabulary for famine early warning. Measures such as accuracy, false positives, and false negatives are often borrowed from medical or meteorological literature but are not as useful for famine early warning (P. W. Howe & Naumova, 2022). Previous analyses of the same dataset have utilized forecast metrics such as Bias, Skill, and Accuracy (R. J. Choularton & Krishnamurthy, 2019b; Krishnamurthy et al., 2020). However, these measures fail to sufficiently account for the asymmetric probability distribution highlighted in this paper, as well as inherent properties of the underlying famine system. Accuracy in our analysis only describes the diagonal presented in Figure 30 and Figure 34. Traditional measures of Type 1 (false positive; below the diagonal) and Type 2 (false negative; above the diagonal) errors are also not meaningful for FEWS since extensive political and humanitarian effort is directed towards avoiding transitions to higher IPC phases, particularly when regions are classified as Phase 4 or Phase 5. True error in FEWS refers only to Type 2 error or “missed transitions” (R. J. Choularton & Krishnamurthy, 2019b), which are instances where a lower phase is projected than what is observed. Within the umbrella of Type 1 error, the lack of data on the amount, extent, and utilization of humanitarian aid makes it difficult to distinguish between true error and successful humanitarian efforts that improve food security. In this context, vocabulary such as misalignment or protection rate may be preferrable to error. This distinction can also help emphasize the large cost difference between Type 2 error which endangers lives, and a forecast misalignment that effectively protects nutrition and health. Further, as quantitative models for famine early warning evolve to include artificial intelligence and machine learning methods, we echo the need for semantic consistency to distinguish between model-based, human-informed, and hybrid forecasts of famine (P. W. Howe & Naumova, 2022). FEWS short-term and long-term projections are outputs of structured scenario development processes involving data and expert opinion on ongoing factors which may affect food security. On the other hand, model-based forecasts, or predictions, utilize only data to inform decision-making.

Literature must emphasize the distinct but related domains of projections, predictions, and forecasts to ensure optimum clarity and transparency.

Conclusion

Markov chains are a useful tool for explanatory analysis of FEWS data. We prove that majority of the FEWS study region meets Markovian assumptions, and demonstrate temporal and spatial trends in transition and conditional probabilities across critical phase pairs. These measures can be utilized for high-resolution surveillance of the famine system.

Chapter 7: Conclusions and Future Directions

Overview and Conclusions

This dissertation examines three indicators of food security at the global scale to evaluate these signals' responsiveness to a suite of extreme events. Retail food prices in Chapter 4 are shown to be generally resilient to extreme weather events; however, general supply constriction of Fruits and Vegetables during storm months and for Breads and Cereals during drought months points to specific avenues for climate-sensitive policies and programs to support healthy diets. Chapter 5 establishes significant heterogeneity in seasonal wasting patterns across continental Africa, and affirms the need for flexible analytical specifications alongside spatiotemporal methods to quantify seasonal wasting. Chapter 6 demonstrates the utility of probabilistic methods for investigating accuracy in famine early warning systems and improving forecasting.

The global scale of analysis is a key strength of this investigation. We limit the potential for selection bias by including all available data across the three aims. The global scale further enables the investigation of five different types of extreme weather events, many of which disproportionately affect some geographies over others. This chosen spatial extent allows us to accumulate generalizable evidence from observations at much smaller spatial scales such as markets and administrative regions. Although no global conclusion is fully applicable at local scales, pooling evidence across the world allows for potential statistical amplification of associations, and large sample sizes allow us to test broad hypotheses to develop baseline evidence that can then direct localized investigations. Therefore, this dissertation provides the foundational feasibility analyses across research aims, and demonstrates the utility of multiple analytical techniques applied to complex research questions.

The choice of percentile-based definitions of extreme weather utilized in this dissertation is another decision that may elicit critique. Although literature points to a variety of indicators and

measures for each extreme event, our choice of percentile indicators remains relatively unique. This decision emerged as a practical consideration to ensure sufficient instances of extreme weather to investigate the research question while capturing the underlying variability of climate. By design this definition precludes imposition of particular thresholds, whether experimentally derived (e.g. SPEI below 1.5) or grounded in human experience (e.g. temperatures above 40 °C). In adopting a geographically variant definition of extreme weather, we allow for the possibility of habituation to a range of extreme weather for populations residing in any location. In other words, the experience and expectation of a heatwave in Dhaka is understandably different from a heatwave in N'djamena, and our operational definitions reflect this variability. The percentile formulation further preserves the assumption of quasi-random distribution of extreme events, and ensures that regression analyses represent data from different geographies more equally in comparison to value-based thresholds which may introduce geographic bias in the underlying data. Thus, the flexible definition of extreme weather allows for broader generalizability of calculated associations.

Limitations

Several common limitations emerge across chapters. Firstly, the spatial and temporal resolution of available data remains a challenge. The high spatial resolution of global analyses presented herein comes at the expense of resolution in the temporal domain, as only monthly data was utilized. The need for data collected at higher frequency is evident; weekly retail prices and weekly weight fluctuations or anthropometric measures such as mid-upper arm circumference (MUAC) can provide necessary nuance and inform much richer, localized analyses of extreme weather effects in the food system. Temporal aggregation to month of observation also results in displacement of true peak timings, which translates to higher costs of mistimed policies and program (T. M. Alarcon Falconi et al., 2020). Spatial resolution is also relevant for the analysis of famine systems; the communities from which the underlying data was collected are not

always presented, and spatial aggregation to administrative boundaries may obscure specific hotspots of vulnerability. Thus, data at higher spatial and temporal resolution can be particularly valuable for validation of extreme weather associations at actionable scales.

The sparsity of available data in the temporal and climatological domains is yet another limitation. Although data fusion attempts to address this sparsity, it is difficult to retroactively reconstruct survey cluster locations based on a handful of spatial and temporal fields gathered in large cross-sectional surveys. In the absence of validation data for spatial matching, the techniques utilized herein provide a means of utilizing valuable publicly available data.

A more technical limitation involves the datasets utilized to derive extreme weather for this dissertation. Recent research comparing temperature datasets indicates little alignment between extreme event occurrence across datasets (Coughlan de Perez, Arrighi, & Marunye, 2023). Although greater alignment is observed for flood and drought events (Akinsanola et al., 2016; Naumann et al., 2014), disagreements across weather data indicates that the generalizability of results from this dissertation is limited by the choice of datasets utilized to characterize extreme weather. Further research is needed to document effect sizes across different temperature and precipitation datasets, and extract ensemble estimates of impacts on each of the dependent variables.

Assumed exposures present another category of limitations. We assume study populations are equally affected by weather and do not account for individual, household, and community mediating factors. This naïve framing of exposures allows us to extract community prevalence of wasting and general trends in food insecurity, but it does not provide community-specific results. We also assume that extreme events are exogenous to human health outcomes, but in the context of anthropogenic climate change, climate is affected by human activities and we know human activity mediates the experience of extreme weather. Therefore, endogeneity is a concern across the previous chapters. Although the global scale of analysis potentially dilutes

some of these influences, localized analyses should utilize robust causal inference strategies and take particular care to ensure

Future Directions

This analysis presents several avenues for further research. Metrics and conclusions calculated at the global scale require further validation at local spatial scales and higher temporal frequency for policy relevance. Country ministries and statistics departments may have access to detailed food lists and price databases, and comparable price analysis techniques can be applied to study price responses to locally relevant extreme weather events. Responses of producer and wholesale prices can also be studied to characterize price responses to extreme weather throughout the supply chain. Seasonal wasting patterns also require validation and localization. Beyond the application of multiple harmonic regression to diverse survey datasets, future research can extend the present analysis on wasting to study the effect of extreme weather in early childhood on growth faltering, stunting, and chronic malnutrition. Further study is also needed to investigate the climate sensitivity of anthropometric indicators; the present analysis demonstrates multiple estimation strategies using binary wasting indicators, but the underlying Z-scores and raw anthropometry may be just as valuable and potentially more sensitive to extreme weather. Famine early warning systems can also apply ensemble methods to derive probabilistic measures of real-time uncertainty estimates for improved food insecurity forecasting.

Several factors were not considered in this text due to the limited analytical scope, but require further investigation for nuanced understanding of extreme weather effects in food systems. Such factors include interactions between extreme events, particularly among often concurrent events such as floods and storms. The sequence of disasters is also known to affect coping strategies and resilience (Béné et al., 2016; Béné, Headey, Haddad, & von Grebmer, 2015); therefore, event cascades, feedback loops, and downstream effects on food systems merit

further investigation. As discussed above, establishing alignment of extreme events across environmental datasets remains a critical next step, and future studies would benefit from an 'ensemble' approach to quantifying effects of extreme weather across different source datasets. Studies can also investigate pathways beyond climate and extreme weather, including conflict, mobility, and demographic factors that influence vulnerability and coping capacity. In localized investigations of these factors, studies should also aim to apply robust causal inference methods to isolate the influence of extreme weather in outcomes across the food system.

Finally, this analysis presents several priorities for the research agenda on climate and food systems. The first priority should be improving data quality, and making critical spatial data behind MICS and SMART survey datasets available to researchers. Secondly, existing survey instruments and data partnerships should seek to address temporal sparsity and climatological representativeness in the data. This outcome can be achieved by leveraging synergies across DHS, MICS, and SMART apparatuses, and deploying SMART or other rapid assessment surveys for nutrition surveillance and reporting. These priorities undoubtedly require large-scale investments in improved nutrition data collection and warehousing. Decentralized warehouses can further address concerns of academic access to anonymized data, and improve transparency and interpretability for a wider audience. Parallel investments in data fusion and methodological advancements such as machine learning and artificial intelligence can ensure that the flexible methods developed in this dissertation can be applied in various contexts while preserving plausible structural foundations.

References

Abatzoglou, J. T., Dobrowski, S. Z., Parks, S. A., & Hegewisch, K. C. (2018). TerraClimate, a high-resolution global dataset of monthly climate and climatic water balance from 1958-2015. *Sci Data, 5*, 170191. doi:10.1038/sdata.2017.191

Abiona, O. (2017). Adverse Effects of Early Life Extreme Precipitation Shocks on Short-term Health and Adulthood Welfare Outcomes. *Review of Development Economics, 21*(4), 1229-1254. doi:10.1111/rode.12310

ACF International. (2013). Seasonality: the missing piece of the undernutrition puzzle?

Aguilar, A., & Vicarelli, M. (2022). El Niño and children: Medium-term effects of early-life weather shocks on cognitive and health outcomes. *World Development, 150*. doi:10.1016/j.worlddev.2021.105690

Ahern, M., Kovats, R. S., Wilkinson, P., Few, R., & Matthies, F. (2005). Global health impacts of floods: epidemiologic evidence. *Epidemiol Rev, 27*, 36-46. doi:10.1093/epirev/mxi004

Ahmed, F., Khan, M. S. A., Warner, J., Moors, E., & Terwisscha Van Scheltinga, C. (2018). Integrated Adaptation Tipping Points (IATPs) for urban flood resilience. *Environment and Urbanization, 30*(2), 575-596. doi:10.1177/0956247818776510

Aizer, A., Stroud, L., & Buka, S. (2016). Maternal stress and child outcomes: Evidence from siblings. *Journal of Human Resources, 51*(3), 523-555.

Akinsanola, A. A., Ogunjobi, K. O., Ajayi, V. O., Adefisan, E. A., Omotosho, J. A., & Sanogo, S. (2016). Comparison of five gridded precipitation products at climatological scales over West Africa. *Meteorology and Atmospheric Physics, 129*(6), 669-689. doi:10.1007/s00703-016-0493-6

Akter, S. (2020). The impact of COVID-19 related 'stay-at-home' restrictions on food prices in Europe: findings from a preliminary analysis. *Food Secur, 12*(4), 719-725. doi:10.1007/s12571-020-01082-3

Alarcon Falconi, T. M., Cruz, M. S., & Naumova, E. N. (2018). The shift in seasonality of legionellosis in the USA. *Epidemiol Infect, 146*(14), 1824-1833. doi:10.1017/S0950268818002182

Alarcon Falconi, T. M., Estrella, B., Sempertegui, F., & Naumova, E. N. (2020). Effects of Data Aggregation on Time Series Analysis of Seasonal Infections. *Int J Environ Res Public Health, 17*(16). doi:10.3390/ijerph17165887

Alarcon Falconi, T. M., Estrella, B., Sempértegui, F., & Naumova, E. N. (2020). Effects of Data Aggregation on Time Series Analysis of Seasonal Infections. *International Journal of Environmental Research and Public Health, 17*(16). doi:10.3390/ijerph17165887

Alderman, H. (2006). Long term consequences of early childhood malnutrition. *Oxford Economic Papers, 58*(3), 450-474. doi:10.1093/oep/gpl008

Alderman, H., & Headey, D. (2018). The timing of growth faltering has important implications for observational analyses of the underlying determinants of nutrition outcomes. *PLoS One, 13*(4), e0195904. doi:10.1371/journal.pone.0195904

Alderman, K., Turner, L. R., & Tong, S. (2012). Floods and human health: a systematic review. *Environ Int, 47*, 37-47. doi:10.1016/j.envint.2012.06.003

Alexander, D. E. (1993). *Natural Disasters*: Routledge.

Alexander, D. E. (2005). An interpretation of disaster in terms of changes in culture, society and international relations. In E. L. Quarantelli & R. W. Perry (Eds.), *What is Disaster? New Answers to Old Questions* (pp. 25-38). Philadelphia: Xlibris.

Almond, D., & Currie, J. (2011). Killing Me Softly: The Fetal Origins Hypothesis. *J Econ Perspect, 25*(3), 153-172. doi:10.1257/jep.25.3.153

Amare, M., Jensen, N. D., Shiferaw, B., & Cissé, J. D. (2018). Rainfall shocks and agricultural productivity: Implication for rural household consumption. *Agricultural Systems, 166*, 79-89. doi:10.1016/j.agsy.2018.07.014

American Geological Institute. (1984). *Glossary of Geology*. Falls Church, Virginia: American Geological Institute.

Ampaabeng, S. K., & Tan, C. M. (2013). The long-term cognitive consequences of early childhood malnutrition: the case of famine in Ghana. *J Health Econ, 32*(6), 1013-1027. doi:10.1016/j.jhealeco.2013.08.001

Andalón, M., Azevedo, J. P., Rodríguez-Castelán, C., Sanfelice, V., & Valderrama-González, D. (2016). Weather Shocks and Health at Birth in Colombia. *World Development, 82*, 69-82. doi:10.1016/j.worlddev.2016.01.015

Anderson, M. B. (1991). Vulnerability to Disaster and Sustainable Development: A General Framework for Assessing Vulnerability. In *Disaster Prevention for Sustainable Development: Economic and Policy Issues*. Washington, DC: World Bank.

Ara Begum, R., Lempert, R., Ali, E., Benjaminsen, T. A., Bernauer, T., Cramer, W., . . . Wester, P. (2022). Point of Departure and Key Concepts. In H.-O. Pörtner, D. C. Roberts, M. Tignor, E. S. Poloczanska, K. Mintenbeck, A. Alegría, M. Craig, S. Langsdorf, S. Löschke, V. Möller, A. Okem, & B. Rama (Eds.), *Climate Change 2022: Impacts, Adaptation and Vulnerability. Contribution of Working Group II to the Sixth Assessment Report of the Intergovernmental Panel on Climate Change* (pp. 121-196). Cambridge, United Kingdom and New York, NY, USA: Cambridge University Press.

Armstrong McKay, D. I., Staal, A., Abrams, J. F., Winkelmann, R., Sakschewski, B., Loriani, S., . . . Lenton, T. M. (2022). Exceeding 1.5 degrees C global warming could trigger multiple climate tipping points. *Science, 377*(6611), eabn7950. doi:10.1126/science.abn7950

Arndt, C., Hussain, M. A., Salvucci, V., & Osterdal, L. P. (2016). Effects of food price shocks on child malnutrition: The Mozambican experience 2008/2009. *Econ Hum Biol, 22*, 1-13. doi:10.1016/j.ehb.2016.03.003

Aven, T. (2012). The risk concept—historical and recent development trends. *Reliability Engineering & System Safety, 99*, 33-44. doi:10.1016/j.ress.2011.11.006

Backer, D., & Billing, T. (2019). *Report on FEWS NET Validation Assessment*. Retrieved from

Bai, Y., Alemu, R., Block, S. A., Headey, D., & Masters, W. A. (2021). Cost and affordability of nutritious diets at retail prices: Evidence from 177 countries. *Food Policy, 99*, 101983. doi:10.1016/j.foodpol.2020.101983

Bai, Y., Naumova, E. N., & Masters, W. A. (2020). Seasonality of diet costs reveals food system performance in East Africa. *Science Advances, 6*.

Baker, R. E., & Anttila-Hughes, J. (2020). Characterizing the contribution of high temperatures to child undernourishment in Sub-Saharan Africa. *Sci Rep, 10*(1), 18796. doi:10.1038/s41598-020-74942-9

Bakhtsiyarava, M., Ortigoza, A., Sanchez, B. N., Braverman-Bronstein, A., Kephart, J. L., Rodriguez Lopez, S., . . . Diez Roux, A. V. (2022). Ambient temperature and term birthweight in Latin American cities. *Environ Int, 167*, 107412. doi:10.1016/j.envint.2022.107412

Barker, D. J. P. (1994). *Mothers, babies, and disease in later life*: BMJ publishing group London.

Barrett, C. B., & Constas, M. A. (2014). Toward a theory of resilience for international development applications. *Proc Natl Acad Sci U S A, 111*(40), 14625-14630. doi:10.1073/pnas.1320880111

Baye, K., & Hirvonen, K. (2020). Seasonality: a missing link in preventing undernutrition. *The Lancet Child & Adolescent Health, 4*(1). doi:10.1016/s2352-4642(19)30343-8

Beck, H. E., Zimmermann, N. E., McVicar, T. R., Vergopolan, N., Berg, A., & Wood, E. F. (2018). Present and future Koppen-Geiger climate classification maps at 1-km resolution. *Sci Data, 5*, 180214. doi:10.1038/sdata.2018.214

Beguería, S., Vicente-Serrano, S. M., & Angulo-Martínez, M. (2010). A Multiscalar Global Drought Dataset: The SPEIbase: A New Gridded Product for the Analysis of Drought Variability and Impacts. *Bulletin of the American Meteorological Society, 91*(10), 1351-1356. doi:10.1175/2010bams2988.1

Beguería, S., Vicente-Serrano, S. M., Reig, F., & Latorre, B. (2014). Standardized precipitation evapotranspiration index (SPEI) revisited: parameter fitting, evapotranspiration models, tools, datasets and drought monitoring. *International Journal of Climatology, 34*(10), 3001-3023. doi:10.1002/joc.3887

Belesova, K., Agabiirwe, C. N., Zou, M., Phalkey, R., & Wilkinson, P. (2019). Drought exposure as a risk factor for child undernutrition in low- and middle-income countries: A systematic review and assessment of empirical evidence. *Environ Int, 131*, 104973. doi:10.1016/j.envint.2019.104973

Bell, G. D., Halpert, M. S., Schnell, R. C., Higgins, R. W., Lawrimore, J., Kousky, V. E., . . . Artusa, A. (2000). Climate Assessment for 1999. *Bulletin of the American Meteorological Society, 81*(6), S1-S50.

Béné, C., Al-Hassan, R. M., Amarasinghe, O., Fong, P., Ocran, J., Onumah, E., . . . Mills, D. J. (2016). Is resilience socially constructed? Empirical evidence from Fiji, Ghana, Sri Lanka, and Vietnam. *Global Environmental Change, 38*, 153-170. doi:10.1016/j.gloenvcha.2016.03.005

Béné, C., Frankenberger, T., & Nelson, S. (2015). *Design, Monitoring and Evaluation of Resilience Interventions: Conceptual and Empirical Considerations*. Retrieved from
Béné, C., Headey, D., Haddad, L., & von Grebmer, K. (2015). Is resilience a useful concept in the context of food security and nutrition programmes? Some conceptual and practical considerations. *Food Security, 8*(1), 123-138. doi:10.1007/s12571-015-0526-x
Bhaskaran, K., Gasparrini, A., Hajat, S., Smeeth, L., & Armstrong, B. (2013). Time series regression studies in environmental epidemiology. *Int J Epidemiol, 42*(4), 1187-1195. doi:10.1093/ije/dyt092
Bischiniotis, K., van den Hurk, B., Jongman, B., Coughlan de Perez, E., Veldkamp, T., de Moel, H., & Aerts, J. (2018). The influence of antecedent conditions on flood risk in sub-Saharan Africa. *Natural Hazards and Earth System Sciences, 18*(1), 271-285. doi:10.5194/nhess-18-271-2018
Bivand, R., Keitt, T., & Rowlingson, B. (2019). rgdal: Bindings for the 'Geospatial' Data Abstraction Library (Version R package version 1.4-8). Retrieved from https://CRAN.R-project.org/package=rgdal
Bivand, R., & Rundel, C. (2018). rgeos: Interface to Geometry Engine - Open Source ('GEOS') (Version R package version 0.4-2). Retrieved from https://CRAN.R-project.org/package=rgeos
Bivand, R. S., Pebesma, E., & Gomez-Rubio, V. (2013). *Applied spatial data analysis with R* (Second edition ed.): Springer, NY.
Black, R. E., Victora, C. G., Walker, S. P., Bhutta, Z. A., Christian, P., de Onis, M., . . . Child Nutrition Study, G. (2013). Maternal and child undernutrition and overweight in low-income and middle-income countries. *Lancet, 382*(9890), 427-451. doi:10.1016/S0140-6736(13)60937-X
Block, S., Haile, B., You, L., & Headey, D. (2021). Heat shocks, maize yields, and child height in Tanzania. *Food Security, 14*(1), 93-109. doi:10.1007/s12571-021-01211-6
Brown, M. E., Backer, D., Billing, T., White, P., Grace, K., Doocy, S., & Huth, P. (2020). Empirical studies of factors associated with child malnutrition: highlighting the evidence about climate and conflict shocks. *Food Security, 12*(6), 1241-1252. doi:10.1007/s12571-020-01041-y
Brown, M. E., & Kshirsagar, V. (2015). Weather and international price shocks on food prices in the developing world. *Global Environmental Change, 35*, 31-40. doi:10.1016/j.gloenvcha.2015.08.003
Buchanan-Smith, M., & Davies, S. (1995). *Famine early warning and response: the missing link*. London: Intermediate Technology Publications Ltd.
Bujones, A. K., Jaskiewicz, K., Linakis, L., & McGirr, M. (2013). *A Framework for Analyzing Resilience in Fragile and Conflict-Affected Situations. USAID Final Report*. Retrieved from
Burgert, C. R., Zachary, B., & Colston, J. (2013). *Incorporating Geographic Information into Demographic and Health Surveys: A Field Guide to GPS Data Collection*. Retrieved from Calverton, Maryland, USA:
Burton, I., Kates, R. W., & White, G. F. (1978). *The environment as hazard*: New York: Oxford University Press.
Burton, I., Kates, R. W., & White, G. F. (1993). *The Environment as Hazard*. New York: The Guilford Press.
Cai, Y., Chang, H. W., Chang, T., Țăran, A.-M., & Pirtea, M. (2023). Time-varying causal impacts of the continental US weather risks on food price. *Applied Economics Letters*, 1-7. doi:10.1080/13504851.2023.2186344
Cameron, A. C., & Trivedi, P. K. (2013). *Regression Analysis of Count Data* (Vol. 53). London: Cambridge University Press.
Carletto, G., Banerjee, R., & Zezza, A. (2015). *Household Data Sources for Measuring and Understanding Resilience. Resilience Measurement Technical Working Group. Technical Series No. 3*. Retrieved from Rome: http://www.fsincop.net/fileadmin/user_upload/fsin/docs/resources/FSIN_TechnicalSeries_3.pdf
Cedrez, C. B., Chamberlin, J., & Hijmans, R. J. (2020). Seasonal, annual, and spatial variation in cereal prices in Sub-Saharan Africa. *Glob Food Sec, 26*, 100438. doi:10.1016/j.gfs.2020.100438
Chacón-Montalván, E. A., Taylor, B. M., Cunha, M. G., Davies, G., Orellana, J. D. Y., & Parry, L. (2021). Rainfall variability and adverse birth outcomes in Amazonia. *Nature Sustainability, 4*(7), 583-594. doi:10.1038/s41893-021-00684-9
Chambers, R. (2007). Health, agriculture, and rural poverty: Why seasons matter. *The Journal of Development Studies, 18*(2), 217-238. doi:10.1080/00220388208421828
Chambers, R., & Conway, G. R. (1991). *Sustainable Rural Livelihoods: practical concepts for the 21st century. IDS Discussion Paper 296*. Retrieved from

Chatzopoulos, T., Pérez Domínguez, I., Zampieri, M., & Toreti, A. (2020). Climate extremes and agricultural commodity markets: A global economic analysis of regionally simulated events. *Weather and Climate Extremes, 27*. doi:10.1016/j.wace.2019.100193

Chersich, M. F., Pham, M. D., Areal, A., Haghighi, M. M., Manyuchi, A., Swift, C. P., . . . Heat-Health Study, G. (2020). Associations between high temperatures in pregnancy and risk of preterm birth, low birth weight, and stillbirths: systematic review and meta-analysis. *BMJ, 371*, m3811. doi:10.1136/bmj.m3811

Chotard, S., Mason, J. B., Oliphant, N. P., Mebrahtu, S., & Hailey, P. (2010). Fluctuations in wasting in vulnerable child populations in the Greater Horn of Africa. *Food and Nutrition Bulletin, 31*(3).

Choularton, R., Frankenberger, T., Kurtz, J., & Nelson, S. (2015). *Measuring Shocks and Stressors as Part of Resilience Measurement. Resilience Measurement Technical Working Group. Technical Series No. 5*. Retrieved from Rome: http://www.fsincop.net/fileadmin/user_upload/fsin/docs/resources/FSIN_TechnicalSeries_5.pdf

Choularton, R. J., & Krishnamurthy, P. K. (2019a). How accurate is food security early warning? Evaluation of FEWS NET accuracy in Ethiopia. *Food Security, 11*, 333-344. doi:10.1007/s12571-019-00909-y

Choularton, R. J., & Krishnamurthy, P. K. (2019b). How accurate is food security early warning? Evaluation of FEWS NET accuracy in Ethiopia. *Food Security, 11*(2), 333-344. doi:10.1007/s12571-019-00909-y

Cohen, M. J., & Garrett, J. L. (2010). The food price crisis and urban food (in)security. *Environment and Urbanization, 22*(2), 467-482. doi:10.1177/0956247810380375

Collins, S. L., Carpenter, S. R., Swinton, S. M., Orenstein, D. E., Childers, D. L., Gragson, T. L., . . . Whitmer, A. C. (2010). An integrated conceptual framework for long-term social–ecological research. *Frontiers in Ecology and the Environment, 9*(6), 351-357. doi:10.1890/100068

Constas, M. A., Frankenberger, T. R., & Hoddinott, J. (2014). *Resilience Measurement Principles: Toward an Agenda for Measurement Design. Resilience Measurement Technical Working Group. Technical Series No. 1*. Retrieved from Rome:

Constas, M. A., Frankenberger, T. R., Hoddinott, J., Mock, N., Romano, D., Béné, C., & Maxwell, D. (2015). *A Common Analytical Model for Resilience Measurement: Causal Framework and Methodological Options. Resilience Measurement Technical Working Group. Technical Series No. 2*. Retrieved from Rome:

Cooper, M., Brown, M. E., Azzarri, C., & Meinzen-Dick, R. (2019). Hunger, nutrition, and precipitation: evidence from Ghana and Bangladesh. *Population and Environment, 41*(2), 151-208. doi:10.1007/s11111-019-00323-8

Cornwell, K., & Inder, B. (2015). Child Health and Rainfall in Early Life. *The Journal of Development Studies, 51*(7), 865-880. doi:10.1080/00220388.2014.976618

Cottrell, R. S., Nash, K. L., Halpern, B. S., Remenyi, T. A., Corney, S. P., Fleming, A., . . . Blanchard, J. L. (2019). Food production shocks across land and sea. *Nature Sustainability, 2*(2), 130-137. doi:10.1038/s41893-018-0210-1

Coughlan de Perez, E., Arrighi, J., & Marunye, J. (2023). Challenging the universality of heatwave definitions: gridded temperature discrepancies across climate regions. *Climatic Change, 176*(12). doi:10.1007/s10584-023-03641-x

Cuesta, J., Htenas, A., & Tiwari, S. (2014). Monitoring global and national food price crises. *Food Policy, 49*, 84-94. doi:10.1016/j.foodpol.2014.06.001

Cutter, S. L. (1996). Vulnerability to environmental hazards. *Progress in Human Geography, 20*(4), 529-539.

Cutter, S. L. (2003). The Vulnerability of Science and the Science of Vulnerability. *Annals of the Association of American Geographers, 93*(1), 1-12. doi:10.1111/1467-8306.93101

Cutter, S. L. (2018). Compound, Cascading, or Complex Disasters: What's in a Name? *Environment: Science and Policy for Sustainable Development, 60*(6), 16-25. doi:10.1080/00139157.2018.1517518

Cutter, S. L., Barnes, L., Berry, M., Burton, C., Evans, E., Tate, E., & Webb, J. (2008). A place-based model for understanding community resilience to natural disasters. *Global Environmental Change, 18*(4), 598-606. doi:10.1016/j.gloenvcha.2008.07.013

Dale, V. H., Lugo, A. E., MacMahon, J. A., & Pickett, S. T. A. (1998). Ecosystem Management in the Context of Large, Infrequent Disturbances. *Ecosystems, 1*(6), 546-557.

Darrouzet-Nardi, A. F., & Masters, W. A. (2017). Nutrition Smoothing: Can Proximity to Towns and Cities Protect Rural Children against Seasonal Variation in Agroclimatic Conditions at Birth? *PLoS One, 12*(1), e0168759. doi:10.1371/journal.pone.0168759
Davenport, F., Dorélien, A., & Grace, K. (2020). Investigating the linkages between pregnancy outcomes and climate in sub-Saharan Africa. *Population and Environment, 41*(4), 397-421. doi:10.1007/s11111-020-00342-w
Davis, K. F., Downs, S., & Gephart, J. A. (2020). Towards food supply chain resilience to environmental shocks. *Nature Food, 2*(1), 54-65. doi:10.1038/s43016-020-00196-3
Davis, K. F., Downs, S., & Gephart, J. A. (2021). Towards food supply chain resilience to environmental shocks. *Nat Food, 2*(1), 54-65. doi:10.1038/s43016-020-00196-3
Delbiso, T. D., Rodriguez-Llanes, J. M., Donneau, A. F., Speybroeck, N., & Guha-Sapir, D. (2017). Drought, conflict and children's undernutrition in Ethiopia 2000-2013: a meta-analysis. *Bull World Health Organ, 95*(2), 94-102. doi:10.2471/BLT.16.172700
Dercon, S., Hoddinott, J., & Woldehanna, T. (2005). Shocks and Consumption in 15 Ethiopian Villages, 1999–2004. *Journal of African Economies, 14*(4), 559-585. doi:10.1093/jae/eji022
Deschenes, O., Greenstone, M., & Guryan, J. (2009). Climate Change and Birth Weight. *Am Econ Rev, 99*(2), 211-217. doi:10.1257/aer.99.2.211
deWaal, A. (2017). *Mass starvation: The history and future of famine*: John Wiley & Sons.
Dewey, K. G., & Begum, K. (2011). Long-term consequences of stunting in early life. *Matern Child Nutr, 7 Suppl 3*(Suppl 3), 5-18. doi:10.1111/j.1740-8709.2011.00349.x
DFID. (2011). *Defining Disaster Resilience: A DFID Approach Paper*. Retrieved from
Didan, K. (2021). *MOD13A3 MODIS/Terra vegetation Indices Monthly L3 Global 1km SIN Grid V006 [Data set]*.
Dijkstra, L., Brandmüller, T., Kemper, T., Khan, A. A., & Veneri, P. (2020). *Applying the Degree of Urbanisation: A methodological manual to define cities, towns and rural areas for international comparisons*. Retrieved from
Dijkstra, L., Poelman, H., & Veneri, P. (2019). *The EU-OECD definition of a functional urban area*. Retrieved from Paris: https://www.oecd.org/cfe/regional-policy/THE%20EU-OECD20
Dillon, A., McGee, K., & Oseni, G. (2015). Agricultural Production, Dietary Diversity and Climate Variability. *The Journal of Development Studies, 51*(8), 976-995. doi:10.1080/00220388.2015.1018902
Dimitrova, A. (2021). Seasonal droughts and the risk of childhood undernutrition in Ethiopia. *World Development, 141*. doi:10.1016/j.worlddev.2021.105417
Donohue, I., Hillebrand, H., Montoya, J. M., Petchey, O. L., Pimm, S. L., Fowler, M. S., . . . Yang, Q. (2016). Navigating the complexity of ecological stability. *Ecol Lett, 19*(9), 1172-1185. doi:10.1111/ele.12648
Drabek, T. E. (1989). Disasters as Nonroutine Social Problems. *International Journal of Mass Emergencies and Disasters, 7*(3), 253-264.
Dynes, R. R. (2005). Coming to terms with community disaster. In E. L. Quarantelli & R. W. Perry (Eds.), *What is a disaster?: New answers to old questions* (pp. 127-144): Routledge.
Edwards, B., Gray, M., & Borja, J. B. (2021). Measuring Natural Hazard-Related Disasters through Self-Reports. *International Journal of Disaster Risk Science, 12*(4), 540-552. doi:10.1007/s13753-021-00359-1
Eyring, V., Gillett, N. P., Rao, K. M. A., Barimalala, R., Parrillo, M. B., Bellouin, N., . . . Sun, Y. (2021). Human Influence on the Climate System. In V. Masson-Delmotte, P. Zhai, A. Pirani, S. L. Connors, S. B. C. Péan, N. Caud, Y. Chen, L. Goldfarb, M. I. Gomis, M. Huang, K. Leitzell, E. Lonnoy, J. B. R. Matthews, T. K. Maycock, T. Waterfield, O. Yelekçi, R. Yu, & B. Zhou (Eds.), *Climate Change 2021: The Physical Science Basis. Contribution of Working Group I to the Sixth Assessment. Report of the Intergovernmental Panel on Climate Change* (pp. 423–552). Cambridge, United Kingdom and New York, NY, USA: Cambridge University Press.
FAO. (2015). *Global Administrative Unit Layers (GAUL)*. Retrieved from: http://www.fao.org/geonetwork/srv/en/metadata.show%3Fid%3D12691
FAO. (2021a). FAO Food Price Index. Retrieved from https://www.fao.org/worldfoodsituation/foodpricesindex/en/
FAO. (2021b). Global Information and Early Warning System on Food and Agriculture [dataset]. Retrieved from https://www.fao.org/giews/en/

FAO. (2021c). *The impact of disasters and crises on agriculture and food security: 2021*. Retrieved from Rome:
FAO, IFAD, IMF, OECD, UNCTAD, WFP, . . . UNHLTF. (2011). *Price Volatility in Food and Agricultural Markets: Policy Responses*. Retrieved from
FAO, IFAD, UNICEF, WFP, & WHO. (2021). *The State of Food Security and Nutrition in the World 2021: Transforming food systems for food security, improved nutrition and affordable healthy diets for all*. Rome: FAO.
FAO, IFAD, UNICEF, WFP, & WHO. (2023). *The State of Food Security and Nutrition in the World 2023: Urbanization, agrifood systems transformation and healthy diets across the rural–urban continuum*. Rome: FAO. https://doi.org/10.4060/cc6550en.
FAO and Tufts University. (2019). *Twin peaks: the seasonality of acute malnutrition, conflict and environmental factors – Chad, South Sudan and the Sudan*. Retrieved from Rome:
FAOSTAT. (2021). Consumer Price Index. Retrieved from https://www.fao.org/faostat/en/#data/CP
FEWSNET. (2018). *Scenario Development for Food Security Early Warning*. Retrieved from Washington DC:
FEWSNET. (2019). *FEWSNET Food Security Data*. Retrieved from: http://shapefiles.fews.net.s3.amazonaws.com/HFIC/FEWS_NET_Food_Security_Data_v3.pdf
Fewster, R. (2013). Chapter 8 Markov Chains. Retrieved from https://www.stat.auckland.ac.nz/~fewster/325/notes/ch8.pdf
Florczyk A.J., C. C., Ehrlich D., Freire S., Kemper T., Maffenini L., Melchiorri M., Pesaresi M., Politis P., Schiavina M., Sabo F., Zanchetta L. (2019). *GHSL Data Package 2019* (Vol. EUR 29788 EN JRC 117104). Luxembourg: Publications Office of the European Union.
Freudenreich, H., Aladysheva, A., & Brück, T. (2022). Weather shocks across seasons and child health: Evidence from a panel study in the Kyrgyz Republic. *World Development, 155*. doi:10.1016/j.worlddev.2021.105801
Fritz, C. E. (1961). Disaster, contemporary social problems. *Harcourt: N ew York, 65*, 1-694.
FSIN, & Global Network Against Food Crises. (2023). *Global Report on Food Crises*. Retrieved from Rome. https://www.fsinplatform.org/global-report-food-crises-2023:
Funk, C., Peterson, P., Landsfeld, M., Pedreros, D., Verdin, J., Shukla, S., . . . Michaelsen, J. (2015). The climate hazards infrared precipitation with stations--a new environmental record for monitoring extremes. *Sci Data, 2*, 150066. doi:10.1038/sdata.2015.66
Funk, C., Shukla, S., Thiaw, W. M., Rowland, J., Hoell, A., McNally, A., . . . Verdin, J. (2019). Recognizing the Famine Early Warning Systems Network: Over 30 Years of Drought Early Warning Science Advances and Partnerships Promoting Global Food Security. *Bulletin of the American Meteorological Society, 100*(6), 1011-1027. doi:10.1175/bams-d-17-0233.1
Gibson, J., & Kim, B. (2019). Quality, quantity, and spatial variation of price: Back to the bog. *Journal of Development Economics, 137*, 66-77. doi:10.1016/j.jdeveco.2018.11.008
Global Administrative Areas (GADM). (2012). *Database of Global Administrative Areas, Version 2.0.* . Retrieved from: www.gadm.org
Grace, K., Brown, M., & McNally, A. (2014). Examining the link between food prices and food insecurity: A multi-level analysis of maize price and birthweight in Kenya. *Food Policy, 46*, 56-65. doi:10.1016/j.foodpol.2014.01.010
Grace, K., Davenport, F., Hanson, H., Funk, C., & Shukla, S. (2015). Linking climate change and health outcomes: Examining the relationship between temperature, precipitation and birth weight in Africa. *Global Environmental Change, 35*, 125-137. doi:10.1016/j.gloenvcha.2015.06.010
Green, R., Cornelsen, L., Dangour, A. D., Turner, R., Shankar, B., Mazzocchi, M., & Smith, R. D. (2013). The effect of rising food prices on food consumption: systematic review with meta-regression. *BMJ, 346*, f3703. doi:10.1136/bmj.f3703
Grimm, N. B., Pickett, S. T. A., Hale, R. L., & Cadenasso, M. L. (2017). Does the ecological concept of disturbance have utility in urban social–ecological–technological systems? *Ecosystem Health and Sustainability, 3*(1). doi:10.1002/ehs2.1255
Grimmett, G., & Welsh, D. (2014). Chapter 12 Markov chains. In *Probability: An Introduction*: OUP Oxford.
Guha-Sapir, D., & Below, R. (2022). *EM-DAT: The CRED/OFDA International Disaster Database*. Retrieved from: www.emdat.be

Hallegatte, S., Bangalore, M., Laura Bonzanigo, Fay, M., Kane, T., Narloch, U., . . . Vogt-Schilb, A. (2016). *Shock Waves: Managing the Impacts of Climate Change on Poverty*

Retrieved from Washington DC:
Harris, I., Osborn, T. J., Jones, P., & Lister, D. (2020). Version 4 of the CRU TS monthly high-resolution gridded multivariate climate dataset. *Sci Data, 7*(1), 109. doi:10.1038/s41597-020-0453-3
Hart, A., & Martínez, S. (2019). *spgs: Statistical Patterns in Genomic Sequences. R package version 1.0-3.* . Retrieved from: https://CRAN.R-project.org/package=spgs
Hasegawa, T., Sakurai, G., Fujimori, S., Takahashi, K., Hijioka, Y., & Masui, T. (2021). Extreme climate events increase risk of global food insecurity and adaptation needs. *Nature Food, 2*(8), 587-595. doi:10.1038/s43016-021-00335-4
Headey, D., & Fan, S. (2008). Anatomy of a crisis: the causes and consequences of surging food prices. *Agricultural Economics, 39*, 375-391. doi:10.1111/j.1574-0862.2008.00345.x
Herforth, A., Bai, Y., Venkat, A., Mahrt, K., Ebel, A., & Masters, W. A. (2020). *Cost and affordability of healthy diets across and within countries: Background paper for The State of Food Security and Nutrition in the World 2020*. Retrieved from
Hertel, T. W., Burke, M. B., & Lobell, D. B. (2010). The poverty implications of climate-induced crop yield changes by 2030. *Global Environmental Change, 20*(4), 577-585. doi:10.1016/j.gloenvcha.2010.07.001
Hewitt, K. (1983). *Interpretations of calamity: From the viewpoint of human ecology*. Boston: Allen & Unwin.
Hewitt, K., & Burton, I. (1973). The Hazardousness of a Place: A Regional Ecology of Damaging Events. In *Geographical Review* (Vol. 63).
Hijmans, R. J. (2019). raster: Geographic Data Analysis and Modeling (Version R package version 2.9-1). Retrieved from https://www.rspatial.org/
Hill, R. V., & Porter, C. (2017). Vulnerability to Drought and Food Price Shocks: Evidence from Ethiopia. *World Development, 96*, 65-77. doi:10.1016/j.worlddev.2017.02.025
Hosking, J. R. M. (1990). L-Moments: Analysis and Estimation of Distributions Using Linear Combinations of Order Statistics

Author(s):

Source: ., 1990, Vol. 52, No. 1 (1990), pp. 105-124 Published by: . *Journal of the Royal Statistical Society, Series B (Methodological), 52*(1), 105-124. doi:https://www.jstor.org/stable/2345653
Howe, P. (2010). Archetypes of famine and response. *Disasters, 34*(1), 30-54. doi:10.1111/j.1467-7717.2009.01113.x
Howe, P. (2018). Famine systems: A new model for understanding the development of famines. *World Development, 105*, 144-155. doi:10.1016/j.worlddev.2017.12.028
Howe, P. W., & Naumova, E. N. (2022). Poverty and famines 2.0: the opportunities and challenges of crisis modeling and forecasting. *J Public Health Policy, 43*(3), 329-334. doi:10.1057/s41271-022-00354-w
Hyndman, D., & Hyndman, D. (2016). *Natural hazards and disasters*: Cengage Learning.
ICF. (2019). *The DHS Program Spatial Data Repository.* Retrieved from: spatialdata.dhsprogram.com
Imai, K. S., Kaicker, N., & Gaiha, R. (2021). Severity of the COVID-19 pandemic in India. *Rev Dev Econ, 25*(2), 517-546. doi:10.1111/rode.12779
IMF. (2021). Country Indexes and Weight: Food and Non-Alcoholic Beverages [dataset]. Retrieved from https://data.imf.org/regular.aspx?key=61015892
International Comparison Program, & World Bank. (2021). PPP conversion factor, private consumption (LCU per international $) [dataset]. *World Development Indicators database, World Bank.* Retrieved from https://data.worldbank.org/indicator/PA.NUS.PRVT.PP
IPC Global Partners. (2019). *Integrated Food Security Phase Classification Technical Manual Version 3.0. Evidence and Standards for Better Food Security and Nutrition Decisions*. Retrieved from Rome:
IPCC. (2022). *Climate Change 2022: Mitigation of Climate Change. Contribution of Working Group III to the Sixth Assessment Report of the Intergovernmental Panel on Climate Change* Retrieved from
IRDR. (2014). *Peril Classification and Hazard Glossary*. Retrieved from Beijing:

Isanaka, S., Boundy, E. O., Grais, R. F., Myatt, M., & Briend, A. (2016). Improving Estimates of Numbers of Children With Severe Acute Malnutrition Using Cohort and Survey Data. *Am J Epidemiol, 184*(12), 861-869. doi:10.1093/aje/kww129
Isen, A., Rossin-Slater, M., & Walker, R. (2017). Relationship between season of birth, temperature exposure, and later life wellbeing. *Proc Natl Acad Sci U S A, 114*(51), 13447-13452. doi:10.1073/pnas.1702436114
Ivanic, M., & Martin, W. (2014). *Short- and Long-Run Impacts of Food Price Changes on Poverty. Policy Research Working Paper 7011.* . Retrieved from Washington DC:
Ives, A. R., & Carpenter, S. R. (2007). Stability and Diversity of Ecosystems. *Science, 317*(5834), 58-62. doi:10.1126/science.1133258
Jones, A. D., Ngure, F. M., Pelto, G., & Young, S. L. (2013). What are we assessing when we measure food security? A compendium and review of current metrics. *Adv Nutr, 4*(5), 481-505. doi:10.3945/an.113.004119
Kakpo, A., Mills, B. F., & Brunelin, S. (2022). Weather shocks and food price seasonality in Sub-Saharan Africa: Evidence from Niger. *Food Policy, 112*. doi:10.1016/j.foodpol.2022.102347
Kaminski, J., Christiaensen, L., & Gilbert, C. L. (2016). Seasonality in local food markets and consumption: evidence from Tanzania. *Oxford Economic Papers, 68*(3), 736-757. doi:10.1093/oep/gpw013
Keller, E. A., & DeVecchio, D. E. (2016). *Natural hazards: earth's processes as hazards, disasters, and catastrophes*: Routledge.
Kim, J. J., Humphrey, A., Marshak, A., Gathuoy, N. M., & Krishnan, V. (2020). *The Currency of Connections: Why Do Social Connections Matter for Household Resilience in South Sudan?* Retrieved from Boston:
Kinyoki, D. K., Moloney, G. M., Uthman, O. A., Kandala, N. B., Odundo, E. O., Noor, A. M., & Berkley, J. A. (2017). Conflict in Somalia: impact on child undernutrition. *BMJ Glob Health, 2*(2), e000262. doi:10.1136/bmjgh-2016-000262
Kjellstrom, T., & Crowe, J. (2011). Climate change, workplace heat exposure, and occupational health and productivity in Central America. *Int J Occup Environ Health, 17*(3), 270-281. doi:10.1179/107735211799041931
Klomp, J., & Bulte, E. (2013). Climate change, weather shocks, and violent conflict: a critical look at the evidence. *Agricultural Economics, 44*(s1), 63-78. doi:10.1111/agec.12051
Knapp, K. R., Kruk, M. C., Levinson, D. H., Diamond, H. J., & Neumann, C. J. (2010). The International Best Track Archive for Climate Stewardship (IBTrACS). *Bulletin of the American Meteorological Society, 91*(3), 363-376. doi:10.1175/2009bams2755.1
Knoben, W. J. M., Woods, R. A., & Freer, J. E. (2019). Global bimodal precipitation seasonality: A systematic overview. *International Journal of Climatology, 39*(1), 558-567. doi:10.1002/joc.5786
Kreps, G. A. (1989). Future Directions in Disaster Research: The Role of Taxonomy. *International Journal of Mass Emergencies and Disasters, 7*(3), 215-241.
Kreps, G. A. (1989). *Social structure and disaster*. Newark NJ: University of Delaware Press.
Krishnamurthy, P. K., Choularton, R. J., & Kareiva, P. (2020). Dealing with uncertainty in famine predictions: How complex events affect food security early warning skill in the Greater Horn of Africa. *Global Food Security, 26*. doi:10.1016/j.gfs.2020.100374
Krishnamurthy R, P. K., Fisher, J. B., Schimel, D. S., & Kareiva, P. M. (2020). Applying Tipping Point Theory to Remote Sensing Science to Improve Early Warning Drought Signals for Food Security. *Earth's Future, 8*(3). doi:10.1029/2019ef001456
Lautze, S., Bell, W., Alinovi, L., & Russo, L. (2012). Early warning, late response (again): The 2011 famine in Somalia. *Global Food Security, 1*(1), 43-49. doi:10.1016/j.gfs.2012.07.006
Lawlor, K., Handa, S., Seidenfeld, D., & Zambia Cash Transfer Evaluation, T. (2019). Cash Transfers Enable Households to Cope with Agricultural Production and Price Shocks: Evidence from Zambia. *J Dev Stud, 55*(2), 209-226. doi:10.1080/00220388.2017.1393519
Lazzaroni, S., & Wagner, N. (2016). Misfortunes never come singly: Structural change, multiple shocks and child malnutrition in rural Senegal. *Econ Hum Biol, 23*, 246-262. doi:10.1016/j.ehb.2016.10.006
Le, K., & Nguyen, M. (2021). The impacts of rainfall shocks on birth weight in Vietnam. *Journal of Development Effectiveness, 14*(2), 143-159. doi:10.1080/19439342.2021.1986114

Lenton, T. M., & Ciscar, J.-C. (2012). Integrating tipping points into climate impact assessments. *Climatic Change, 117*(3), 585-597. doi:10.1007/s10584-012-0572-8
León, J. C. V. D. (2006). *Vulnerability: A Conceptual and Methodological Review*. Retrieved from Bonn:
Leroy, J. L., Ruel, M., Frongillo, E. A., Harris, J., & Ballard, T. J. (2015). Measuring the Food Access Dimension of Food Security: A Critical Review and Mapping of Indicators. *Food Nutr Bull, 36*(2), 167-195. doi:10.1177/0379572115587274
Letta, M., Montalbano, P., & Pierre, G. (2021). Weather shocks, traders' expectations, and food prices. *American Journal of Agricultural Economics*. doi:10.1111/ajae.12258
Lobell, D. B., & Gourdji, S. M. (2012). The influence of climate change on global crop productivity. *Plant Physiol, 160*(4), 1686-1697. doi:10.1104/pp.112.208298
Lofgren, E., Fefferman, N., Doshi, M., & Naumova, E. N. (2007). *Assessing Seasonal Variation in Multisource Surveillance Data: Annual Harmonic Regression*, Berlin, Heidelberg.
M, T. (2018). tmap: Thematic Maps in R. *Journal of Statistical Software, 84*(6), 1-39. doi:10.18637/jss.v084.i06
Maccini, S., & Yang, D. (2009). Under the Weather: Health, Schooling, and Economic Consequences of Early-Life Rainfall. *Am Econ Rev, 99*(3), 1006-1026. doi:10.1257/aer.99.3.1006
Maidment, D. R. (1993). *Handbook of hydrology*: McGraw-Hill.
Marshak, A., Venkat, A., Young, H., & Naumova, E. N. (2021). How Seasonality of Malnutrition Is Measured and Analyzed. *Int J Environ Res Public Health, 18*(4). doi:10.3390/ijerph18041828
Mawejje, J. (2016). Food prices, energy and climate shocks in Uganda. *Agricultural and Food Economics, 4*(1). doi:10.1186/s40100-016-0049-6
Maxwell, D., Constas, M., Frankenberger, T. R., Klaus, D., & Mock, N. (2015). *Qualitative Data and Subjective Indicators for Resilience Measurement. Resilience Measurement Technical Working Group. Technical Series No. 4*. Retrieved from Rome: http://www.fsincop.net/fileadmin/user_upload/fsin/docs/resources/FSIN_TechnicalSeries_4.pdf
Maxwell, D., & Fitzpatrick, M. (2012). The 2011 Somalia famine: Context, causes, and complications. *Global Food Security, 1*(1), 5-12. doi:10.1016/j.gfs.2012.07.002
Maxwell, D., & Hailey, P. (2020). *Towards Anticipatory Information Systems and Action: Notes on Early Warning and Early Action in East Africa*. Retrieved from Boston: Feinstein International Center, Tufts University; Nairobi: Centre for Humanitarian Change:
Maxwell, D. G., & Majid, N. (2016). *Famine in Somalia: competing imperatives, collective failures, 2011-2012*: Hurst.
May, R. M. (1974). *Stability and complexity in model ecosystems* (2nd ed.). Princeton, NJ: Princeton University Press.
Mbow, C., Rosenzweig, C., Barioni, L. G., Benton, T. G., Herrero, M., Krishnapillai, M., . . . Xu, Y. (2019). Food security. In P. R. Shukla, J. Skea, E. C. Buendia, V. Masson-Delmotte, H.-O. Pörtner, D. C. Roberts, P. Zhai, R. Slade, S. Connors, R. v. Diemen, M. Ferrat, E. Haughey, S. Luz, S. Neogi, M. Pathak, J. Petzold, J. P. Pereira, P. Vyas, E. Huntley, K. Kissick, M. Belkacemi, & J. Malley (Eds.), *Climate Change and Land: an IPCC special report on climate change, desertification, land degradation, sustainable land management, food security, and greenhouse gas fluxes in terrestrial ecosystems* (pp. 437-550).
McPhillips, L. E., Chang, H., Chester, M. V., Depietri, Y., Friedman, E., Grimm, N. B., . . . Shafiei Shiva, J. (2018). Defining Extreme Events: A Cross-Disciplinary Review. *Earth's Future, 6*(3), 441-455. doi:10.1002/2017ef000686
Mileti, D. (1999). *Disasters by design: A reassessment of natural hazards in the United States*: Joseph Henry Press.
Minot, N. (2014). Food price volatility in sub-Saharan Africa: Has it really increased? *Food Policy, 45*, 45-56. doi:10.1016/j.foodpol.2013.12.008
Minten, B., Koru, B., & Stifel, D. (2013). The last mile(s) in modern input distribution: Pricing, profitability, and adoption. *Agricultural Economics, 44*(6), 629-646. doi:10.1111/agec.12078
Molina, O., & Saldarriaga, V. (2017). The perils of climate change: In utero exposure to temperature variability and birth outcomes in the Andean region. *Econ Hum Biol, 24*, 111-124. doi:10.1016/j.ehb.2016.11.009
Moltedo, A., Troubat, N., Lokshin, M., & Sajaia, Z. (2014). *Analyzing Food Security Using Household Survey Data: Streamlined Analysis with ADePT Software*. Retrieved from Washington, DC:

Moran, J. M. (2012). Chapter 12: Tropical Weather Systems. In *Weather studies: introduction to atmospheric science*. Boston, MA: American Meteorological Society.
Myatt, M., Khara, T., Schoenbuchner, S., Pietzsch, S., Dolan, C., Lelijveld, N., & Briend, A. (2018). Children who are both wasted and stunted are also underweight and have a high risk of death: a descriptive epidemiology of multiple anthropometric deficits using data from 51 countries. *Arch Public Health, 76*, 28. doi:10.1186/s13690-018-0277-1
Narayanan, S., & Saha, S. (2021). Urban food markets and the COVID-19 lockdown in India. *Global Food Security, 29*. doi:10.1016/j.gfs.2021.100515
Naumann, G., Dutra, E., Barbosa, P., Pappenberger, F., Wetterhall, F., & Vogt, J. V. (2014). Comparison of drought indicators derived from multiple data sets over Africa. *Hydrology and Earth System Sciences, 18*(5), 1625-1640. doi:10.5194/hess-18-1625-2014
Naumova, E. N., Jagai, J. S., Matyas, B., DeMaria, A., Jr., MacNeill, I. B., & Griffiths, J. K. (2007). Seasonality in six enterically transmitted diseases and ambient temperature. *Epidemiol Infect, 135*(2), 281-292. doi:10.1017/S0950268806006698
Naumova, E. N., & MacNeill, I. B. (2007a). Seasonality Assessment for Biosurveillance Systems. In J.-L. Auget, N. Balakrishnan, M. Mesbah, & G. Molenberghs (Eds.), *Advances in Statistical Methods for the Health Sciences: Applications to Cancer and AIDS Studies, Genome Sequence Analysis, and Survival Analysis* (pp. 437-450). Boston, MA: Birkhäuser Boston.
Naumova, E. N., & MacNeill, I. B. (2007b). Seasonality Assessment for Biosurveillance Systems. In *Advances in Statistical Methods for the Health Sciences* (pp. 437-450).
Niles, M. T., Emery, B. F., Reagan, A. J., Dodds, P. S., & Danforth, C. M. (2019). Social media usage patterns during natural hazards. *PLoS One, 14*(2), e0210484. doi:10.1371/journal.pone.0210484
Noy, I. (2016). A Global Comprehensive Measure of the Impact of Natural Hazards and Disasters. *Global Policy, 7*(1), 56-65. doi:10.1111/1758-5899.12272
Omiat, G., & Shively, G. (2020). Rainfall and child weight in Uganda. *Econ Hum Biol, 38*, 100877. doi:10.1016/j.ehb.2020.100877
Oxley, M. C. (2013). A “People-centred Principles-based” post-Hyogo framework to strengthen the resilience of nations and communities. *International Journal of Disaster Risk Reduction, 4*, 1-9. doi:10.1016/j.ijdrr.2013.03.004
Palm, R. I. (1990). Natural Hazards: An Integrative Framework for Research and Planning. *JOHNS HOPKINS UNIVERSITY PRESS, BALTIMORE, MD(USA). 1990.*
Park, J., Seager, T. P., Rao, P. S., Convertino, M., & Linkov, I. (2013). Integrating risk and resilience approaches to catastrophe management in engineering systems. *Risk Anal, 33*(3), 356-367. doi:10.1111/j.1539-6924.2012.01885.x
Paul, B. K. (2011). History and Development of Hazard Studies in Geography. In B. K. Paul (Ed.), *Environmental Hazards and Disasters* (pp. 37-66): John Wiley & Sons.
Pebesma, E. (2018). Simple Features for R: Standardized Support for Spatial Vector Data. *The R Journal*.
Peri, M. (2017). Climate variability and the volatility of global maize and soybean prices. *Food Security, 9*(4), 673-683. doi:10.1007/s12571-017-0702-2
Perry, R. W. (2007). What is a Disaster? In H. Rodríguez, E. L. Quarantelli, & R. R. Dynes (Eds.), *Handbook of Sociology and Social Research*. New York: Springer Science and Business Media.
Pesaresi, M., Florczyk, A., Schiavina, M., Melchiorri, M., & Maffenini, L. (2019). *GHS settlement grid, updated and refined REGIO model 2014 in application to GHS-BUILT R2018A and GHS-POP R2019A, multitemporal (1975-1990-2000-2015), R2019A.* Retrieved from: http://data.europa.eu/89h/42e8be89-54ff-464e-be7b-bf9e64da5218
Peters, D. P. C., Lugo, A. E., Chapin, F. S., Pickett, S. T. A., Duniway, M., Rocha, A. V., . . . Jones, J. (2011). Cross-system comparisons elucidate disturbance complexities and generalities. *Ecosphere, 2*(7). doi:10.1890/es11-00115.1
Phalkey, R. K., Aranda-Jan, C., Marx, S., Hofle, B., & Sauerborn, R. (2015). Systematic review of current efforts to quantify the impacts of climate change on undernutrition. *Proc Natl Acad Sci U S A, 112*(33), E4522-4529. doi:10.1073/pnas.1409769112
Pickett, S. T. A., & Cadenasso, M. L. (2008). Altered resources, disturbance, and heterogeneity: A framework for comparing urban and non-urban soils. *Urban Ecosystems, 12*(1), 23-44. doi:10.1007/s11252-008-0047-x

Pickett, S. T. A., Kolasa, J., Armesto, J. J., & Collins, S. L. (1989). The Ecological Concept of Disturbance and Its Expression at Various Hierarchical Levels. *Oikos, 54*(2), 129-136. doi:https://www.jstor.org/stable/3565258
Pimm, S. L. (1984). The complexity and stability of ecosystems. *Nature, 307*, 321-326.
Porter, C. (2012). Shocks, Consumption and Income Diversification in Rural Ethiopia. *Journal of Development Studies, 48*(9), 1209-1222. doi:10.1080/00220388.2011.646990
Quarantelli, E. L., & Perry, R. W. (2005). A social science research agenda for the disasters of the 21st century: Theoretical, methodological and empirical issues and their professional implementation. In *What is a Disaster?* (Vol. 325, pp. 396). Philadelphia: Xlibris.
Quarantelli, E. L., & Perry, R. W. (2005). *What is a disaster?: New answers to old questions*: Xlibris Corporation.
Raleigh, C., Choi, H. J., & Kniveton, D. (2015). The devil is in the details: An investigation of the relationships between conflict, food price and climate across Africa. *Glob Environ Change, 32*, 187-199. doi:10.1016/j.gloenvcha.2015.03.005
Ramanathan, K., Thenmozhi, M., George, S., Anandan, S., Veeraraghavan, B., Naumova, E. N., & Jeyaseelan, L. (2020). Assessing Seasonality Variation with Harmonic Regression: Accommodations for Sharp Peaks. *Int J Environ Res Public Health, 17*(4). doi:10.3390/ijerph17041318
Randell, H., & Gray, C. (2016). Climate variability and educational attainment: Evidence from rural Ethiopia. *Glob Environ Change, 41*, 111-123. doi:10.1016/j.gloenvcha.2016.09.006
Rocha, R., & Soares, R. R. (2015). Water scarcity and birth outcomes in the Brazilian semiarid. *Journal of Development Economics, 112*, 72-91. doi:10.1016/j.jdeveco.2014.10.003
Rosales-Rueda, M. (2018). The impact of early life shocks on human capital formation: evidence from El Nino floods in Ecuador. *J Health Econ, 62*, 13-44. doi:10.1016/j.jhealeco.2018.07.003
Roth, D. E., Krishna, A., Leung, M., Shi, J., Bassani, D. G., & Barros, A. J. D. (2017). Early childhood linear growth faltering in low-income and middle-income countries as a whole-population condition: analysis of 179 Demographic and Health Surveys from 64 countries (1993-2015). *Lancet Glob Health, 5*(12), e1249-e1257. doi:10.1016/S2214-109X(17)30418-7
Rustad, S. A., Rosvold, E. L., & Buhaug, H. (2019). Development Aid, Drought, and Coping Capacity. *The Journal of Development Studies, 56*(8), 1578-1593. doi:10.1080/00220388.2019.1696958
Sajid, O., & Bevis, L. E. M. (2021). Flooding and child health: Evidence from Pakistan. *World Development, 146*. doi:10.1016/j.worlddev.2021.105477
Sanderson, D. (2000). Cities, disasters and livelihoods. *Environment & Urbanization, 12*(2).
Schlenker, W., & Lobell, D. B. (2010). Robust negative impacts of climate change on African agriculture. *Environmental Research Letters, 5*(1). doi:10.1088/1748-9326/5/1/014010
Seneviratne, S. I., Zhang, X., Adnan, M., Badi, W., Dereczynski, C., Luca, A. D., . . . Zhou, B. (2021). Weather and Climate Extreme Events in a Changing Climate. In V. Masson-Delmotte, P. Zhai, A. Pirani, S. L. Connors, C. Péan, S. Berger, N. Caud, Y. Chen, L. Goldfarb, M. I. Gomis, M. Huang, K. Leitzell, E. Lonnoy, J. B. R. Matthews, T. K. Maycock, T. Waterfield, O. Yelekçi, R. Yu, & B. Zhou (Eds.), *Climate Change 2021: The Physical Science Basis. Contribution of Working Group I to the Sixth Assessment Report of the Intergovernmental Panel on Climate Change* (pp. 1513–1766). Cambridge, United Kingdom and New York, NY, USA: Cambridge University Press.
Shah, M., & Steinberg, B. M. (2017). Drought of Opportunities: Contemporaneous and Long-Term Impacts of Rainfall Shocks on Human Capital. *Journal of Political Economy, 125*(2), 527-561. doi:0022-3808/2017/12502-0003
Shively, G., & Thapa, G. (2016). Markets, Transportation Infrastructure, and Food Prices in Nepal. *American Journal of Agricultural Economics, 99*(3), 660-682. doi:10.1093/ajae/aaw086
Shively, G. E. (2017). Infrastructure mitigates the sensitivity of child growth to local agriculture and rainfall in Nepal and Uganda. *Proc Natl Acad Sci U S A, 114*(5), 903-908. doi:10.1073/pnas.1524482114
Simpson, R. B., Zhou, B., & Naumova, E. N. (2020). Seasonal synchronization of foodborne outbreaks in the United States, 1996-2017. *Sci Rep, 10*(1), 17500. doi:10.1038/s41598-020-74435-9
Skoufias, E. (2003). Economic Crises and Natural Disasters: Coping Strategies and Policy Implications. *World Development, 31*(7), 1087-1102. doi:10.1016/s0305-750x(03)00069-x
Skoufias, E., & Vinha, K. (2012). Climate variability and child height in rural Mexico. *Econ Hum Biol, 10*(1), 54-73. doi:10.1016/j.ehb.2011.06.001

SMART. (2017). *Standardized Monitoring and Assessment for Relief and Transitions (SMART) Manual 2.0*. Retrieved from
Spedicato, G. (2017). Discrete Time Markov Chains with R. *The R Journal, 9*(2), 84-108.
Stanke, C., Kerac, M., Prudhomme, C., Medlock, J., & Murray, V. (2013). Health effects of drought: a systematic review of the evidence. *PLoS Curr, 5*. doi:10.1371/currents.dis.7a2cee9e980f91ad7697b570bcc4b004
Takayama, T. J. G. G. (1971). *Spatial and temporal price and allocation models*. Amsterdam: North-Holland Pub. Co.
Thapa, G., & Shively, G. (2018). A dose-response model of road development and child nutrition in Nepal. *Research in Transportation Economics, 70*, 112-124. doi:10.1016/j.retrec.2018.11.002
The Integrated Food Security Phase Classification (IPC) Global Partners. (2019). *IPC Technical Manual Version 3.0*. Retrieved from
Thiede, B. C., & Strube, J. (2020). Climate Variability and Child Nutrition: Findings from Sub-Saharan Africa. *Glob Environ Change, 65*. doi:10.1016/j.gloenvcha.2020.102192
Tierney, K. (2014a). Chapter 6: Communities and Societies at Risk. In *The Social Roots of Risk*: Stanford University Press.
Tierney, K. (2014b). The social roots of risk. In *The Social Roots of Risk*: Stanford University Press.
Tierney, K. J. (2007). From the Margins to the Mainstream? Disaster Research at the Crossroads. *Annual Review of Sociology, 33*(1), 503-525. doi:10.1146/annurev.soc.33.040406.131743
Tobin, G. A., & Montz, B. E. (1997a). *Natural hazards: explanation and integration*. New York, NY: Guilford Press.
Tobin, G. A., & Montz, B. E. (1997b). Physical Dimensions of Natural Hazards. In *Natural hazards: explanation and integration*. New York, NY: Guilford Press.
Turner, B. A. (1976). The Development of Disasters - A Sequence Model for the Analysis of the Origins of Disasters. *The Sociological Review, 24*(4), 753-774. doi:https://doi.org/10.1111/j.1467-954X.1976.tb00583.x
Tusting, L. S., Bradley, J., Bhatt, S., Gibson, H. S., Weiss, D. J., Shenton, F. C., & Lindsay, S. W. (2020). Environmental temperature and growth faltering in African children: a cross-sectional study. *Lancet Planet Health, 4*(3), e116-e123. doi:10.1016/S2542-5196(20)30037-1
Twigg, J. (2001). *Corporate social responsibility and disaster reduction: A global overview*: Benfield Greig Hazard Research Centre London.
Ubilava, D., & Abdolrahimi, M. (2019). The El Niño impact on maize yields is amplified in lower income teleconnected countries. *Environmental Research Letters, 14*(5). doi:10.1088/1748-9326/ab0cd0
UN/ISDR. (2009). *Global assessment report on disaster risk reduction*. Retrieved from Geneva, Switzerland:
UNDRR. (2017). *UNDRR Terminology on Disaster Risk Reduction*. Retrieved from
UNDRR. (2019). *Global Assessment Report on Disaster Risk Reduction*. Retrieved from Geneva, Switzerland:
UNICEF, WHO, & IBRD/WB. (2020). *Levels and trends in child malnutrition: Key Findings of the 2020 Edition of the Joint Child Malnutrition Estimates*. Retrieved from Geneva:
UNISDR. (2009). *UNISDR Terminology on Disaster Risk Reduction*. Retrieved from Geneva, Switzerland: https://www.preventionweb.net/files/7817_UNISDRTerminologyEnglish.pdf
US Department of Agriculture Agricultural Research Service. (2016). USDA National Nutrient Database for Standard Reference, Release 28 (Slightly revised). Version Current: May 2016. Retrieved from http://www.ars.usda.gov/nea/bhnrc/mafcl
Vaitla, B., Devereux, S., & Swan, S. H. (2009). Seasonal hunger: a neglected problem with proven solutions. *PLoS Med, 6*(6), e1000101. doi:10.1371/journal.pmed.1000101
van Herk, S., Schot, P. P., Gersonius, B., & Koukoui, N. (2015). Adaptation tipping points and opportunities for urban flood risk management. *Journal of Water and Climate Change, 6*(4), 695-710. doi:10.2166/wcc.2015.093
Vargo, E., Pasupathy, R., & Leemis, L. (2010). Moment-Ratio Diagrams for Univariate Distributions. *Journal of Quality Technology, 42*(3).
Venkat, A., Marshak, A., Young, H., & Naumova, E. N. (2023). Seasonality of Acute Malnutrition in African Drylands: Evidence From 15 Years of SMART Surveys. *Food Nutr Bull, 44*(2_suppl), S94-S108. doi:10.1177/03795721231178344

Vickerstaff, V., Omar, R. Z., & Ambler, G. (2019). Methods to adjust for multiple comparisons in the analysis and sample size calculation of randomised controlled trials with multiple primary outcomes. *BMC Med Res Methodol, 19*(1), 129. doi:10.1186/s12874-019-0754-4
Vincent, A., Grande, F., Compaoré, E., Amponsah Annor, G., Addy, P. A., Aburime, L. C., . . . Charrondière, U. R. (2020). *Food Composition Table for Western Africa*. Retrieved from Rome:
Vogel, E., Donat, M. G., Alexander, L. V., Meinshausen, M., Ray, D. K., Karoly, D., . . . Frieler, K. (2019). The effects of climate extremes on global agricultural yields. *Environmental Research Letters, 14*(5). doi:10.1088/1748-9326/ab154b
Wan, Z., Hook, S., & Hulley, G. (2015). MOD11C3 MODIS/Terra Land Surface Temperature/Emissivity Monthly L3 Global 0.05Deg CMG V006 [Data set]. Retrieved from https://doi.org/10.5067/MODIS/MOD11C3.006
WFP. (2021). Vulnerability Analysis and Mapping [dataset]. Retrieved from https://dataviz.vam.wfp.org/
White, G. F. (1974). *Natural hazards, local, national, global*: Oxford University Press.
WHO. (2000). *The management of nutrition in major emergencies*. Retrieved from
WHO, & UNICEF. (2009). *WHO child growth standards and the identification of severe acute malnutrition in infants and children*. Retrieved from
Wisner, B., Blaikie, P., Cannon, T., & Davis, I. (2004). *At risk: natural hazards, people's vulnerability and disasters* (2nd ed.). London: Routledge.
Wisner, B., Gaillard, J.-C., & Kelman, I. (2012). *Handbook of hazards and disaster risk reduction*: Routledge.
Yamano, T., Alderman, H., & Christiaensen, L. (2005). Child Growth, Shocks, and Food Aid in Rural Ethiopia. *American Journal of Agricultural Economics, 87*(2), 273-288. doi:10.1111/j.1467-8276.2005.00721.x
Young, H. (2020). *Nutrition in Africa's drylands: A conceptual framework for addressing acute malnutrition*. Retrieved from Boston:
Young, H., & Jaspars, S. (2006). *The meaning and measurement of acute malnutrition in emergencies: a primer for decision-makers*. Retrieved from
Zhao, M., Lee, J. K. W., Kjellstrom, T., & Cai, W. (2021). Assessment of the economic impact of heat-related labor productivity loss: a systematic review. *Climatic Change, 167*(1-2). doi:10.1007/s10584-021-03160-7
Zseleczky, L., & Yosef, S. (2014). *Are Shocks Really Increasing? a selective reivew of the global frequency, severity, scope, and impact of five types of shocks*. Retrieved from Washington DC:

Appendix 1: Retail Items Included in Early Warning Systems

Food Group	*Item Name*	*Number of Observations*	*Frequency*
Breads and Cereals	Barley	127	0.02
	Bread	24004	3.87
	Buckwheat	1296	0.21
	Maize	157816	25.48
	Millet	58572	9.46
	Pasta	9107	1.47
	Rice	211188	34.09
	Sorghum	76726	12.39
	Teff	579	0.09
	Wheat	80053	12.92
Dairy and Eggs	Cheese	5128	11.10
	Egg	11128	24.09
	Milk	27383	59.27
	Yogurt	2561	5.54
Fats and Oils	Butter	1060	1.10
	Cotton Oil	1019	1.05
	Ghee	4177	4.32
	Groundnut Oil	6050	6.26
	Maize Oil	876	0.91
	Mustard Oil	8526	8.82
	Other Oils	1015	1.05
	Olive Oil	1141	1.18
	Palm Oil	25781	26.67
	Soybean Oil	5276	5.46
	Sunflower Oil	11806	12.21
	Vegetable Oil	29947	30.98
Meats	Beef	30678	40.48
	Camel	910	1.20
	Chicken	15093	19.91
Fruits and Vegetables	Apple	6106	1.79
	Apples	739	0.22
	Avocados	3281	0.96
	Banana	14952	4.38
	Beans	2882	0.84
	Beetroots	467	0.14
	Bitter Melon	891	0.26
	Bitterball	165	0.05
	Bottle Gourd	741	0.22
	Cabbage	13501	3.95
	Calamansi	840	0.25
	Carrot	11066	3.24
	Cassava	105716	30.94
	Cauliflower	1111	0.33
	Choko	776	0.23
	Coconut	4048	1.18
	Cocoyam	2652	0.78
	Cucumbers	3553	1.04
	Dates	1075	0.31
	Egg	5853	1.71
	Guava	619	0.18
	Kale	49	0.01
	Leafy Vegetables	502	0.15
	Lettuce	1837	0.54
	Mandarins	201	0.06
	Mangoes	3444	1.01
	Okra	1307	0.38
	Onion	30119	8.81
	Orange	5406	1.58

Food Group	*Item Name*	*Number of Observations*	*Frequency*	*Food Group*	*Item Name*	*Number of Observations*	*Frequency*
	Pork	12463	16.44		Papaya	3573	1.05
	Sheep	8653	11.42		Passion Fruit	3963	1.16
	Other	7992	10.55		Peppers	5681	1.66
Pulses, Nuts, and Seeds	Beans	76669	44.68		Pineapples	498	0.15
	Cashew Nut	197	0.11		Plantains	4477	1.31
	Chickpea	5981	3.49		Pork	435	0.13
	Cowpea	10861	6.33		Potato	38135	11.16
	Gram	122	0.07		Potato Leaves	143	0.04
	Groundnut	35178	20.50		Pumpkin	821	0.24
	Horse Beans	261	0.15		Radish	324	0.09
	Lentils	24386	14.21		Snake Gourd	391	0.11
	Peas	6672	3.89		Spinach	2712	0.79
	Pigeon Peas	1042	0.61		Squashes	837	0.24
	Pulses	2379	1.39		Sweet Potato Leaves	570	0.17
	Sesame	2054	1.20		Sweet Potatoes	14737	4.31
	Soybean	4909	2.86		Swiss Chard	20	0.01
	Walnuts	870	0.51		Taro	798	0.23
Fish and Seafoods	Crab	591	1.47		Tomato	25578	7.49
	Egg	114	0.28		Tomato Paste	1486	0.43
	Fish	38199	94.91		Water Spinach	1007	0.29
	Shrimp	1246	3.10		Watermelons	1285	0.38
	Snail	98	0.24		Wax Gourd	434	0.13
Sugar and Confectionery	Sugar	5132	100.00		Yam	8244	2.41
				Fruits and Vegetables	Zucchini	1653	0.48

Appendix 2: Sensitivity Analysis of Retail Prices

Refer to attachment.

Appendix 3: Sensitivity Analysis of Seasonal Wasting Curves

Refer to attachment.

Appendix 4: Extreme Weather and Underprediction of Critical Phase Transitions

Refer to attachment.